eman ta zabal zazu

Universidad del País Vasco
Euskal Herriko Unibertsitatea

CHARACTERIZATION AND PHARMACOLOGICAL MODULATION OF CALCIUM HANDLING PROTEINS IN LIMB-GIRDLE MUSCLE DYSTROPHY TYPE R1

DOCTORAL THESIS

by

Jaione Lasa Elgarresta

Memory to achieve a PhD in Molecular Biology and Biomedicine

by

The University of the Basque Country

Department of Neurosciences

Donostia / San Sebastian, January 2021

(c) 2021 Jaione Lasa Elgarresta

Hegoak emateaz gain,

haietaz baliatzen irakatsi zidanari.

Amari

This thesis project has been developed at Biodonostia Health Research Institute, in the group of Neuromuscular Diseases, under the supervision of Dr Adolfo López de Munain Arregui and Dr Ainara Vallejo Illarramendi.

Funding received for developing the current thesis

Ayudas destinadas a la financiación de la realización de una tesis doctoral mediante un contrato predoctoral. Departamento de Educación del Gobierno Vasco (PRE_2015_1_0016, PRE_2016_2_0215, PRE_2017_2_0056 y PRE_2018_2_0046).

Ayudas para estancias en centros distintos al de aplicación del programa de formación de personal investigador (EP_2019_1_0074)

EMBO Short-Term Fellowship Number 8365 (2019)

Diputación de Guipúzcoa (2018-000117-01-B y 2019-00362-01-B)

Programa de Becas reservadas a titulados superiores de la Fundación Jesús Gangoiti Barrera (2016)

Articles and presentations related to the subject of the current thesis

Published papers, book chapters and reviews

1. **Calpain 3 deficiency affects SERCA expression and function in the skeletal muscle**

Iván Toral-Ojeda[+], Garazi Aldanondo[,+], Jaione Lasa-Elgarresta, Haizpea Lasa-Fernández, Roberto Fernández-Torrón, Adolfo López de Munain, and Ainara Vallejo-Illarramendi[*].

[*] Corresponding author

[+] These authors contributed equally to this work

Expert Reviews in Molecular Medicine. 2016, *Vol. 18; e7.*

DOI: 10.1017/erm.2016.9

2. **A novel functional in vitro model that recapitulates human muscle disorders**

Iván Toral-Ojeda[+], Garazi Aldanondo[,+], Jaione Lasa-Elgarresta[,+], Haizpea Lasa-Fernández, Camila Vesga-Castro, Vincent Mouly, Adolfo López de Munain, and Ainara Vallejo-Illarramendi[*]

[*] Corresponding author

[+] These authors contributed equally to this work

Muscle Cell and Tissue - Current Status of Research Field. 2018*; pp.pp 133–153.*

DOI: 10.5772/intechopen.75903.

3. **Calcium mechanisms in Limb-Girdle Muscular Dystrophy with CAPN3 mutations**

Jaione Lasa-Elgarresta, Laura Mosqueira-Martín, Neia Naldaiz-Gastesi, Amets Sáenz, Adolfo López de Munain[*], and Ainara Vallejo-Illarramendi[*]

[*] Corresponding authors

International Journal of Molecular Sciences. 2019*, 20.*

DOI: 10.3390/ijms20184548.

Congress presentations

1. **Targeting calcium homeostasis in LGMD2A. Presented in the 6th International congress of myology, Bordeaux, France (2019)**

Jaione Lasa-Elgarresta, Haizpea Lasa-Fernández,Camila Vesga, Laura Mosqueira-Martín, Adolfo López de Munain and Ainara Vallejo-Illarramendi

2. **Alteration of calcium handling proteins in human in vitro models of limb girdle muscular dystrophy type 2A (LGMD2A). Presented in Neurogune 2016, Bilbao, Spain (2016)**

Jaione Lasa-Elgarresta[+], Iván Toral-Ojeda[+], Garazi Aldanondo, Haizpea Lasa-Fernández, Adolfo López de Munain and Ainara Vallejo-Illarramendi

[+] These authors contributed equally to this work

3. **Alteration of calcium homeostasis in human *in vitro* models of limb girdle muscular dystrophy type 2A (LGMD2A). Presented in the 5th International congress of myology, Lyon, France (2016)**

Jaione Lasa-Elgarresta[+], Iván Toral-Ojeda[+], Garazi Aldanondo, Haizpea Lasa-Fernández, Adolfo López de Munain and Ainara Vallejo-Illarramendi

[+] These authors contributed equally to this work

4. **New evidence for calcium mishandling in human Calpain 3 deficient myotubes. Presented in Neurogune 2014, San Sebastian, Spain (2014)**

Ivan Toral-Ojeda, Garazi Aldanondo, Jaione Lasa-Elgarresta, Roberto Fernández-Torrón, Adolfo López de Munain, and Ainara Vallejo-Illarramendi

INDEX

INDEX 5

FIGURE INDEX 7

TABLE INDEX 9

ABBREVIATIONS AND ACRONYMS 11

RESUMEN 19

SUMMARY 27

INTRODUCTION 35

- Muscle tissue - Skeletal muscle 37
- Calcium homeostasis in skeletal muscle 41
- Limb-Girdle Muscle Dystrophy type R1 47
- Calpain 3 51
- CAPN3 functions in skeletal muscle 56
- Muscle atrophy and degradation 63
- Therapeutic strategies 65

HYPOTHESIS AND OBJECTIVES 69

- Working hypothesis 71
- Aims and objectives 71

MATERIALS AND METHODS 73

- Cell culture 75
- Animal models 76
- Protein analysis 76
- SERCA activity assay 78
- Real-time quantitative PCR (qPCR) 79
- Calcium imaging 81
- Serum creatine kinase 81
- Grip Strength test 81
- Fatigue resistance 81
- Diaphragm strength *in vitro* measurement 82
- Open field test 83
- Voluntary exercise 83
- Histological analysis 83
- Ubiquitin proteasome activity 84

Data analysis and statistical procedures 85
RESULTS 87
Downregulation of SERCA protein in CAPN3 deficient *in vitro* models 89
Effect of Bortezomib (BTZ) over CAPN3 deficient myotubes 93
SERCA protein deficiency in human primary immortalized myoblasts from LGMDR1 patients and BTZ treatment. 96
SERCA protein expression in C3KO model.. 99
Effect of BTZ treatment in C3KO mice 108
SERCA protein expression in *C3 null* rat model and the effect of UPS inhibition. 114
DISCUSSION 123
CAPN3 deficiency generates SERCA deficiency in human *in vitro* myotubes..... 125
Bortezomib treatment can restore SERCA2 expression and functionality in CAPN3-deficient *in vitro* human myotubes but induces SR stress 128
LGMDR1 animal models show mild LGMDR1 phenotype though SERCA deficiency is observed. 130
Future direction 137
CONCLUSIONS 139
REFERENCES 143

FIGURE INDEX

Figure 1. Representation of the skeletal muscle structure. 38

Figure 2. Representation of the sarcomere structure. 39

Figure 3. Representation of the muscle fibre. 40

Figure 4. Representation of Ca^{2+} fluxes in the muscle fibre. 42

Figure 5. Schematic representation of UPR signalling pathways. 45

Figure 6. Illustration of pathological features of CAPN3 deficiency in the skeletal muscle 51

Figure 7. Muscle biopsy of a LGMDR1 patient. 51

Figure 8. Schematic representation of CAPN3 structure. 52

Figure 9. Schematic representation of recognized Ca^{2+}-mediated pathogenic mechanisms triggered by CAPN3 deficiency. 58

Figure 10. Scheme of the hypothesis. 71

Figure 11. Schematic representation of the enzymatic reactions determining SERCA activity. 79

Figure 12. CAPN3-deficiency in human LHCN-M2 myotubes. 90

Figure 13. Intracellular Ca^{2+} imaging of human LHCN-M2 myotubes. 90

Figure 14. Analysis of mRNA expression in CAPN3 deficient LHCN-M2 myotubes. 91

Figure 15. Analysis of Ca^{2+} handling proteins in CAPN3 deficient 8220 myotubes. 92

Figure 16. Analysis of mRNA expression in LGMDR1 model based on CAPN3 silencing in 8220 control myotubes. 92

Figure 17. Intracellular Ca^{2+} imaging of 8220 myotubes after being loaded by ratiometric dye Fura 2AM. 93

Figure 18. Effect of BTZ treatment over calcium handling proteins in CAPN3-deficient 8220 myotubes. 94

Figure 19. Gene expression analysis in BTZ treated CAPN3-deficient 8220 myotubes. 95

Figure 20. Intercellular Ca2+ imaging of BTZ treated and no-treated CAPN3-deficient 8220 myotubes by loading with ratiometric marker Fura 2AM. 95

Figure 21. Immortalized human LGMDR1 myotubes. 96

Figure 22. Gene expression analysis in primary immortalized LGMDR1 and control human myotubes. 97

Figure 23. Characterization of human primary immortalized LGMDR1 and control myotubes at the protein level. 98

Figure 24. Effect of BTZ treatment on protein and mRNA expression in immortalized human primary LGMDR1 myotubes. 99

Figure 25. Forelimb grip strength of young control and C3KO mice. 100

Figure 26. Results of run-to-exhaustion test in young control and C3KO mice. 100

Figure 27. Characterization of SERCA expression in *soleus* muscle of young control and C3KO mice. 101

Figure 28. Characterization of SERCA expression in the diaphragm of young control and C3KO mice. 101

Figure 29. *In vitro* diaphragm force analysis in young control and C3KO mice. 102

Figure 30. Serum creatine kinase (CK) levels of young control and C3KO mice. 102

Figure 31. Resting intracellular calcium levels of FDB-isolated myofibres from young control and C3KO mice. 103

Figure 32. Forelimb grip strength of young and adult control and C3KO mice. 104

Figure 33. Voluntary exercise performed for 24h by adult control and C3KO mice.105

Figure 34. Six-min-walk test in open field of adult control and C3KO mice. 105

Figure 35. Analysis of muscle fibres CSA of adult control and C3KO mice diaphragms. 106

Figure 36. Percentage of fast and slow fibres among total fibres in adult control and C3KO mice diaphragms. 107

Figure 37. Analysis of central nucleation of control and C3KO adult mouse diaphragm cryosections by immunofluorescence. 107

Figure 38. Body weight evolution during BTZ treatment of adult mice. 108

Figure 39. Forelimb grip strength of adult mice after BTZ treatment. 108

Figure 40. Voluntary exercise of adult mice after BTZ treatment. 109

Figure 41. Six-min-walk test in the open-field of adult mice after BTZ treatment. 109

Figure 42. Analysis of muscle fibres CSA in adult mice after BTZ treatment. 110

Figure 43. Proportion of fast and slow fibres in *soleus* from adult mice after BTZ treatment. 111

Figure 44. Analysis of central nucleation of adult mouse diaphragms after BTZ treatment. 111

Figure 45. Gene expression analysis of adult mouse diaphragms after BTZ treatment. 112

Figure 46. Gene expression analysis of mitochondrial biosynthesis marker Ppargc1 and myogenic inhibitor *Tgfb1* of adult mouse diaphragm. 113

Figure 47. Characterization of SERCAs and p-CaMKII expression in diaphragms from adult BTZ-treated mice. 113

Figure 48. Ubiquitin proteasome activity in *soleus* muscle of adult mice after BTZ treatment. 114

Figure 49. Characterization of SERCA expression in diaphragms from adult rats. 115

Figure 50. Body weight evolution during BTZ treatment of adult rats. 116

Figure 51. Forelimb grip strength of adult rats after BTZ treatment. 116

Figure 52. Serum creatine kinase (CK) levels of adult rats after BTZ treatment. 117

Figure 53. Analysis of central nucleation of adult rat *soleus*. 117

Figure 54. Characterization of adult rat *soleus* CSA after BTZ treatment. 118

Figure 55. Fast / slow myofibre proportion of adult rat *soleus* after BTZ treatment. 119

Figure 56. Analysis of fibrosis in adult rat *soleus* after BTZ treatment. 119

Figure 57. Characterization of SERCA expression in adult rat *soleus* after BTZ treatment. 120

Figure 58. Characterization of SERCA expression in adult rat diaphragms after BTZ treatment. 121

Figure 59. Gene expression analysis in adult rat diaphragms after BTZ treatment. 122

Figure 60. Hypothetic model of SERCA deficiency upon CAPN3 reduction in SR network. 128

TABLE INDEX

Table 1. Description of the clusters for calpainopathy. 48

Table 2. Therapeutic strategies for LGMDR1. 66

Table 3. Summary of molecular data of the cell lines from LGMDR1 patients. 75

Table 4. List of antibodies employed for western blot and immunohistochemistry. 78

Table 5. Sequence of primers used for real-time qPCR analysis. 80

ABBREVIATIONS AND ACRONYMS

	%	**Percent**
	[ ]	Concentration
	ºC	Degree Celsius
	µg	Microgram
	µl	Microlitre
	µm	Micrometre
	Δ	Delta
	ε	Extinction coefficient
A	A	Ampere
	AAV	Adeno-associated virus
	Ach	Acetylcholine
	ADP	Adenosine diphosphate
	Akt	Protein kinase B
	AldoA	Aldolase isoform A
	AMBMP	N4-(1,3-benzo-dioxol-5-ylmethyl)-6-(3-methoxyphenyl)-2,4-pyrimidinediaminehydrochlorid
	AMP	Adenosine monophosphate
	AMPK	AMP-activated protein kinase
	ANOVA	Analysis of variance
	ARN	Ácido ribonucleico
	ATF4	Activating transcription factor 4
	ATF6	Activating transcription factor 6
	ATP	Adenosine triphosphate
	ATP2A1	Sarco/endoplasmic reticulum Ca^{2+}-ATPase isoform 1 gene
	ATP2A2	Sarco/endoplasmic reticulum Ca^{2+}-ATPase isoform 2 gene
	ATP2A3	Sarco/endoplasmic reticulum Ca^{2+}-ATPase isoform 3 gene
	Atp5d	Rodent ATP synthase subunit delta gen
B	BiP/GRP78	Endoplasmic reticulum chaperone BiP/glucose-regulated protein 78
	Bnip3	BCL2 Interacting Protein 3 gene
	BSA	Bovine serum albumin
	BCN	Barcelona
	BTZ	Bortezomib
C	C3 null/ *C3-/-*	Calpain 3 knockout rat
	C3KO	Calpain 3 knockout
	Ca^{2+}	Calcium ion
	$CaCl_2$	Calcium chloride
	CaM	Calmodulin
	CAMK	Ca^{2+}/calmodulin-dependent protein kinase
	CAMKII	Ca^{2+}/calmodulin-dependent protein kinase II
	Capn3	Rodent Calpain 3 gene
	CAPN1	Calpain 1

	CAPN2	Calpain 2
	CAPN3	Human Calpain 3 gene
	CAPN3	Calpain 3 protein
	Capn3$^{-/-}$	Calpain 3 knockout mouse
	Capn3$^{cs/cs}$	Calpain 3 C129S mouse
	CBSW	Calpain-type beta-sandwich domain
	CDK-4	Cyclin dependent kinase 4
	cDNA	Complementary DNA
	c-FLIP	Cellular FLICE inhibitory protein
	CHOP	CCAAT-enhancer-binding protein homologous protein
	CK	Creatine Kinase gene
	CK	Creatine Kinase protein
	Ckmt2	Creatin kinase, mitochondrial 2
	cm	Centimetre
	CMA	Chaperone-mediated autophagy
	Cn	Calcineurin
	CNIC	Centro Nacional de Investigaciones Cardiovasculares
	CRISPR/Cas9	Clustered Regularly Interspaced Short Palyndromic Repeats Cas9
	CSA	Cross-sectional area
	CSQ	Calsequestrin
	CTX	Cardiotoxin
	Cys	Cystein
	Cyt	Cytoplasm
	CysPC	Cystein protease domain
	Cyt-c	Cytochrome C
D	D	Density
	DAPI	4',6-diamidino-2-phenylindole
	DHPR	Dihydropyridine receptor
	Dhpra1	Rodent dihydropyridine receptor isoform alpha 1 gene
	DHPRα2	Dihydropyridine receptor isoform alpha 2
	Dmd	Animal Dystrophin gene
	DMD	Duchenne muscular dystrophy
	DMEM	Dulbecco's Modified Eagle Medium
	DNA	Deoxyribonucleic acid
	DNase	Deoxyribonuclease
	DOX	Doxypacycline
	DPBS	Dulbecco's phosphate buffered saline
	Dr	Doctor (English)
	Dr.	Doctor (Spanish)
	Dra.	Doctora (Spanish)
	DSHB	The Developmental Studies Hybridoma Bank
	DTT	Dithiothreitol
	DWORF	Dwarf open reading frame
	DYST	Human dytrophin gene

	Dyst	Rodent dytrophin gene
E	ECC	Excitation-contraction coupling
	ECM	Extracellular matrix
	EDL	*Extensor digitorum longus*
	EGTA	Ethylene glycol-bis(β-aminoethyl ether)-N,N,N′,N′-tetraacetic acid
	EMA	European Medicines Agency
	ER	Endoplasmic reticulum
	ERAD	ER-associated degradation
	EX	Exon
F	FBS	Fetal bovine serum
	FDA	The United States Food and Drug Administration
	FDB	*Flexor digitorum brevis*
	FITC	5/6-fluorescein isothiocyanate
	FKBP12	Peptidyl-prolyl cis-trans isomerase FKBP12
	FRZB	Frizzled Related Protein
G	g	G-force
	Gapdh	Rodent glyceraldehyde 3-phosphate dehydrogenase gene
	GAPDH	Human glyceraldehyde 3-phosphate dehydrogenase
	GS	Goat serum
	GRP78	HumanGlucose-regulated protein 78 gene
	GSK-3β	Glycogen synthase kinase 3 Beta
H	h	Hour
	HCl	Hydrochloric acid
	HE	Haematoxylin & Eosin
	HEK	Human embryonic kidney cells
	HEPES	4-(2-hydroxyethyl)-1-piperazineethanesulfonic acid
	HERP	Homocysteine-induced endoplasmic reticulum protein
	hESC	Human embryonic stem cells
	HPRT1	Human hypoxanthine phosphoribosyltransferase 1 gene
	Hprt1	Rodent hypoxanthine phosphoribosyltransferase 1 gene
	hiPSC	Human induced pluripotent stem cell
	hTERT	Human telomerase reverse transcriptase
	Hz	Hertz
I	IC50	Half maximal inhibitory concentration
	IgM	Immunoglobulin M
	IHC	Immunohistochemistry
	Ikβα	Nuclear factor of kappa light polypeptide gene enhancer in B-cells inhibitor, isoform alpha
	Inc.	Incorporation
	iMOC	Intermolecular complementation
	IP	Intraperitoneal
	IP3R	Inositol 1,4,5-triphosphate receptors
	iPSC	Induced pluripotent stem cell
	IREI	Inositol-requiring protein 1

	IS1	Insertion sequence 1
	IS2	Insertion sequence 2
	IV	Intravenous
K	kb	Kilobase
	KCl	Potassium chloride
	kg	kilogram
	KLF4	Kruppel-like factor 4
	KO	Knockout
L	L	optical pathlength
	L_0	Optimum length
	LC3	Microtubule-associated protein 1A/1B-light chain 3
	LC3 II	Lipid modified form of LC3
	LDH	Lactic Dehydrogenase
	L_f	Tissue length/fibre length
	LG1	LGMDR1 sample 1
	LG2	LGMDR1 sample 2
	LGMD	Limb girdle muscular dystrophy
	LGMD2A	Limb girdle muscular dystrophy type 2A, renamed LGMDR1
	LGMD2B	Limb girdle muscular dystrophy type 2B, renamed LGMDR2
	LGMDD4	Limb girdle muscular dystrophy dominant 4
	LGMDR1	Limb girdle muscular dystrophy recessive 1, caused by mutations in CAPN3
	LGMDR2	Limb girdle muscular dystrophy recessive 2, caused by mutations in dysferlin
	LGMDR4	Limb girdle muscular dystrophy recessive 4, caused by mutations in α-sarcoglycan
	LKB1	Liver kinase B1
	LLVY-R110	Leu-Leu-Val-Tyr-R110
	Lpl	Rodent lipoprotein lipase gene
M	M	Molar
	m	Metre
	m^2	Square metre
	mAb	Monoclonal antibody
	MAM	Mitochondria-associated sarcoplasmic reticulum membrane
	MARP-2	Muscle Ankyrin repeat protein-2
	MEF2	Myocyte enhancer factor-2
	mg	milligram
	$MgCl_2$	Magnesium chloride
	$MgSO_4$	Magnesium sulfate
	min	Minutes
	miRNA	Micro ribonucleic acid
	ml	Millilitre
	MLN	Myoregulin protein
	mM	Millimolar
	mmol	Millimol

	Mmp9	Rodent metalloprotease 9 gene
	MN	Motor neuron
	mo	Months
	MOI	Multiplicity of infection
	MOPS	(3-(N-morpholino)propanesulfonic acid)
	MRF4	Myogenic regulatory factor 4 protein
	MRF	Myogenic regulatory factor
	MRI	Magnetic resonance imaging
	mRNA	Messenger ribonucleic acid
	msec	Milliseconds
	mtDNA	Mitochondrial deoxyribonucleic acid
	mTORC1	Mammalian target of rapamycin complex 1
	MuRF1	Muscle RING-finger protein 1
	MYF5	Myogenic factor 5 protein
	MyHC	Myosin heavy chain
	Myl2	Rodent myosin light chain 2 gene
	MYL2	Human myosin light chain 2 protein
	Myo18b	Rodent myosin XVIIIb gene
	MYOD	Myogenic differentiation protein 1
	MYOD	Myogenic differentiation protein 1 gene
	MYOG	Myogenin
	Myom3	Mouse Myomesin 3
N	Na^+	Sodium ion
	NaCl	Sodium chloride
	NAD^+	Oxidized form of nicotinamide adenine dinucleotide
	NADH	Reduced form of nicotinamide adenine dinucleotide
	NADPH	Reduced form of nicotinamide adenine dinucleotide phosphate
	$NaHCO_3$	Sodium bicarbonate
	NaH_2PO_4	Monosodium phosphate
	NaN_3	Sodium azide
	NCX	Na^+/Ca^{2+} exchanger
	NCX3	Na^+/Ca^{2+} exchanger isoform 3
	ND	Non-drug
	Nedd4-1	Neuronal precursor cell-expressed developmentally downregulated protein 4
	NFAT	Nuclear factor of activated T-cells
	NF-κβ	Nuclear factor kappa-light-chain-enhancer of activated B cells
	NIH	National Institutes of Health
	nM	Nanomolar
	nm	Nanometre
	NMJ	Neuromuscular junction
	NS	N-terminal addition sequence
	NS-shRNA	Non-sense shRNA
O	OCT	Optimal cutting temperature compound

	OCT3/4	Octamer-binding transcription factor 3 or 4 protein
	OD	Optical density
P	pAb	Polyclonal antibody
	Pax7	Mouse paired box transcription factor 7 gene
	PAX7	Human paired box transcription factor 7 gene
	PBS	Phosphate buffered saline
	PC1	Protease core 1
	PC2	Protease core 2
	PCR	Polymerase chain reaction
	PEF	Penta E-F hand domain
	PERK	PKR-like endoplasmic reticulum kinase
	PGC1α	Peroxisome proliferator activated receptor gamma coactivator 1 alpha
	pH	Potential of hydrogen
	PK	Pyruvate Kinase
	PKA	Protein kinase A
	PKR	Protein kinase R
	PLEIAD	Platform element for inhibition of autolytic degradation
	PLN	Phospholamban
	PMCA	Plasma membrane calcium ATPase
	Pnpla2	Rodent patatin like phospholipase domain containing 2 gene
	Ppargc	Rodent peroxisome proliferator-activated receptor gamma coactivator 1-alpha gene
	Prot.	Protein
	PTP	Permeability transmission pore
	PVDF	Polyvinylidene difluoride
Q	qPCR	Quantitative Polymerase chain reaction
R	R1	Recessive 1
	RNA	Ribonucleic acid
	ROS	Reactive oxygen species
	rpm	Revolutions per min
	RPS6A	Ribosomal protein S6
	RyR	Ryanodine receptor
	RyR1	Ryanodine receptor isoform 1
S	s	Seconds
	S1P	Site 1 protease
	S2P	Site 2 protease
	SC	Satellite cell
	SDS	Sodium Dodecyl Sulphate
	SEM	Standard error of the mean
	Ser	Serine
	SERCA	Sarco/endoplasmic reticulum Ca^{2+}-ATPase
	SERCA1	Sarco/endoplasmic reticulum Ca^{2+}-ATPase isoform 1
	SERCA2	Sarco/endoplasmic reticulum Ca^{2+}-ATPase isoform 2
	SERCA3	Sarco/endoplasmic reticulum Ca^{2+}-ATPase isoform 3

	SGM	Skeletal muscle growth medium
	shRNA	Small hairpin ribonucleic acid
	SLN	Sarcolipin
	SOD	Superoxide dismutase
	SOX2	Sex determining region Y-box 2
	sP	Specific force
	SR	Sarcoplasmic reticulum
T	TA	*Tibialis anterior*
	TBS	Tris-buffered saline
	Tgfb1	Rodent transforming growth factor beta-1 proprotein gene
	TRIM32	Tripartite motif 32
	T-tubule	Transverse tubule
U	U	Enzyme unit
	UB	Ubiquitin
	UCLA	University of California Los Ángeles
	UK	The United Kingdom
	UPR	Unfolded protein response
	UPS	Ubiquitin-proteasome system
	USA	The United States of America
V	ViVU	Viral vector unit
	V	Voltage
	vs.	Versus
W	WB	Western blot
	Wnt	Wingless-related integration site
	WT	Wild type
X	*XBP1*	Human X-box binding protein gene
	XBP1s	Human Spliced Xbp1 gene
	XBP1	X-box binding protein
	XBP1s	Spliced Xbp1

RESUMEN

Las distrofias musculares son un grupo de enfermedades de origen genético que causan debilidad muscular disminuyendo la movilidad y dificultando las actividades de la vida diaria. Dentro de este grupo, las distrofias de cinturas, también llamadas LGMD, forman un gran subgrupo heterogéneo de enfermedades caracterizadas por la debilidad proximal que afecta a la cintura escapular y pélvica. La forma más frecuente de distrofia de cinturas es la causada por mutaciones en el gen *CAPN3.* Esta enfermedad conocida previamente como LGMD2A ha sido recientemente renombrada como LGMDR1. A pesar de que comúnmente se ha considerado una enfermedad recesiva, los últimos hallazgos indican la existencia de una forma con un patrón hereditario dominante, que recibe la nomenclatura LGMDD4. Actualmente estas enfermedades carecen de tratamiento eficaz.

El gen *CAPN3* codifica la proteína calpaína 3 (CAPN3), una cisteín-proteasa no lisosomal necesaria para el correcto funcionamiento del músculo. Por el momento se desconoce en detalle la función principal de CAPN3 en el músculo esquelético y los mecanismos fisiopatológicos que subyacen en la enfermedad. Diversos estudios indican que la CAPN3 posee una función proteolítica y una función estructural. Esto podría explicar en parte las diferentes características fenotípicas de la enfermedad.

Los mecanismos fisiopatológicos de la enfermedad han sido estudiados mediante el uso de herramientas como las biopsias musculares de pacientes y los cultivos de mioblastos derivados de las mismas. Sin embargo, en la actualidad la disponibilidad de biopsias de pacientes con LGMDR1 para la investigación es muy limitada, ya que el diagnóstico de la enfermedad se realiza mediante estudios moleculares a partir de muestras sanguíneas. A ello habría que sumarle la baja capacidad de los mioblastos humanos para proliferar al aumentar el tiempo de cultivo, especialmente en el caso de las enfermedades neuromusculares. Por ello, la generación de nuevas herramientas como los modelos *in vitro* de mioblastos humanos inmortalizados o los modelos animales se ha hecho imprescindible para avanzar en el conocimiento de los mecanismos fisiopatológicos de estas enfermedades.

En el presente proyecto nos hemos centrado en la alteración de la homeostasis del calcio como mecanismo patogénico de LGMDR1. Así, hemos caracterizado varios modelos *in vitro* generados a partir de mioblastos humanos inmortalizados. Por un lado, hemos empleado dos muestras de donantes sanos en los que hemos silenciado la expresión de *CAPN3* mediante partículas lentivirales portadores de una pequeña

molécula de ARN interferente (shRNA). Por otro lado, hemos empleado mioblastos humanos inmortalizados procedentes de dos pacientes de LGMDR1 con diferentes mutaciones en el gen *CAPN3.* De este modo, los miotubos de pacientes nos han permitido estudiar diferentes escenarios debido a la naturaleza de las mutaciones en *CAPN3*, ya que una de las muestras expresa CAPN3 mientras que la otra prácticamente carece de CAPN3.

Los modelos *in vitro* de mioblastos silenciados han demostrado que la deficiencia de CAPN3 genera una reducción concomitante de los niveles de proteína SERCA1 y SERCA2, sin que su expresión génica se vea alterada. Esto, a su vez, afecta a la homeostasis del calcio, lo que resulta en una mayor concentración de calcio intracelular en estado basal en los miotubos distróficos. Por otro lado, los datos obtenidos de los miotubos derivados de pacientes LGMDR1 evidencian que la reducción de las proteínas SERCA1 y SERCA2 es más evidente cuando los niveles de CAPN3 están disminuidos. Esto sugiere que la función no proteolítica de CAPN3 juega un papel esencial en la estabilización de las proteínas SERCA. Por ello, planteamos la hipótesis de que la desregulación del calcio observada en LGMDR1 es en parte resultado de un déficit de SERCA, y proponemos que las proteínas SERCA pueden ser dianas terapéuticas para esta enfermedad.

El déficit de las proteínas SERCA, junto con la mayor ubiquitinación de SERCA1 y SERCA2 observada previamente en miotubos silenciados, sugiere que en los modelos deficientes en CAPN3 las proteínas SERCA se degradan anormalmente. Por ello, hemos utilizado el Bortezomib (BTZ), un inhibidor específico del proteosoma, como estrategia para evitar la degradación exacerbada de las proteínas SERCA que se produce en los modelos *in vitro* de LGMDR1. El BTZ ha sido aprobado por la Administración Estadounidense de Alimentos y Medicamentos (FDA) para el tratamiento del mieloma múltiple. Además, se ha utilizado en estudios preclínicos y clínicos de distrofias musculares como Duchenne y LGMDR2.

Hemos podido observar que el tratamiento con BTZ es capaz de normalizar la concentración de calcio intracelular basal que se encuentra aumentada en los miotubos deficientes en CAPN3. Además, el BTZ aumenta los niveles de proteína SERCA2 en los miotubos distróficos, aunque no parece afectar a los niveles de SERCA1. Hemos descubierto que el BTZ también aumenta los niveles de la proteína CAPN3 en miotubos de pacientes con LGMDR1. Reforzando este resultado, previamente se ha observado un efecto similar en modelos animales de distrofia muscular de Duchenne, con mutaciones puntuales en el gen *Dmd* que codifica la proteína distrofina. En estos modelos se ha demostrado que el tratamiento con BTZ aumenta los niveles de la distrofina mutada en las fibras musculares, recuperando parcialmente su función estructural. Esto indica que en los pacientes con LGMDR1 el BTZ podría rescatar las deficiencias tanto de SERCA2 como de CAPN3 en las fibras musculares. Cabe mencionar, además, que el tratamiento con BTZ aumenta la expresión génica de marcadores de estrés del retículo y la respuesta a las proteínas mal plegadas en los miotubos silenciados, al mismo tiempo que aumenta la expresión génica de la proteína anti-apoptótica c-FLIP. A pesar de ello, los miotubos tratados con BTZ durante 24h no muestran cambios morfológicos en comparación con los miotubos controles.

Los modelos animales son una herramienta esencial para el estudio de la fisiopatología de diferentes enfermedades. En concreto, se han generado diversos modelos animales de LGMDR1, entre los que se destaca el ratón *knockout* para *CAPN3*, C3KO, que ha sido generado por el grupo de la Dra. Spencer y es actualmente uno de los más utilizados en el campo. La caracterización de este modelo indica un fenotipo distrófico leve, junto con alteraciones mitocondriales y desregulación de la homeostasis del calcio.

En el presente trabajo hemos ampliado la caracterización del fenotipo distrófico en ratones C3KO de 2 meses de edad, los cuales se encuentran en un estadio pre-sintomático de la enfermedad. Estos ratones presentan niveles reducidos de la proteína SERCA1 en el músculo sóleo y niveles reducidos de proteína SERCA1 y SERCA2 en el diafragma. También se encontraron déficits de SERCA2 en los mismos músculos de ratones C3KO de 9 meses, mientras que en esta edad las alteraciones de SERCA1 no fueron evidentes. A su vez, hemos observado que los ratones C3KO tienen una tendencia a aumentar la expresión de *Ppargc,* un regulador principal de la biogénesis mitocondrial, y *Tgfb1*, una citoquina inflamatoria capaz de inhibir la miogénesis. Interesantemente, el tratamiento con BTZ parece revertir los aumentos observados en la expresión de estos genes. No obstante, la posología de BTZ empleada en este trabajo (0.8mg/kg cada 3,5 días) no ha mostrado ningún efecto sobre la actividad del proteasoma en el músculo, ni tampoco se observó un efecto claro sobre los niveles de las proteínas SERCA1 y SERCA2. En cualquier caso, no se han observado diferencias relevantes entre los ratones C3KO y los ratones control respecto al área transversal de las fibras o la distribución de éstas, la capacidad de ejercicio voluntario, ni tampoco respecto al porcentaje de fibras con núcleos centrales. A su vez, estos fenómenos no parecen verse afectados por el tratamiento con BTZ.

Debido al fenotipo leve de los ratones C3KO, decidimos analizar la eficacia del BTZ en el modelo de rata de LGMDR1, un modelo *knockout* de *Capn3*, *C3 null*, generado recientemente por el grupo de la Dra. Richard, que muestra un fenotipo más grave. En primer lugar, hemos analizado los niveles de las proteínas SERCA1 y SERCA2, y observamos que los niveles de ambas proteínas están reducidos en el diafragma de ratas jóvenes *C3 null*, comparadas con las ratas control. En edades más adultas, a los 6 meses de edad, las ratas *C3 null* muestran menor fuerza de agarre en las patas delanteras respecto a las ratas controles. Además, las ratas *C3 null* muestran un aumento evidente de marcadores de daño muscular como son el incremento observado en la actividad Creatina Quinasa (CK, de sus siglas en inglés) del suero, y el mayor porcentaje de fibras con núcleos centrales, que alcanza el 8%, respecto al 4% observado en ratas controles. Por contra, no se han observado diferencias en el área transversal de las fibras ni en la proporción de fibras rápidas y lentas.

De acuerdo a las características moleculares, observamos que los genes que hacen que las fibras sean de fenotipo lento no muestran cambios en su expresión, o se incrementaron ligeramente en las ratas *C3 null*, como en el caso de *Pnpla2, Lpl* o *Myo18b*. A su vez, la sobreexpresión de *Tgfb1* y *Mmp9* observada en las ratas *C3 null* puede ser indicativa de una mayor inflamación y fibrosis en estos animales. Finalmente, mientras que los niveles de SERCA2 están reducidos en los diafragmas de las ratas distróficas, encontramos un aumento en los niveles de SERCA1 en el sóleo de estas ratas. Estos resultados concuerdan con la actividad de SERCA observada en estos músculos.

En las ratas el tratamiento con BTZ se ajustó a 0,2mg/kg cada 3,5 días, teniendo en cuenta estudios previos y el volumen corporal de las ratas. Sin embargo, en vista de la pérdida de peso observada en los animales tratados con BTZ, que es indicativa de una posible toxicidad, la dosis tuvo que reducirse aún más a 0,15mg/kg. Si bien el tratamiento con BTZ parece mejorar la fuerza de agarre de las ratas *C3 null*, cuando se normalizan los valores con el peso corporal, este resultado es difícil de interpretar dado que los animales tratados con BTZ mostraron una pérdida de peso significativa durante el estudio. En cualquier caso, el tratamiento no empeora los valores de actividad CK sérica, la nucleación central o la fuerza de agarre. Tampoco hay cambios importantes en el área transversal de las fibras, o en la proporción de fibras rápidas y lentas. Sin embargo, el tratamiento con BTZ parece normalizar la expresión de genes relacionados con el programa miogénico de fibras lentas, al igual que reduce la expresión de genes relacionados con la fibrosis como *Tgfb1* y *Mmp9.* Finalmente, no se han observado cambios tras el tratamiento con BTZ respecto a los niveles de las proteínas SERCA1 o SERCA2.

En conclusión, las deficiencias en CAPN3 pueden dar lugar a niveles reducidos de proteínas SERCA, lo que resulta en una alteración de la homeostasis del calcio. El tratamiento con BTZ constituye una estrategia terapéutica para la recuperación de SERCA que repercute en la homeostasis del calcio. Los estudios *in vitro* realizados demuestran la eficacia del BTZ para recuperar la expresión proteica de SERCA2 y los niveles de calcio citosólico. Estos estudios han revelado además el potencial del BTZ para recuperar la expresión de la CAPN3 mutada, recuperando parcialmente su función estructural, en miotubos de pacientes con ciertas mutaciones puntuales en el gen *CAPN3.* Los estudios *in* vivo desarrollados en los modelos múridos C3KO y *C3 null* no han resultado concluyentes en cuanto a la eficacia del tratamiento de BTZ para recuperar los niveles de proteínas SERCA, probablemente debido a que no se ha alcanzado la posología óptima de BTZ en ninguno de los dos modelos. A su vez, el fenotipo leve que presenta el ratón C3KO dificulta el ensayo de fármacos en este modelo. Por el contrario, las ratas *C3 null* presentan un fenotipo distrófico más severo, por lo que en principio sería un modelo más adecuado para el ensayo de fármacos que el ratón C3KO. Desafortunadamente, las ratas son más susceptibles a la toxicidad generada por BTZ, por lo que el modelo de rata de LGMDR1 no sería el más apropiado para testar la eficacia de este tratamiento. En cualquier caso, nuestros resultados apoyan a SERCA2 como diana terapéutica prometedora para las terapias frente a LGMDR1, dado que los niveles de esta proteína están reducidos en los modelos celulares y animales de esta enfermedad, así como en pacientes con LGMDR1. Asimismo, nuestros resultados indican que el tratamiento con BTZ también puede aumentar los niveles de la proteína CAPN3 mutada en algunos pacientes LGMDR1 portadores de mutaciones puntuales, recuperando parcialmente su función estructural. En el futuro, los estudios deberían estar dirigidos hacia la generación de nuevos modelos animales de LGMDR1 con mutaciones de CAPN3 similares a las humanas y un fenotipo distrófico más similar al observado en los pacientes con LGMDR1. Estos modelos también ayudarían a comprender los mecanismos fisiopatológicos subyacentes a esta enfermedad y permitirían avanzar en el desarrollo de nuevas terapias para LGMDR1.

SUMMARY

Muscular dystrophies are a group of genetic diseases that cause muscle weakness, reducing mobility and making daily live activities challenging. Within this group, limb-girdle muscular dystrophies or LGMDs comprise a large heterogeneous subgroup of diseases characterized by proximal weakness of shoulder and pelvic girdle muscles. LGMDR1, previously known as LGMD2A, is the most common form of limb-girdle dystrophy and is caused by mutations in the *CAPN3* gene. This disease has been considered a strictly recessive illness; however, recent studies have reported different mutations with a dominant inheritance pattern, categorizing them as LGMDD4. Currently, there is no effective treatment for these diseases.

CAPN3 gene encodes calpain 3 protein (CAPN3), a non-lysosomal cysteine protease necessary for proper muscle function. The main function of CAPN3 in skeletal muscle and the pathophysiological mechanisms underlying the disease remain to be clarified. However, previous studies indicate that CAPN3 has both proteolytic and structural functions. This may partly explain the different phenotypic characteristics of this disorder.

The pathophysiological mechanisms of the disease have been mainly studied using muscle biopsies from patients and myoblast cultures obtained from them. However, nowadays availability of LGMDR1 muscle biopsies for research is greatly diminished due to the fact that diagnosis is currently performed through molecular studies from blood samples. It must also be considered the low proliferation capability of human myoblasts in long-term cultures, and in particular, when myoblasts are derived from patients with neuromuscular diseases. For these reasons, the generation of new tools such as immortalized human *in vitro* models or animal models has become essential to gain further insight into the pathophysiological mechanisms of these diseases.

The present study focuses on the dysregulation of calcium homeostasis as a pathogenic mechanism of LGMDR1. We have characterized several *in vitro* models generated from immortalized human myoblasts. First, we have generated a novel LGMDR1 *in vitro* model by silencing *CAPN3* expression in myoblasts from two healthy donors with lentiviral particles carrying a small hairpin RNA. On the other hand, we have used immortalized human myoblasts from two LGMDR1 patients carrying different mutations in the *CAPN3* gene. The nature of the different *CAPN3* mutations in these patients has allowed us to study different scenarios in LGMDR1

illness since one of the samples expresses CAPN3 whereas in the other sample CAPN3 is virtually absent.

Silenced myoblast *in vitro* models have shown that CAPN3 deficiency generates a concomitant reduction of SERCA1 and SERCA2 protein levels, with no modification in gene expression. This, in turn, affects calcium homeostasis, resulting in a higher concentration of basal cytosolic calcium in dystrophic myotubes. On the other hand, data obtained from LGMDR1 myotubes show that the reduction of SERCA1 and SERCA2 protein levels is more evident when CAPN3 levels are greatly diminished, suggesting that the non-proteolytic CAPN3 function plays an essential role in stabilizing SERCAs. Hence, we hypothesize that calcium dysregulation observed in LGMDR1 is partly a result of SERCA deficiency, and we propose SERCAs as therapeutic targets for this disease.

The deficit in SERCA proteins, together with the higher ubiquitination levels previously found in SERCA1 and SERCA2 proteins observed in CAPN3 knockdown myotubes, suggest that in CAPN3-deficient models SERCA proteins are abnormally degraded. Therefore, we have used Bortezomib (BTZ), a specific proteasome inhibitor, as a strategy to prevent the exacerbated degradation of SERCA proteins occurring in LGMDR1 models. BTZ has been approved by the American Food and Drug Administration (FDA) for the treatment of multiple myeloma. In addition, it has been used in preclinical and clinical studies of muscular dystrophies such as in Duchenne and LGMDR2.

We have found that BTZ treatment is able to normalize basal intracellular calcium levels that are increased in CAPN3 knockdown myotubes. Moreover, BTZ increases SERCA2 protein levels in dystrophic myotubes but does not seem to affect SERCA1 levels. Interestingly, we have also found that BTZ increases CAPN3 protein levels in myotubes from LGMDR1 patients. A similar effect has been previously observed in Duchenne muscular dystrophy animal models carrying missense mutations in the *Dmd* gene, where BTZ has been shown to increase mutated dystrophin protein levels in the muscle fibres, recovering partially its structural function. This indicates that BTZ could target CAPN3 as well as SERCA2 deficiencies in LGMDR1 patients. Remarkably, we also found that BTZ treatment increases the expression of sarcoplasmic reticulum stress and unfolded protein response markers in myotubes, while also increasing *c-FLIP* mRNA levels, which encodes a major antiapoptotic protein. All in all, myotubes treated with BTZ for 24 hours did not show morphological alterations compared to control myotubes.

Animal models are essential tools to study the pathophysiology of different diseases. Specifically, several animal models of LGMDR1 have been generated, though the murine CAPN3 knockout model generated by Dr Spencer's group, C3KO, is currently one of the most commonly used in the field. Previous studies characterizing this C3KO mouse model report a mild dystrophic phenotype, together with alterations in mitochondria, and calcium dysregulation.

In this study, we have performed a thorough characterization of the C3KO phenotype in 2-month-old mice, which are at an early pre-symptomatic stage of the disease. These mice show reduced SERCA1 protein levels in the *soleus* muscle, and reduced SERCA1 and SERCA2 levels in the diaphragm. SERCA2 deficits were also found in older C3KO mice, while no clear changes in SERCA1 levels were observed. We have also found that C3KO mice have a tendency to increased expression of *Ppargc*, a master regulator of mitochondrial biogenesis, and *Tgfb1*, an inflammatory cytokine that represses muscle growth. Interestingly, BTZ treatment seemed to revert increases observed in the expression of these genes. However, BTZ treatment used in this study (0.8 mg/kg every 3.5 days) did not show any effect on the ubiquitin-proteasome activity in the muscles analysed, neither it showed a clear effect on SERCA1 and SERCA2 protein levels. In any case, we did not find any obvious difference between C3KO and control mice in myofibre area and distribution, voluntary exercise, or percentage of centrally nucleated myofibres, nor did we find any apparent difference in these outcomes with BTZ treatment.

Due to the mild phenotype of C3KO mice, we decided to test the efficacy of BTZ in *C3 null* rats, a CAPN3 knockout model recently developed by the group of Dr Richard, reported to display a more severe phenotype. First, we have analysed SERCA1 and SERCA2 protein levels and found that both proteins are indeed reduced in the diaphragms of adult *C3 null* rats compared to controls. Six-month-old rats show lower forelimb grip strength compared to controls and markers of muscle damage are apparent in *C3 null* rats, such as increased serum creatin kinase (CK) activity, and higher percentage of centrally nucleated myofibres, 8% vs. 4% in control animals. However, no differences in the cross-sectional area or in the ratio fast / slow myofibres have been observed. According to their molecular characteristics, genes related to the slow myogenic program show no change or were slightly increased in

C3 null rats, such as *Pnpla2, Lpl* or *Myo18b*. Likewise, upregulation of *Tgfb1* and *Mmp9* observed in *C3 null* rats may be indicative of a higher inflammation and fibrosis in these animals. Finally, we have found contrary trends in diaphragm and *soleus* muscles regarding SERCA proteins. While SERCA2 levels are reduced in *C3 null* diaphragms, we find an increase in SERCA1 levels in the *soleus*. These results are concordant with the SERCA activity values present in these muscles.

In rats, BTZ dosing was adjusted to 0.2mg/kg every 3.5 days, taking into account their body volume and previous reports. However, as BTZ-treated animals lost weight, indicative of potential toxicity, BTZ dose had to be further lowered to 0.15mg/kg. While BTZ treatment of *C3 null* rats seems to improve grip strength when normalized to body weight, this result is difficult to interpret given that BTZ-treated animals had significant weight loss. In any case, BTZ treatment does not seem to worsen serum CK activity, central nucleation or grip strength. There are also no major changes in myofibre mean cross-sectional areas, or in the ratio fast / slow myofibres. BTZ treatment appears to normalize the expression of genes related to the slow myogenic program, and also to reduce fibrosis-related genes such as *Tgfb1* and *Mmp9*. Finally, no changes in SERCA1 or SERCA2 protein levels are observed after BTZ treatment.

In conclusion, CAPN3 deficiency leads to reduced SERCA protein levels, which results in abnormal calcium homeostasis. Treatment with BTZ constitutes a therapeutic strategy for the recovery of SERCA, affecting calcium homeostasis. *In vitro* studies have demonstrated the efficacy of BTZ in recovering SERCA2 protein levels and intracellular calcium levels. Most interestingly, these studies have further revealed BTZ potential to recover CAPN3 mutated protein, recovering its structural function, in patients with missense mutations in the *CAPN3* gene. *In vivo* studies performed in mouse and rat models of LGMDR1 have proved inconclusive, in terms of the efficacy of BTZ, in rescuing SERCA levels, due to the fact that optimal doses were not reached in any of the models. Furthermore, the extremely mild phenotype of the C3KO mouse model makes testing drug efficacy very challenging. In contrast, *C3 null* rats display a more apparent dystrophic phenotype, and thus, it seems to be a more suitable model of LGMDR1 to test the efficacy of potential therapies. Unfortunately, rats are also more susceptible to BTZ toxicity, and therefore *C3 null* rats are not appropriate for testing BTZ efficacy. In any case, our results support SERCA2 as a promising molecular target for LGMDR1 therapies, given that this

protein is reduced in cellular and animal LGMDR1models, as well as in LGMDR1 patients. Our results further indicate that BTZ may also increase CAPN3 levels in some LGMDR1 patients carrying missense mutations. Further studies should focus on the generation of new animal models with human-like *CAPN3* mutations, giving rise to more similar dystrophic phenotype as the observed in human patients. These models would also pave the way to a better understanding of the different pathophysiological mechanisms underlying this disease and move forward towards the development of new therapies for LGMDR1.

INTRODUCTION

Muscle tissue - Skeletal muscle

Muscle tissue is one of the most relevant/important tissues in the body, characterized by allowing movement of internal organs as well as the skeleton. It is a very complex tissue containing many different cell types and well supplied with blood vessels. This tissue is elastic and excitable, generating cell contraction after receiving stimuli from the nervous system. Depending on the structure and the function, this tissue can be classified in 3 types: smooth muscle (non-striated and involuntary), cardiac muscle (striated and involuntary) and skeletal muscle (striated and voluntary) [1],[2].

Skeletal muscle, the higher representative muscle tissue, is attached to bones by tendons and, under the voluntary control of the nervous system, triggers the movement of the skeleton, being essential for breathing and whole-body metabolism. Its mass depends on the balance between protein synthesis and degradation, which can be modulated by different mechanisms as nutrition, hormones, physical activity, injury or disease [3].

Skeletal muscle is a tissue integrated by various cell types, including skeletal muscle fibres, blood vessels, nerve fibres, and connective tissue, among others [4]. The organization of this tissue is well defined and organized, based on assembling long, cylindrical, multinucleated myofibres in fascicles. Each structure within the skeletal muscle is covered by different layers of connective tissue. Muscle fibres are surrounded by a layer called *endomysium*, while fascicles are covered by the *perimysium*. These fascicles are grouped forming skeletal muscle, which is protected by the *epimysium*, the outer layer of connective tissue in skeletal muscles [3] (Figure 1).

Skeletal muscle has a robust regenerative capacity that is tightly regulated by specific transcription factors. This process is supported by the satellite cells (SC), a pool of undifferentiated resident myogenic stem cells, which supply myoblasts for both muscle homeostasis and repair [5]. SCs are characterized by the expression of *paired box transcription factor 7* (*Pax7*), which controls the activation of the myogenic program, by regulating myogenic regulatory factors (MRFs) [5]. Once SCs get activated, they enter the cell cycle proliferating and expanding the myogenic population. Proliferative myogenic cells are known as myoblasts and they express determination protein 1 (MYOD) and myogenic factor 5 (MYF5), although MYF5 can be expressed by quiescent SCs as well. Up-regulation of secondary MRFs such as myogenin (MYOG) and MRF4 induces terminal differentiation of myoblasts into myocytes, that eventually fuse to form myotubes that express myosin heavy chain (MyHC) [5]–[7].

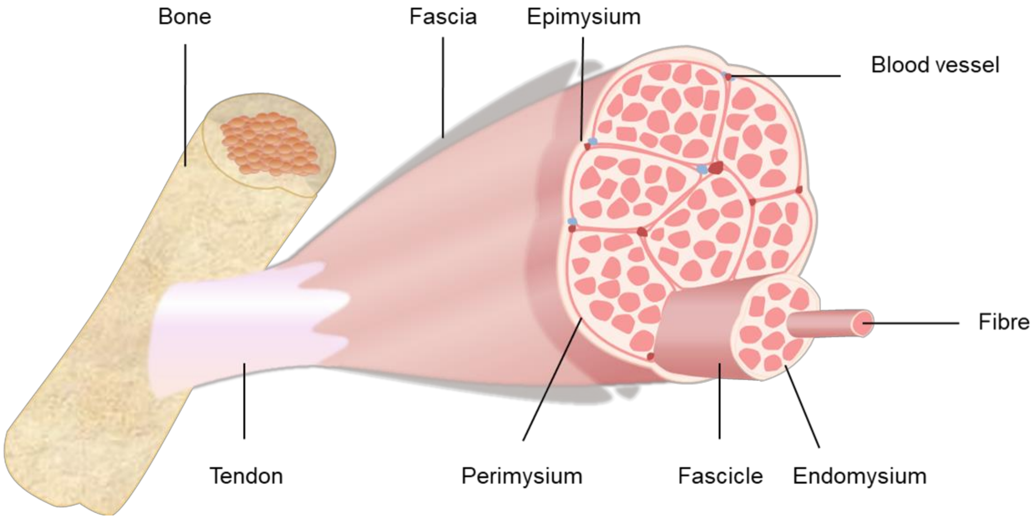

Figure 1. Representation of the skeletal muscle structure. Different fascicles are surrounded by the epimysium. Each fascicle is covered by the endomysium and fascicles are formed by myofibres that are surrounded by the endomysium.

Muscle fibre o myofibre is the functional unit of the skeletal muscle, which is a multinucleated structure, built by fusion of myoblasts and covered by a membrane called sarcolemma. Myofibres are composed of myofibrils, which are mainly formed by thick myosin filaments and thin actin filaments. These myofibrils are organized creating the contractile unit of the myofibre, the sarcomere [8]. Besides myosin and actin, other proteins are present at the sarcomere contributing to its structure, excitation-contraction coupling process, energy release and force generation [3].

Sarcomeres have very defined organization due to the distribution of actin and myosin filaments, as they generate cross-bridges leading to a repetitive specific pattern of transversal bands. I-bands are the regions where only actin is present. These bands are divided by Z-dishes, where actin filaments of two consecutive sarcomeres join together. On the other hand, A-bands are regions where myosin filaments overlap with actin. In these bands, it is possible to distinguish a region where only myosin is present, the H-bands. In the middle of those bands, M-lines are found, where myosin filaments come together [9] (Figure 2). Noteworthily, sarcomeres are linked to the sarcolemma by some protein complexes associated with Z-line, called costameres. These characteristic structures are composed by different protein complexes, as the dystrophin-glycoprotein complex and the integrin–vinculin–talin complex, and have important roles in force transmission from the sarcomere to the sarcolemma and extracellular matrix [10].

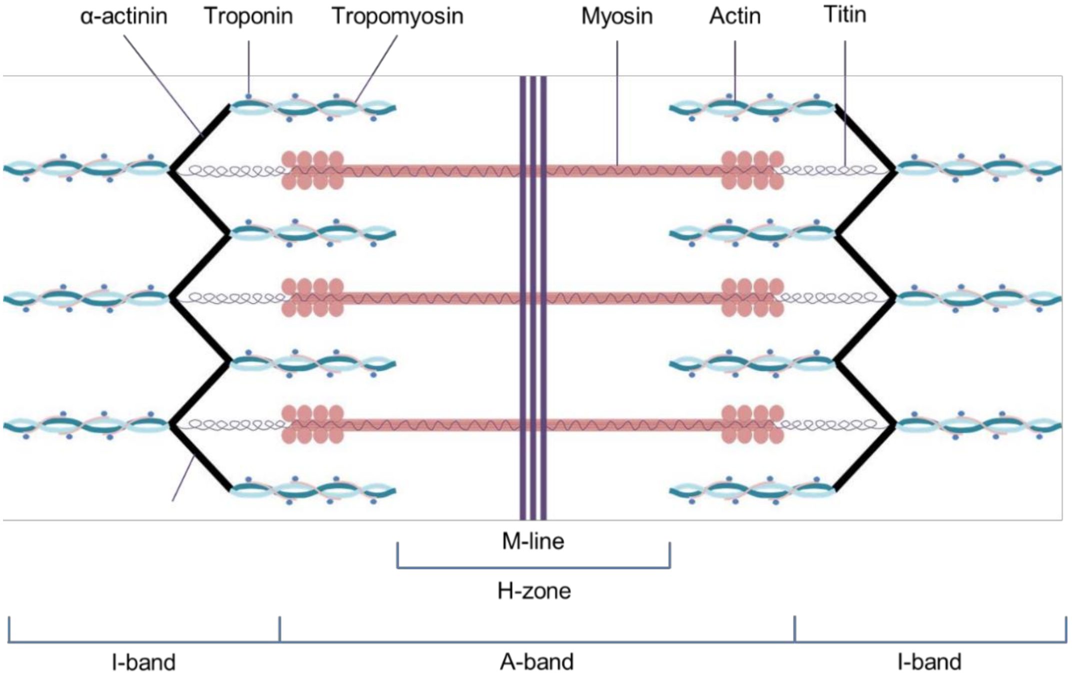

Figure 2. Representation of the sarcomere structure. Schematic representation of the sarcomere, showing the protein composition of different bands.

The contraction of the sarcomere is produced by the cross-bridge between actin and myosin, and it requires ATP consumption. This interaction is modulated by troponin and tropomyosin. Troponin is able to change its conformation in presence of calcium (Ca^{2+}) producing tropomyosin movement and letting myosin bind to actin. This interaction triggers muscle contraction [11]. In addition to the sarcomere, other components in the muscle fibre are required to reach muscle contraction. On one hand, the energy required for this process is supplied by mitochondria, which are distributed between myofibrils. On the other hand, the nuclei, which are located right below the sarcolemma in the periphery of the myofibre, contain the genetic information for the production of large amounts of proteins and enzymes needed for contraction (Figure 3).

The sarcolemma and sarcoplasmic reticulum (SR) also play important roles in the contraction process. The sarcolemma has specialized regions called neuromuscular junctions (NMJ) where a motor neuron's (MN) terminal meets the muscle fibre. The releasement of acetylcholine (Ach) by these MNs generates sarcolemma depolarization, which propagates along the sarcolemma reaching transverse-tubules (T-tubule). These membrane invaginations ensure that the membrane can get close to the SR to trigger the release of Ca^{2+} from SR. A T-tubule with the membranes of SR on both sides integrates a very specialized structure called triad, critical for the excitation – contraction coupling process [12],[13].

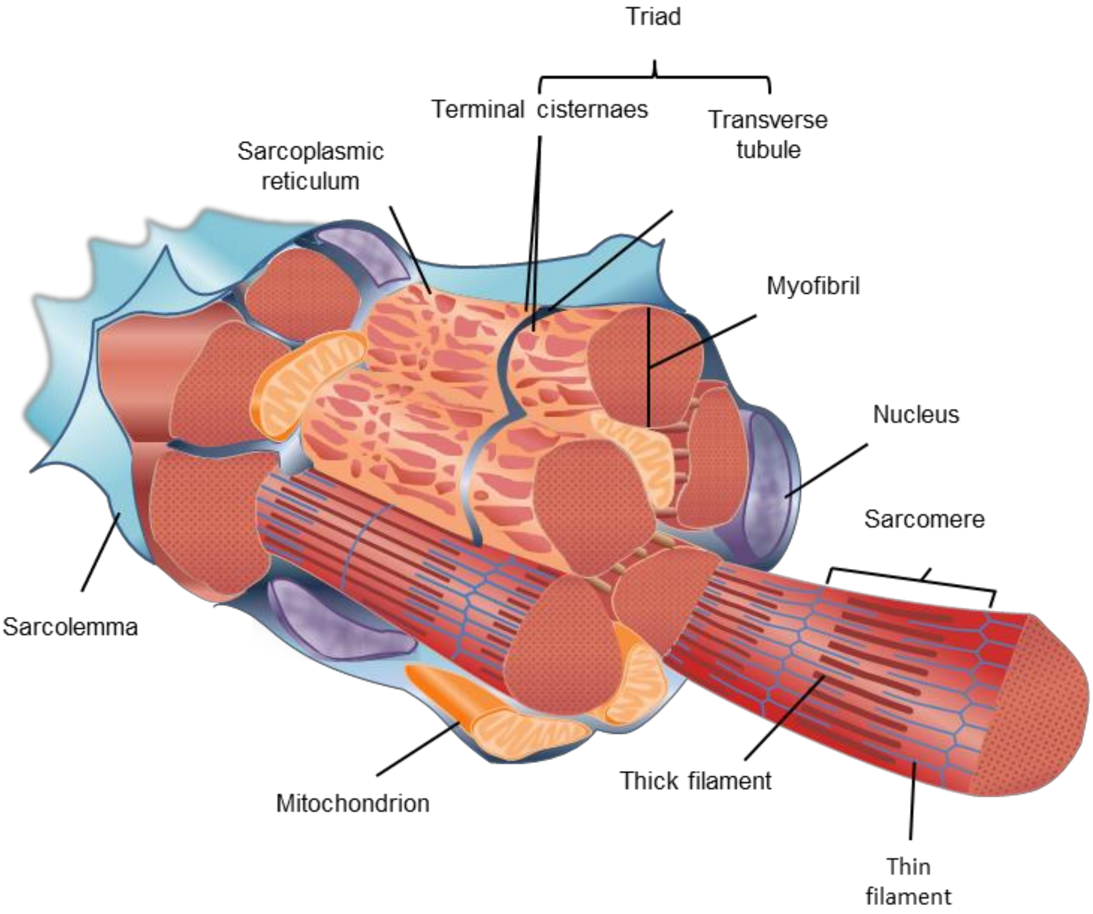

Figure 3. Representation of the muscle fibre. Sarcolemma is the membrane surrounding the myofibre were different organelles like mitochondria, nucleus and sarcoplasmic reticulum (SR) can be found around the myofibrils. Each myofibril is formed by organised thick (myosin) and thin (actin) filaments creating sarcomeres. Finally, the invaginations of the sarcolemma and the terminal cisternae from SR integrate the triad.

Muscle fibres are broadly classified as slow (type I) and fast (type II) fibres. This classification is based on their movement rate, response to neural inputs and metabolic style. Regarding their myosin heavy chain (MyHC) expression, fast fibres can be subclassified as IIA, IIX or IIB, being type IIB the fastest ones. Their energy production is also different. Type I and IIA fibres primarily use oxidative metabolism while type IIX and IIB are more glycolytic [14]. IIB fibre type has been probably lost in large mammals in accordance with energy conservation. Therefore, in normal adult human skeletal muscle, type I, IIA, and IIX fibres predominate, but vary with functional differences in individual muscles [15].

In mammalian skeletal muscles, a single muscle group can be made by multiple fibre types and their proportions can be variable. These proportions are plastic and fibres have the ability to remodel their phenotypes to help muscles to adapt to different uses. Remarkably, there are many inherited myopathies and other acquired muscle-related disorders that preferentially affect specific skeletal muscle fibre types [14]. For instance, in sarcopenia and in muscle dystrophies such as Duchenne Muscular Dystrophy (DMD), fast to slow muscular transition occurs [16]–[18] whereas, in limb-girdle muscular dystrophy type R1 (LGMDR1) slow fibres are preferentially affected [19].

Calcium homeostasis in skeletal muscle

Calcium (Ca^{2+}) plays a vital role in a wide range of cellular processes such as gene transcription, membrane resealing, secretion, neurotransmission, as well as cell differentiation, proliferation, or survival [20],[21]. In skeletal muscle fibres, Ca^{2+} is crucial for both, electric activation along the motor endplate and skeletal muscle contraction. In addition, Ca^{2+} is involved in many other functions such as protein synthesis, protein degradation, fibre type shifting, Ca^{2+}-regulated proteolysis, transcription factor modulation, mitochondrial adaptation, cell plasticity and respiration [22]. In skeletal muscle, changes in cytosolic Ca^{2+} levels are particularly frequent and diverse, and therefore, tight regulation of Ca^{2+} levels is essential in this tissue (Figure 4).

Muscle contraction

Muscle contraction initiates upon Ach release from the MNs in the NMJ, which trigger sarcolemma depolarization. The action potential propagates into the triads, which play an essential role in excitation-contraction coupling (ECC). Membrane depolarization activates dihydropyridine receptors (DHPRs) in the T-tubules, generating a conformational change, which results in activation of the closely apposed ryanodine receptors (RyRs) [23]. RyR1 is the predominant RyR isoform in skeletal muscle, being the main Ca^{2+} release channels in the SR [24]. Either activation by DHPRs or increased cytosolic Ca^{2+} levels can trigger Ca^{2+} release from the SR into the cytosol [25]. RyR1 function can be modulated by post-translational modifications, such as S-nitrosylation, S-glutathionylation, and phosphorylation by both, Protein Kinase A (PKA) and Ca^{2+}/calmodulin-dependent protein kinase II (CaMKII) [26] (Figure 4).

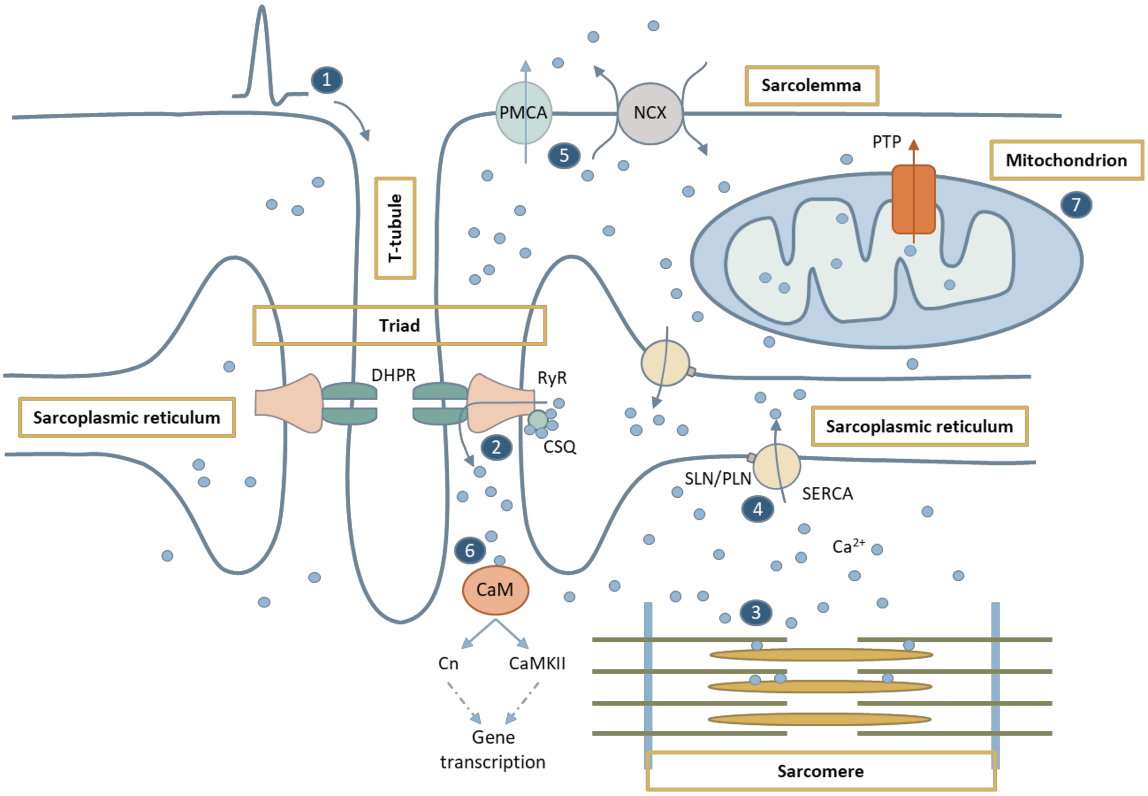

Figure 4. Representation of Ca^{2+} fluxes in the muscle fibre. Upon sarcolemmal depolarization reaching T-tubules, DHPRs undergo a conformational change that activates RyR1 channels and results in Ca^{2+} release from the SR (sarcoplasmic reticulum). Ca^{2+} diffuses to the sarcomere where it initiates muscle contraction. Muscle relaxation takes place when Ca^{2+} is sequestered into the SR by SERCAs or pumped out from the myofibre by membrane channels (NCX, PMCA). Cytosolic Ca^{2+} also binds calmodulin (CaM), which activates Ca^{2+}-dependent signalling pathways resulting in muscle gene regulation. Cytosolic Ca^{2+} also reaches mitochondria, where it stimulates metabolism and ATP synthesis required for muscle contraction and relaxation [27].

In order to maintain the balance between Ca^{2+} release, Ca^{2+} storage, and Ca^{2+} reuptake, RyRs operate in coordination with other proteins [28]. Indeed, a variety of proteins and small molecules both, in the SR lumen and cytosol, are needed for this tight coordination [26]. On the cytosolic side, calmodulin (CaM), a Ca^{2+} sensor, has a dual effect on RyR1, functioning as an activator at low cytosolic Ca^{2+} levels and as an inhibitor at high cytosolic Ca^{2+} levels [29]. On the SR luminal side, calsequestrin (CSQ) forms a complex with junctin and triadin, which activates or inhibits RyR1 in a Ca^{2+}-dependent manner [30]. CSQ is the main Ca^{2+}-binding protein in the SR lumen, functioning as an endogenous regulator of Ca^{2+} fluxes and as a Ca^{2+} reservoir with a moderate affinity but high capacity to bind Ca^{2+} [31].

After Ca^{2+} release into the cytosol, Ca^{2+} binds to various cytosolic Ca^{2+} buffers, such as ATP and CaM, and it can also be up-taken by mitochondria. On the other hand, at the sarcomere, troponin C undergoes a Ca^{2+}-dependent conformational change that results in myosin and actin cross-bridge and consequently in muscle contraction [32]. Muscle relaxation initiates by lowering of cytosolic Ca^{2+} back to resting levels, which mainly relies on sarco/endoplasmic reticulum Ca^{2+} ATPase (SERCA) pumps [33], sarcolemmal Ca^{2+} transporters such as Na^{+}/Ca^{2+} exchangers (NCX1-3) and plasmalemmal Ca^{2+}-ATPase (PMCA) [22].

Sarcoplasmic Reticulum (SR)

The SR is a very specialized form of endoplasmic reticulum, which embraces myofibres. It works as Ca^{2+} storage and it includes Ca^{2+} release channels as well as Ca^{2+}-ATPase pumps for Ca^{2+} reuptake to achieve tuned control of the storing and the ECC.

RyR receptors

RyR receptors as well as IP3R (inositol 1,4,5-triphosphate receptors) are the main Ca^{2+} release channels in ER. The main isoform in skeletal muscle and therefore, the one in SR, is RyR1. Mutations in the gene coding for RyR1 underlie diseases such as central core disease and malignant hyperthermia. In both cases, an abnormal release of Ca^{2+} has been described [34],[35].

RyR is composed by four identical subunits and three domains can be distinguished: a luminal, a transmembrane and a cytoplasmic domain. At the triads, the luminal domain of RyR and DHPR are located very close to each other: an essential contact for the voltage-induced Ca^{2+} release performed by RyR1 [34]. Therefore, DHPR can modulate RyR activity. Moreover, various ions, small molecules and proteins as PKA, FKBP12, CaM, CaMKII, CSQ, triadin and junction can also regulate Ca^{2+} release through RyR1 [25].

SR Ca^{2+}-ATPase (SERCA) pumps

SERCA is the most abundant protein in SR. It belongs to the family of P-type ATPases, using the energy from the hydrolysis of ATP to move ions across a biological membrane. In case of SERCA, this energy is used to transport Ca^{2+} from the sarcoplasm to the SR against the gradient. [36]. Since SERCA pumps are major ATP consumers, they are strongly affected by changes in cell energetics and ATP supply [37].

SERCA is a single polypeptide chain formed by a transmembrane region and a cytoplasmic region which contains 3 domains: the nucleotide binding domain, the domain that gets phosphorylated with the phosphate from ATP, and the actuator domain that coordinates the phosphorylation [38].

SERCA pump isoforms are encoded by three genes, SERCA 1, 2, and 3, which are differentially expressed in muscle and determine SR Ca^{2+} dynamics by affecting the rate and amount of Ca^{2+} uptake, thus, affecting SR store and release of Ca^{2+} in muscle [36]. Between them, there is a 75-84% of homology, which suggests that there is almost no difference in their tertiary structure. Two of these genes (SERCA1 and SERCA2) have alternative splicing products. SERCA1a isoform is predominantly expressed in fast twitch skeletal muscle, whereas its alternative splicing product, SERCA1b, is expressed in neonatal skeletal muscle. Conversely, SERCA2a, which is the predominant isoform expressed in cardiac muscle, is expressed in relatively high levels in slow skeletal muscle, while SERCA2b, is expressed in smooth muscle. Finally, SERCA3 isoform appears to be ubiquitously expressed in low levels, having lower Ca^{2+} affinity than the other isoforms [33]

Regulation of SERCA pumps is performed by PLN, SLN, myoregulin (MLN) or Dwarf Open Reading Frame (DWORF) [39]–[42]. Previous studies suggest that PLN can modulate SERCA2 while MLN does it over SERCA1. On the other hand, SLN can regulate SERCA1 and SERCA2. Finally, DWORF has been proposed to regulate the 3 isoforms [33],[39]–[41]. The mechanism to modulate SERCA is also different for each regulator. It is known that PLN and SLN inhibit SERCA function in a Ca^{2+}-dependent manner. However, the mechanism for MLN and DWORF are still unknown, although it has been suggested that MLN inhibits SERCA while DWORF activates it. Further studies would be needed to understand their mechanism over SERCA [43]–[46]. On the other hand, post-transcriptional modifications such as N-glycosylation, S-glutathionylation, and phosphorylation can also regulate SERCA function[47].

SR stress

Apart from being one of the main Ca^{2+} storages in myotubes, SR has an essential function orchestrating the synthesis, folding, and structural maturation of cellular proteins. To accomplish these functions, different chaperons and enzymes are needed in SR, requiring high levels of Ca^{2+} for their proper activity [48]. By contrast, upon altered activity, unfolded proteins accumulate in SR generating unfolded protein response (UPR). Different physiological or pathological events, including alterations in Ca^{2+} levels, inflammatory challenges or oxidative stress may underlie the capacity for protein folding [49]. UPR involves transcriptional induction of SR chaperon proteins to increase the folding process to avoid aggregation, translational attenuation to reduce protein overload, and removal of misfolding proteins through degradation by the ubiquitin proteasome system (UPS) [50]. This answer is mediated by the SR transmebrane sensors: protein kinase R (PKR)-like endoplasmic reticulum kinase (PERK), inositol-requiring protein 1a (IRE1a) and activating transcription factor 6 (ATF6) [51]–[53] (Figure 5).

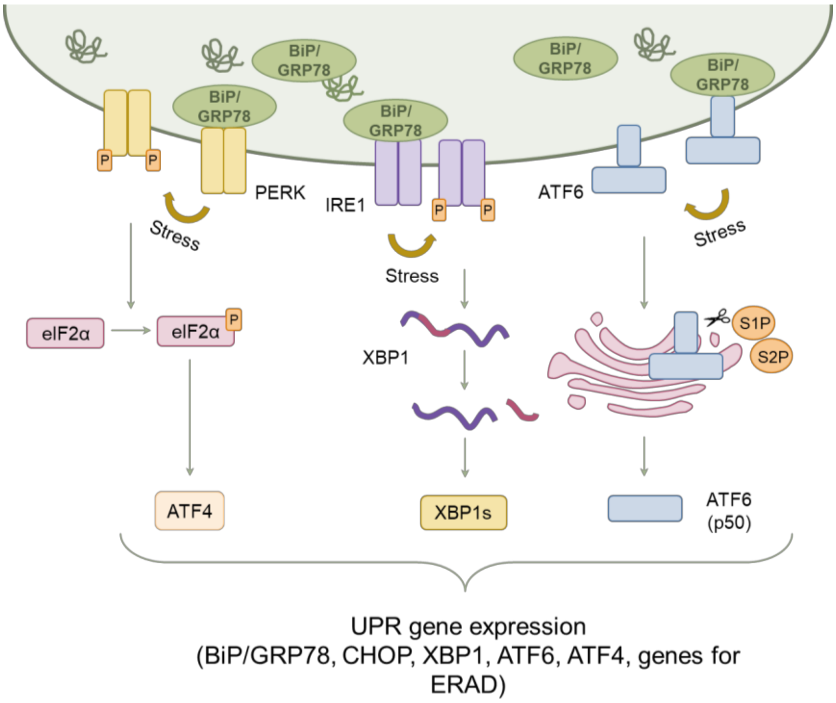

Figure 5. Schematic representation of UPR signalling pathways. Upon stress conditions, for instance ER (endoplasmic reticulum) Ca^{2+} decrease, unfolded proteins accumulate in the ER lumen, which triggers the dissociation of BiP/GRP78 from the three ER stress sensors, IRE1α, ATF6α and PERK. Therefore, these three sensors get active and, through different pathways, some transcription factors translocate to the nucleus to induce the expression of genes involved in protein folding, ER-associated degradation (ERAD), autophagy, and amino acid metabolism. Upon persistent ER stress, pro-apoptotic signalling is induced and the cell undergoes programmed cell death.

In normal state, one of the best-characterized ER chaperones, 78-kDa glucose-regulated protein GRP78, also referred as BiP, binds to these three proteins blocking their activity [54]. Nevertheless, upon SR stress, GRP78 binds unfolded proteins letting those stress sensors get active. As a result, the expression of CHOP, a transcriptional factor promoting apoptosis through down-regulation of pro-survival proteins, is increased [55]. On the other hand, splicing of a 26-base intron from X-Box

Binding Protein (XBP1) is promoted. *XBP1* spliced (*XBP1s*)-encoded proteins can translocate into the nucleus to induce the expression of ER-resident chaperones and ER-associated degradation (ERAD) components [56],[57], enabling misfolded proteins to be degraded by UPS or by autophagy-lysosomal system [58],[59]. Noteworthily, UPR is necessary to promote cell survival; however, chronic unmitigated SR stress can lead to death [51] (Figure 5).

Ca^{2+}-mediated signalling pathways

In addition to its key function in muscle contraction, Ca^{2+} has also a main role in the regulation of gene transcription. For instance, the transcriptional changes necessary for muscle adaptation upon different stimuli are mediated by Ca^{2+}-dependent signalling [60]. CaMK pathway and Calcineurin (Cn), a Ca^{2+}/CaM-dependent serine/threonine protein phosphatase, have crucial roles in many of these Ca^{2+}-mediated signalling processes. Cn stimulates the transcription of both NFAT and NF-κB targeted genes [61],[62]. While Cn/NFAT pathway responds preferentially to sustained and low-amplitude elevations of intracellular Ca^{2+}, high amplitude oscillations activate NF-κB [63]. NFAT signalling induces the slow gene program during muscle regeneration and maintains the slow fibre phenotype in the adult muscle tissue. On the other hand, NF-κB regulates the gene program for myoblast proliferation and differentiation [64],[65]. Remarkably, NF-κB can behave either as a booster or antagonist of apoptosis [66], depending on the stimulus nature.

CaMK pathway regulates contraction-induced Ca^{2+}-handling and mitochondrial biogenesis. It is also involved in the regulation of gene expression in skeletal muscle promoting the slow to fast fibre shift [67]. Moreover, during muscle development and adaptation, CaMK may activate crucial transcription factors as MEF2 (myocyte enhancer factor 2) [68]. The main CaMK isoform in skeletal muscle is CaMKII, which is involved in the maintenance of myofibre phenotype and muscle growth.[69],[70]. Additionally, CaMKII is one of the upstream activators of AMP-activated protein kinase (AMPK), an energy sensor that coordinates cell growth and autophagy, which consists in removing misfolded or aggregated proteins and clearing damaged organelles as a survival mechanism [71]. Furthermore, AMPK is able to regulate mitochondrial function and biogenesis. Under low intracellular ATP levels, AMPK promotes catabolic pathways to generate more ATP, and suppresses anabolic pathways, such as the high ATP consuming mTORC1 pathway, to inhibit cell growth [72].

Ca^{2+} in mitochondria

SR and mitochondria are the main Ca^{2+} storages [21]. Mitochondria account for about 15% of the cytosolic volume of muscle fibres,[73] and they are located close to the SR. In fact, there is a significant interplay between both organelles through the mitochondria-associated SR membrane (MAM), structure that is essential for cell physiology and Ca^{2+} homeostasis [74].

Ca^{2+} has several functions related to mitochondria. For instance, it regulates mitochondrial metabolism, biogenesis, motility, distribution, and plasticity [75]–[77]. Likewise, mitochondria can affect intracellular Ca^{2+} levels. ECC triggers transient Ca^{2+} increases in the mitochondrial matrix, which promotes mitochondrial metabolism and ATP synthesis. The last is required to supply the necessary ATP for actomyosin cross-bridge cycling and SERCA pumps during contraction and relaxation, respectively [78]. Alternatively, Ca^{2+} overload in the mitochondria may induce the opening of permeability transient pores (PTP), that results in a massive release of Ca^{2+} and pro-apoptotic factors such as cytochrome C (Cyt-c) into the cytosol, which in turn, activate caspase 9 and initiate the apoptotic program [79],[80]. Regarding mitochondrial biogenesis, Ca^{2+} is involved in its regulation through modulation of the CaMKII pathway. Indeed, Ca^{2+}-mediated activation of CaMKII is in charge of the expression of peroxisome proliferator-activated receptor gamma coactivator 1 alpha (PGC1α), a key regulator of mitochondrial biogenesis [81]. Lastly, mitochondrial motility also relies on cytosolic [Ca^{2+}]. Indeed, myosin-Va, a Ca^{2+} sensor molecule, regulates mitochondria-bound molecular motors allowing mitochondrial movement along cytoskeletal fibres, and controlling mitochondria distribution to enhance Ca^{2+} buffering and ATP production in regions with high cytosolic [Ca^{2+}] [77].

Limb-Girdle Muscle Dystrophy type R1

Limb girdle muscle dystrophy recessive 1 (LGMDR1), or calpainopathy, is caused by mutations in the *CAPN3* gene encoding for the proteolytic enzyme calpain 3 (CAPN3) [82]. This disease is characterized by a slow progressive muscular weakness that affects both scapular and pelvic girdles, as well as proximal lower limb muscles [83]–[85]. Despite it has been described to present an autosomal recessive inheritance pattern, recently, heterozygous mutations in the *CAPN3* gene have been reported to cause autosomal dominant limb-girdle muscular dystrophy-4 (LGMDD4), with a later onset and milder phenotype [86]–[91]. Nevertheless, the underlying mechanisms of these disorders still need some clarification [92].

The prevalence of LGMDR1 ranges from 1 to 9 cases per 100,000 people, and it represents almost 30% of all LGMD cases in open populations [93]–[99], with some ancestral mutations responsible for specific ethnic or geographic clusters (Table 1) [84],[100]–[103].

Table 1. Description of the clusters for calpainopathy.

Geographic location	Mutation	References
Reunion Island in the Indian Ocean	c.946-1G>A	[83]
Old Order Amish Community in Northern Indiana (USA)	c.2306G>A	[104],[105]
Russia, Croatia, Turkey, Czech Republic, Bulgaria, Germany, Italy, Poland	c.550delA	[93],[106],[115],[107]–[114]
Basque Country (Spain), Brazil	c.2362_2363delAGinsTCATCT	[97],[100]
Japan	c.1795_1796insA	[85],[96]
Chioggia village (Venetia, Italy)	c.1469G>A	[109]
Mòcheni community (Fersina River Valley, Italian Alps)	c.1193+6T>A	[103]
Agarwal community (Northern India)	c.2338 G>C, c.2099-1G>T, c.2051-1G>T	[116],[117]
Northern European Countries (UK, Norway, Sweden, Denmark ("dominantly inherited")	c.643_663del21	[86]
Tlaxcala village (central Mexico)	c.348C>A	[102]
The United States of America	c.598_612del15	[89]
France ("dominantly inherited")	c.1333G>A	[118]

Molecular genetics

LGMDR1 is caused by mutations in the *CAPN3* gene, which encodes an enzyme known as calpain 3 or p94 [82]. This gene is located in the chromosome region 15q15.1-q21.1, extends over 50 kb, and contains 24 exons [82]. As a result of the alternative splicing of the gene, and due to different promoters that can activate its transcription in different tissues, several transcript variants have been described

[119],[120]. Among them, the longest and most common isoform leads to an 821 amino acid calpain 3 protein.

Up to day, more than 480 pathogenic variants of CAPN3 have been reported in the Leiden Open Variation database [121]. The molecular spectrum covers all CAPN3 exons, with some hot regions related to either severe or benign phenotypes, as well as intronic variants [97],[122].

Clinical and histological features

LGMDR1 is characterized by progressive muscle weakness and degeneration, with predominant affection of shoulder, pelvic, and proximal limb muscles [93],[123]. Age of onset is highly variable, although initial symptoms usually appear between 8 and 15 years [124]. Patients have difficulties to lift weight, climb stairs, run and/or get up from chair or floor, and they become wheelchair-bound approximately one or two decades after the symptoms begin [84],[100]. Cardiac and facial muscles are not affected, and no cognitive defects have been reported in this disease. Interestingly, benign forms are lately being increasingly reported with preserved ambulation even after reaching 60 or more years old. In general, these benign forms have metabolic symptoms at onset (myalgia, cramps, and exercise intolerance) or even asymptomatic hyper-CKemia, which is a muscle damage biomarker [125], that may carry on for years before muscle weakness. Symptoms of the classical LGMDR1 phenotype fit with the criteria described by Erb in 1884 to define juvenile muscular dystrophy [84]. However, there is certain variability regarding disease progression and severity related to gender, as well as the type and localization of mutations [97]. Moreover, a phenomenon known as *de novo* intermolecular complementation (iMOC) of CAPN3, may also lead to a milder phenotype in compound heterozygotes, as the autolysis of each CAPN3 mutant can generate two autolytic fragments that are able to reconstitute the WT CAPN3 activity [126],[127]. Additionally, in some families, there is considerable phenotypic variability among patients with identical mutations [128], which makes prognosis in LGMDR1 very challenging [93].

Weakness usually begins in the pelvic girdle. Nevertheless, in some patients, shoulder girdle muscles are firstly affected, or both girdles suffer a simultaneous weakness. Trunk muscles and posterior thigh muscles suffer a prominent atrophy. Among these muscles, *adductor magnus* and *semimembranous* are predominantly affected. However, *soleus*, *vastus intermedius* and *biceps femoralis* have been recently described to suffer a pronounced decline in affected patients [123]. Actually, magnetic resonance imaging (MRI) has shown that in the early stages of the disease some distal muscles, such as *soleus*, are also affected [129]. Contractures in hips, knees, elbows and fingers can also be a sign, as well as Achiles tendon contractures [84],[130]. Patients can also develop shoulder bone protrusions known as *scapula alata* [131].

Since the discovery of *CAPN3* mutations as responsible for LGMDR1, several groups have been trying to identify the pathogenic mechanisms underlying LGMDR1. Although these mechanisms are not entirely understood to date, there is solid evidence indicating that CAPN3 is a multifunctional protein. Different studies, performed in animal models and human samples, have shown that CAPN3 deficiency is associated with different features in the skeletal muscle such as oxidative damage [132],[133], Ca^{2+} dysregulation [134],[135], sarcomere disorganization [136], mitochondrial abnormalities [133],[137]–[139], abnormal muscle adaptation [19],[43] and impaired muscle regeneration [138] (Figure 6). Together, all lead to the characteristic inflammation, necrosis, fibrosis, atrophy, central nucleation and progressive muscle degeneration, observed as histological LGMDR1 features [140] (Figure 7). Indeed, patients in the early stages of the disease present increased concentration of serum creatine kinase (CK) [100],[140]. Some patients at this stage present eosinophilic infiltrations associated with peripheral blood eosinophilia, with unclear pathogenic significance [84],[96],[141]. Fibrosis is often present, and it tends to increase with disease progression, while the presence of muscle fibres becomes residual, being finally replaced by adipose tissue [140].

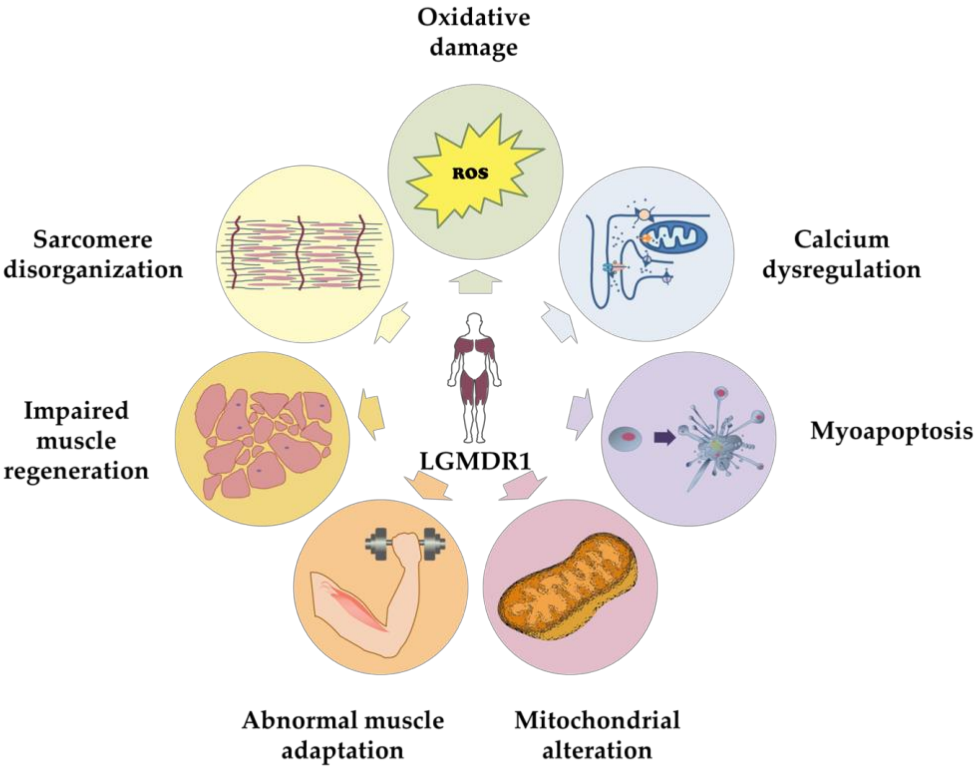
Oxidative damage
ROS
Calcium dysregulation
Myoapoptosis
Mitochondrial alteration
Abnormal muscle adaptation
Impaired muscle regeneration
Sarcomere disorganization
LGMDR1

Figure 6. Illustration of pathological features of CAPN3 deficiency in the skeletal muscle [27].

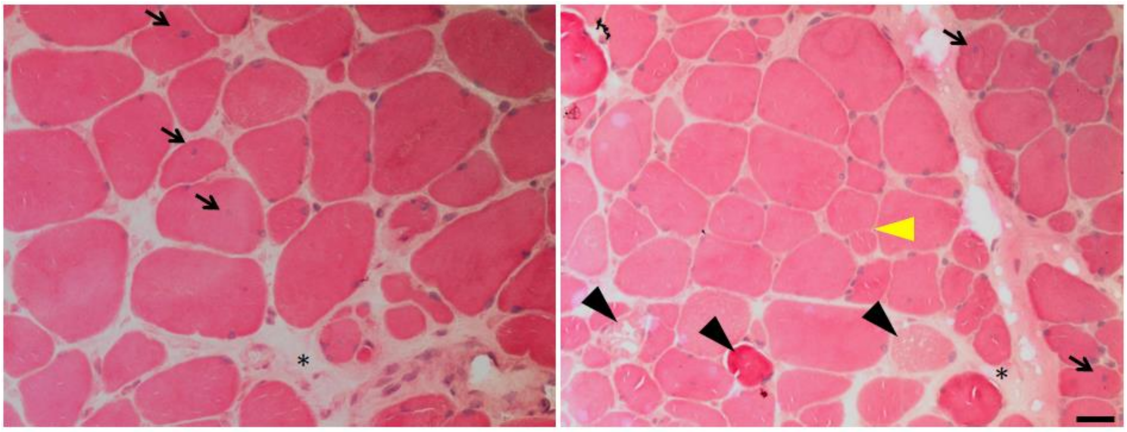

Figure 7. Muscle biopsy of a LGMDR1 patient. Haematoxylin and eosin staining shows endomysial fibrosis (black asterisks), central nuclei (arrows), fibre splitting (yellow arrowhead), necrosis (black arrowheads), and increased variation in fibre size and shape. Scale bar: 25µm [27].

Calpain 3

Calpain 3 (CAPN3) belongs to the calpain superfamily of calcium-dependent non-lysosomal cysteine proteases. Calpains have relevant functions in many cellular processes, including cell motility, apoptosis, cell differentiation and cell-cycle regulation. In these processes, calpains are activated by intracellular Ca^{2+} and they cleave specific substrates [142]–[145]. In mammals, more than a dozen of calpains have been identified, being the ubiquitous CAPN1 (μ-calpain) and CAPN2 (m-calpain) the most extensively studied. The primary structure of the calpain catalytic subunit consists on a multi-domain structure of: i) a cysteine protease domain (CysPc) composed of two protease cores subdomains (PC1 and PC2), ii) a calpain-type beta-sandwich domain (CBSW), and iii) a Penta E-F hand domain (PEF) [146]. CAPN3 shares this catalytic domain structure with CAPN1 and CAPN2. However, CAPN3 has three unique regions namely NS, IS1 and IS2, that confer this protein unusual features such as an extreme instability and fast autodegradation, and Na^+ dependent activation [146] (Figure 8).

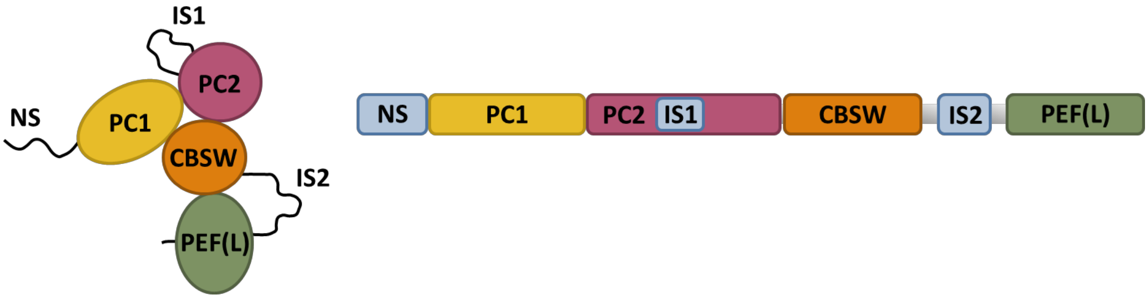

Figure 8. Schematic representation of CAPN3 structure. CAPN3 is comprised of two protease core domains (PC1 and PC2), a calpain-type β-sandwich domain (CBSW), and a Penta E-F hand domain [PEF(L)] that binds four Ca^{2+} ions and may contribute to CAPN3 dimerization. The three specific regions of CAPN3 (NS, IS1 and IS2) are shown in blue. Schematics have been modified from Ye et al., 2018 [147]. The left panel depicts the estimated tertiary structure of CAPN3 [27].

One of the most remarkable features of CAPN3 is its extreme autodegradation rate [148], which has hindered conventional biochemical analysis. Indeed, the native structure of CAPN3 remains unresolved, as well as the accurate interactions of CAPN3 with other proteins. Another extremely unusual characteristic of CAPN3 is its ability to regain proteolytic function after its autolytic dissociation. This occurs through iMOC, a process where two autolytic fragments of CAPN3 reconstitute an active core protease domain [127]. Regarding its proteolytic function, CAPN3 can be activated at physiological intracellular concentrations of Ca^{2+} (100nM) and Na^+ (15mM) [149], and thus, Na^+ is responsible for the low Ca^{2+} levels required to activate CAPN3. In fact, in absence of Na^+, the $[Ca^{2+}]$ required for CAPN3 autolysis is around 0.1mM. Hence, in the skeletal muscle, CAPN3 autolytic activity is suppressed *in vivo* through its binding to connectin/titin [150]. CAPN3 presents both proteolytic as well as non-proteolytic functions [146]. Different studies have identified several mechanisms dependent on CAPN3 proteolytic function, such as mechanosensory transduction and sarcomere remodelling after exercise [146],[151].

Non-proteolytic features of CAPN3, independent of its protease activity, have been identified through comparative studies in CAPN3 knockout and knockin mice. These studies indicate that CAPN3 contributes to the maintenance of Ca^{2+} homeostasis through the stabilization of critical Ca^{2+}-handling proteins, which relies on non-proteolytic CAPN3 functions [152]–[154]. CAPN3 presents a broad distribution within the muscle fibre, having been found at the sarcomere, membrane fraction, SR, cytosol, and even in the nucleus [152],[155],[156].

Research tools for the study of CAPN3 functions

In vitro models

Obtaining human muscle samples for research purposes is getting increasingly more difficult as nowadays diagnosis of muscle dystrophies are performed by less invasive methods, such as genetic diagnosis performed in blood samples [122]. Moreover, the growth rate and myogenic capacity of primary healthy myoblasts decline after few passages [157]. Thus, immortalized myoblasts have come up as a more convenient source of cells compared to primary myoblasts. Actually, immortalized myoblast from healthy rodents are the most common *in vitro* model for investigating myotube fusion or degeneration for instance [158],[159]. Nevertheless, proliferation and differentiation processes in these cells are not always controlled by the same mechanisms as in human myogenic cells [160],[161]. Hence, new protocols have been recently described; for instance, the immortalization of , human primary myoblasts by inducing the expression of human telomerase reverse transcriptase (hTERT) and cyclin dependent kinase 4 (CDK-4) [162]. Myotubes derived from these myoblasts have shown relatively mature sarcomeres and the ability to form NMJs when co-cultured with motor neurons, as well as regenerative capacity after transplantation [162]–[164]. On the other hand, to overcome the limitations of primary myoblasts, new strategies as the use of myogenic cells derived from human embryonic stem cells (hESCs) or human induced pluripotent stem cells (hiPSCs) have emerged [165]. Both, primary myoblasts and myogenic cells derived from stem cells, are compatible with gene editing techniques such as CRISPR/Cas9 [166],[167] or gene silencing by RNA interference [134],[168]. In this way, cell models with the different pathogenic mutations of a specific disease can be obtained, expanding the spectrum of muscle dystrophy *in vitro* models.

Obtention of hESCs or hiPSCs and the subsequent differentiation into myotubes is difficult and time-consuming. Regarding hESCs, myoblasts are obtained by lentiviral-based inducible gene expression of ectopic *MYOD* and exposing them to skeletal muscle media for approximately 10 days [169]. Then, they are cultured in myoblast medium for 4–5 days before triggering myoblasts fusion into myotubes [170]. In hiPSCs, however, the process is even more arduous, as somatic cells must be reprogrammed by introducing four transcription factors (OCT3/4, SOX2, C-MYC and KLF4) into the cells using retroviral vectors in order to behave as hESC [171]. Apart from inducing *MYOD* overexpression, Darabi R. *et al.*[172] suggested using a lentiviral vector encoding DOX-inducible *PAX7* to obtain myogenic cells. This kind of cells may be really useful for studying the differentiation process from muscle stem cells. Nonetheless, when studying terminal differentiation, immortalized human myoblast offer a reliable and less time-consuming model. Moreover, myotubes derived from primary myoblasts show grater maturity compared to myotubes derived from hESCs or hiPSCs [173], which is essential when analysing the expression of the main proteins involved in the pathogenesis of muscular dystrophic proteins that are mainly present in highly mature myotubes as calcium handling proteins [135].

In order to increase maturation and mimic exercise and adaptive responses characteristic of the skeletal muscle, several strategies have been developed, such as exogenous application of electrical pulse stimulation to cultured myotubes [174]–[176] and mixed cultures of human myotubes with either spinal cord explants [177]–[179] or human MNs.[180]. Recently, in our group, we have developed a novel tool based on the human immortalized myoblast cell line LHCN-M2. These cells were transduced by lentiviral particles containing shRNAs to silence the gene of interest. To obtain mature myotubes, we optimized a differentiation media containing several components with reported activity for promoting myotube survival and maturation, such as agrin and neurotrophins [135].

In vivo models

In the last decades, several research groups have developed different models for calpainopathy. These include CAPN3 transgenic and knockout mice.

Transgenic mice

In 2000, a heterozygous transgenic mouse expressing a proteolytically inactive CAPN3 but maintaining its integral structure was generated. In this model, Cys129 was replaced by Ser (p94:C129S) [181]. This mutation has not been described in humans, however, mice show a dystrophic phenotype, including decreased grip strength, increased number of lobulated and split fibres in *soleus* and *extensor digitorum longus* (EDL) muscles from aged transgenic heterozygous mice [181]. On the other hand, a homozygous model with the same mutation was later generated by the same group [182]. In this case, mice showed disrupted fibre membranes, increased central nucleation and higher levels of CK [182]. This mutation reduces autolytic activity and therefore, authors suggest that accumulation of this form of CAPN3 was the cause of these dystrophic features.

Transgenic mice lacking exons 6 and 15 of CAPN3 have also been generated displaying immature muscle fibres by Spencer and colleagues [183]. Moreover, they have developed some transgenic mice carrying missense mutations that show how a less stable but active CAPN3 is able to rescue both, the growth defect in fast fibres and the muscle strength observed in *Capn3*$^{-/-}$ mice [184].

Knockout (KO) mice

The first *Capn3*-deficient mouse model reported was generated by Richard *et al.* [185]. This model was generated by the replacement of exons 2 and 3 of *Capn3* gene with a neomycin resistance cassette. Due to this change, CAPN3 expression was absent. Nevertheless, the cassette employed for the substitution was able to trigger the expression of a recombinant CAPN3 protein with the capability to bind titin, although the autolysis property was absent. The modification was generated in two different backgrounds: 129Sv and a mixed C57BL/6 - 129Svter. In both cases, mice displayed similar dystrophic features as centrally nucleated fibres, necrotic and regenerative areas, inflammatory cell infiltrates, and split fibres. These affections were observed mainly in *psoas*, *soleus*, and *deltoid* muscles, whereas *tibialis anterior* (TA) and *biceps* showed a mild phenotype, and the *quadriceps*, *gastrocnemius*, and *triceps brachii* did not seem to be affected.

Some years later, a full *Capn3* knockout (C3KO) mouse model was developed by Kramerova and colleagues [136]. These mice showed reduced fibre size with inflammation, necrotic and regenerative areas in cross-sections of *gastrocnemius*, *soleus*, TA and diaphragm. The most affected muscles in this model were the *soleus* and diaphragm muscles. These muscle fibres showed that lack of CAPN3 led to delayed myofibrillogenesis and reduced myofibre maturity. This has been the most characterised calpainopathy animal model.

C3 null rat

Just recently, a rat model for LGMDR1 has been generated by Dr Richard's group, following the same procedure as the one employed for generating their mouse model (unpublished data). In these rats, *psoas*, *gastrocnemius*, *soleus*, TA and diaphragm are the most affected muscles. Higher central nucleation and more inflammation signs, especially in TA, have been observed. Moreover, grip strength from their forelimbs is lower compared to wild-type rats (unpublished data).

CAPN3 functions in skeletal muscle

Employing the different *in vitro* and *in vivo* models of calpainopathy, several functions have been attributed to CAPN3. These functions will be further discussed in the following sections.

CAPN3 and sarcomere remodelling

CAPN3 has been mainly implicated in the regulation of muscle contraction and sarcomere stability [149],[156],[186],[187]. Within the sarcomere, CAPN3 is localized in several regions where it interacts with different proteins. CAPN3 interacts at the Z-line with α-actinin-3, tropomyosin and LIM-domain binding protein 3. CAPN3 also interacts with titin, a large scaffold protein that plays a vital role in sarcomere assembly and passive tension of myofibrils, as well as in mechanosensory transduction pathways [156],[188]. Interestingly, CAPN3 binds to titin at the N2A and M-line regions, with different affinity depending on the sarcomere length. Thus, the presence of CAPN3 at the N2A region is increased compared to the M-line region when the sarcomere stretches. This location shift along different titin regions is facilitated by CAPN3 proteolytic activity [186], and it is crucial for the dissociation of Muscle Ankyrin Repeat Protein-2 (MARP-2) from titin, and its translocation to the nucleus to transmit signals of mechanical perturbation [182], suggesting that CAPN3 may function as a sensor of sarcomere integrity.

Titin stabilizes CAPN3 by preventing its autodegradation [136], and therefore, CAPN3 activity may be regulated by titin binding. Moreover, since titin is also a CAPN3 substrate, CAPN3 may be responsible for the fast turnover of titin [189], an aspect that, like accounting for other sarcomere proteins, is necessary for appropriate maintenance of the sarcomere structure [190],[191]. In this line, C3KO mice present abnormal A-bands at the sarcomere and delayed myofibrillogenesis [136], and an accumulation of high molecular weight ubiquitin-protein conjugates [151]. Together, these findings suggest that proper interaction between CAPN3 and titin is essential for sarcomere maintenance and remodelling [192].

Activity of the cytosolic pool of CAPN3, not associated to the sarcomere, has been suggested to be regulated by PLEAID (Platform Element for Inhibition of Autolytic Degradation). Depending on the cellular context, PLEIAD is able to alternate its major role of CAPN3 suppression with the recruitment of CAPN3 substrates [193].

Ca^{2+}-mediated pathogenic mechanisms involved in CAPN3 deficiency

Evidence obtained from animal models and human patients implicates Ca^{2+} homeostasis as a pathophysiological mechanism underlying different muscular dystrophies, including LGMDR1 [194]. Several mouse models of LGMDR1 have been used to understand the pathogenic mechanisms resulting from CAPN3 deficiency. Among these models, the CAPN3 knockout mouse lines *Capn3*$^{-/-}$ and C3KO [136],[185], and the CAPN3 knockin mice *Capn3*$^{CS/CS}$ expressing a structurally intact but inactive CAPN3 [182],[183], have enabled to identify specifically non-proteolytic and proteolytic functions of CAPN3. Noteworthily, the phenotype of these mouse models does not fully recapitulate the severity of LGMDR1 in human patients, likely due to the higher regenerative potential of the murine muscle [195] and/or the increased Ca^{2+} buffering capacity of murine myofibres [134]. Therefore, data from cellular models and muscle samples of patients with LGMDR1 need to be considered in order to unravel the molecular pathways involved in LGMDR1. During the last years, our group has been working on understanding these mechanisms using human biopsies as well as primary and immortalized human myotubes [134],[135],[196]. Here below, recent findings on pathogenic mechanisms associated with CAPN3 deficiency are reviewed, with a particular focus on the involvement of Ca^{2+} dysregulation (summarized in Figure 9).

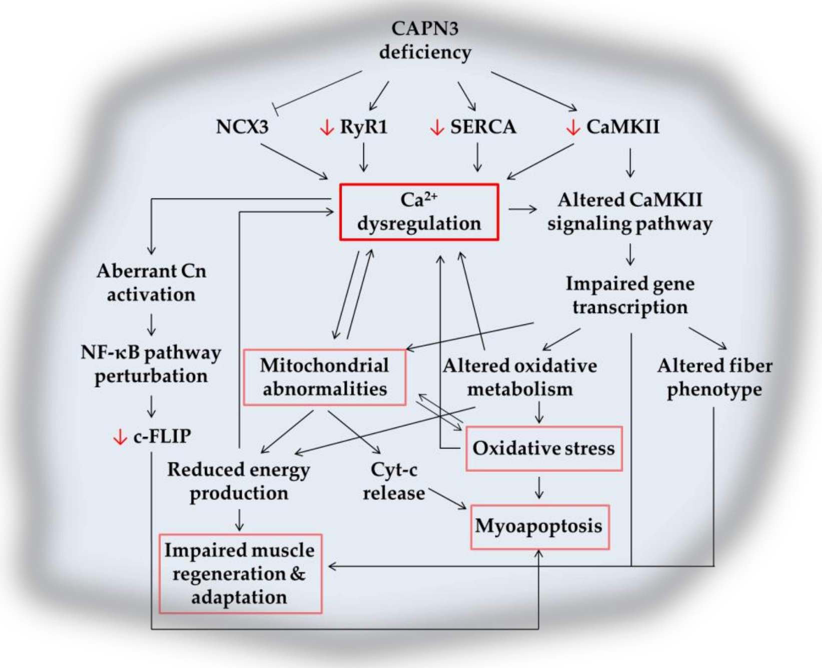
CAPN3 deficiency
NCX3
↓ RyR1
↓ SERCA
↓ CaMKII
Ca2+ dysregulation
Altered CaMKII signaling pathway
Impaired gene transcription
Aberrant Cn activation
NF-κB pathway perturbation
↓ c-FLIP
Mitochondrial abnormalities
Altered oxidative metabolism
Altered fiber phenotype
Oxidative stress
Reduced energy production
Cyt-c release
Myoapoptosis
Impaired muscle regeneration & adaptation

Figure 9. Schematic representation of recognized Ca^{2+}-mediated pathogenic mechanisms triggered by CAPN3 deficiency. CAPN3 deficiency results in reduced levels of RyR1, SERCA, and CaMKII. In addition, NCX3 activity may also be reduced. The decreased function of major Ca^{2+}-handling proteins results in Ca^{2+} dysregulation and increased intracellular [Ca^{2+}]. Reduced CaMKII levels together with Ca^{2+} dysregulation compromise CaMK downstream pathways, which may lead to impaired gene transcription, mitochondrial abnormalities, oxidative stress, altered fibre phenotype, and impaired muscle regeneration. Mitochondrial abnormalities aggravate Ca^{2+} dysregulation and oxidative damage. They may also impact energy production and promote apoptosis through Cyt-c release and activation of caspases. Among these mechanisms, multiple feedback loops lead to altered Ca^{2+} levels and may result in myoapoptosis and muscle waste. Red arrows indicate decreased protein expression. Text in boxes represent several pathological features of CAPN3, as described in Figure 6 [27].

Calcium dysregulation

CAPN3 has been found to interact with several key Ca^{2+}-handling proteins, such as RyR1, CSQ, and SERCA [152]. In this line, several studies have shown that CAPN3 deficiency results in abnormal Ca^{2+}-handling in the skeletal muscle. Indeed, previous studies performed on the CAPN3 knockout mice C3KO and *Capn3$^{-/-}$*, indicate that these mice present reduced RyR1 expression together with a decrease in SR Ca^{2+} release [153],[154]. Furthermore, Capn3$^{-/-}$ knockout myotubes display reduced SR Ca^{2+} levels and a lower response to SERCA inhibitors compared to wild-type myotubes [154]. Notably, the group also contributed to a study showing reduced RyR1 expression and CaMKII signalling in muscles from LGMDR1 patients and C3KO mice [19]. At the triads, CAPN3 is part of a complex comprised of RyR1, AldoA and CaMKII. Interestingly, in the absence of CAPN3 in C3KO mice, both RyR1 and CaMKII protein levels are decreased while AldoA is mislocalized. Thus, CAPN3 has been proposed as a structural stabilizer of RyR1 complexes at the triads [19],[153]. This structural function of CAPN3 may depend on specific genetic regions since a recent study with LGMDR1 patients has reported a new CAPN3 mutation that does not result in diminished RyR1 in the skeletal muscle [137].

Our group had previously found that mouse and human CAPN3-deficient myotubes display decreased SERCA levels as well as impaired Ca^{2+} reuptake into the SR [134],[135]. Moreover, we also found reduced SERCA expression in muscle samples from LGMDR1 patients. In line with these findings, a recent study has shown that in sporadic inclusion body myositis, a common acquired muscle disease associated with aging, there is a secondary calpainopathy and a concomitant reduction of SERCA proteins that leads to Ca^{2+} dyshomeostasis [197]. Interestingly, we have found that SERCA deficiency in CAPN3 knockdown myotubes resulted in increased resting intracellular $[Ca^{2+}]$ in human myotubes, but not in mouse myotubes [134]. This is likely due to the fact that mouse muscle myofibres have a higher Ca^{2+} buffer capacity, since parvalbumin, a major cytosolic Ca^{2+} buffer, is highly expressed in the mouse muscle [135]. In any case, SERCA (*ATP2A1/ATP2A2*) mRNA levels were found unchanged in CAPN3-deficient samples, and therefore, we propose that CAPN3 is necessary to stabilize SERCA proteins and prevent their degradation, similarly to RyR1 and CaMKII. Moreover, SERCA was suggested to be abnormally ubiquitinated, what could lead to its faster degradation by UPS.

Finally, CAPN3 may also regulate Ca^{2+} homeostasis by increasing the activity of NCX3. In HEK293T cells, Michel *et al.* describe an increased activity of the NCX3 muscle isoform, NCX3-AC, following CAPN3 cleavage [198]. This Na^+/Ca^{2+} exchanger is found at the triads and extrudes Ca^{2+} across the sarcolemma to lower intracellular $[Ca^{2+}]$ during relaxation [198]. Nevertheless, more studies need to be performed in order to verify the regulation of NCX3 by CAPN3 in myotubes as well as in LGMDR1 models.

Abnormal muscle adaptation

Skeletal muscle is a remarkably adaptable tissue that responds to physiological and environmental challenges by altering its size and composition [199]. Ca^{2+} plays a fundamental role in muscle adaptation to changes in functional demand by activating specific Ca^{2+}-dependent transcriptional pathways, such those where CaMK is involved, in order to control muscle growth, myofibre type transition, or mitochondrial biogenesis. In particular, CaMKII has been proposed as a major sensor of muscle activity that translates it into phenotypic adaptations by regulating the transcription of specific genes [70]. CaMKII signalling has been found severely compromised in the C3KO mice, and thus, abnormal muscle adaptation has been proposed as a major instrumental mechanism in LGMDR1 [19],[43]. Indeed, in C3KO mice, reduced CaMKII expression results in an impaired slow myogenic program [19]. This may explain why muscles highly enriched in oxidative slow-twitch fibres such as *soleus* and diaphragm are the most severely affected muscles in C3KO mice, and also why it seems to be a preferential involvement of slow fibres in LGMDR1 muscle biopsies [19]. Moreover, after endurance exercise, Capn3-deficient mice muscles fail to upregulate several groups of genes associated with muscle adaptation, such as myofibrillar (*Myl2, Ckmt2, Myom3, Myo18b)*, mitochondrial (*Ppargc1*), and metabolic genes (*Lpl, Pnpla2)* [43].

Mitochondrial abnormalities

Several studies support the notion that CAPN3 is an important modulator of mitochondrial function, and its absence seems to have major consequences over this organelle [139],[200]. LGMDR1 patients and *Capn3* knockout mice present abundant mitochondria with abnormal spatial distribution [96],[139],[201], and a recent study points towards mutation-specific patterns of mitochondrial dysfunction in different LGMDR1 patients [137]. Moreover, in C3KO mice, mitochondria display a swollen appearance with disrupted membranes [139], while in LGMDR1 muscle biopsies, several mitochondrial genes have been found deregulated [202]. Mitochondrial abnormalities would have a direct impact on several pathomechanisms in LGMDR1, including Ca^{2+} dysregulation, energy deficits, oxidative stress, which ultimately, could lead to cell death through the release of different pro-apoptotic factors into the cytosol (Figure 4). Indeed, C3KO muscles present decreased ATP production and increased oxidative stress [139], while LGMDR1 muscles show Cyt-c mislocalization to the cytosol [155], which may promote activation of caspases and apoptosis [203]. Likewise, mitochondria biogenesis and function are severely affected by Ca^{2+} dyshomeostasis [194]. Thus, while Ca^{2+} promotes mitochondrial metabolism and ATP synthesis, sustained high intracellular Ca^{2+} levels, such as those found in CAPN3-deficient myotubes [134],[135], may result in mitochondrial Ca^{2+} overload, and eventually lead to mitochondrial dysfunction and muscle cell degeneration. On the other hand, mitochondria biogenesis is modulated by PGC1α, which is in turn regulated by Cn and CaMK pathway, and therefore, it is highly susceptible to Ca^{2+} dysregulation [81],[204]. In this line, during muscle regeneration, *Capn3* knockout mice have proved unable to increase mitochondrial DNA content, as well as *Ppargc1a* and *Atp5d* transcripts, likely due to diminished CaMKII signalling [138].

Oxidative stress

Oxidative and nitrosative stress have been associated with muscle wasting in several muscular dystrophies, including LGMDR1, where NAPDH oxidase appears to be one potential source of oxidative stress in LGMDR1 muscle biopsies [132]. In LGMDR1 biopsies, elevated reactive oxygen species (ROS), increased oxidized proteins and lipid peroxidation have been reported [132],[133]. Oxidative stress has also been associated with C3KO mouse muscles [139], where defective mitochondria may be a contributing factor since they are considered to generate the majority of cellular free radicals. Reciprocally, oxidative stress may also lead to mitochondrial damage [205], as well as Ca^{2+} dysregulation [206]. Therefore, identification of the cause-effect relationship among these features is very challenging. In any case, oxidative stress can cause cell death through necrotic or apoptotic pathways.

In response to oxidative stress, several protective mechanisms are activated to buffer extra ROS, such as superoxide dismutases (SOD). An increment in their concentration is indicative of oxidative stress. Accordingly, in *Capn3* knockout mouse increased levels of SOD have been reported, indicating a suitable protective response against oxidative stress [133]. In contrast, a reduction of antioxidant defence mechanisms has been described in LGMDR1 biopsies [133], pointing towards a higher vulnerability of human LGMDR1 muscles compared to mouse C3KO muscles.

Impaired muscle regeneration

Impaired muscle regeneration is another main pathological feature of LGMDR1 [138]. Muscle regeneration is a complex process that is initiated upon injury of muscle cells and can be divided into several stages: activation and proliferation of satellite cells, which are the muscle stem cells, differentiation and fusion of the myoblasts, maturation of the newly formed muscle fibres, and the remodelling of muscle fibres. This process requires high levels of protein synthesis, proper mRNA translation, and energy consumption. Different signalling pathways underlie these processes, such as AMP-activated protein kinase (AMPK) signalling, which is regulated by CaMKII and liver kinase B1 (LKB1) [207],[208]. In C3KO mice, during muscle regeneration after cardiotoxin (CTX)-induced damage, muscle fibre growth is arrested due to increased AMPK phosphorylation, inhibition of mTORC1, and energy shortage [138]. Regeneration is one of the most energy-consuming cellular processes, and therefore, C3KO mice fibres are not able to activate genes necessary to adapt to a new situation [209],[210]. Moreover, abnormal sarcomere organization in C3KO mice may also contribute to impaired muscle regeneration [136].

Interestingly, in regenerating C3KO muscles [138], as well as in LGMDR1 biopsies [211], a similar miRNA pattern has been reported to the one described in muscles with impaired myofibre repair/regeneration and subsequent fibrosis, showing increased *Pax7* expression and downregulation of the muscle specific miRNAs miR-1, miR-133a, and miR-206. These miRNAs, also known as dystromirs, are involved in myogenesis by promoting muscle proliferation (miR-133a) and differentiation (miR-1 and miR-206) [212]. Downregulation or inhibition of miR-1 and miR-206 is associated to an increase in satellite cells proliferation and *Pax7* expression *in vivo* [213],[214]. On the other hand, miR-133a is involved in the maintenance of adult skeletal muscle structure, function, bioenergetics and myofibre identity [215]. Remarkably, miR-1, miR-206 and miR-133a have been proposed as disease biomarkers for DMD [212].

Finally, MYOD modulation by CAPN3 has been demonstrated in murine cell cultures, which signals CAPN3 as a potential player during muscle regeneration [216]. Moreover, a defective fusion of C3KO myoblast has been described *in vitro*, due to an accumulation of the β-catenin-M-cadherin complex at the membrane [217]. CAPN3 regulates the localization of β-catenin [217]. At the same time, frizzled-related protein 3 (FRZB), through Wnt pathway inhibition, may prevent the translocation of β-catenin to the nucleus [196]. Interestingly, upregulated FRZB expression has been found in LGMDR1 muscle samples [196]. Therefore, CAPN3 seems to be involved in the fusion and maturation processes of myogenic cells.

Myoapoptosis

Several studies have reported apoptotic myonuclei in muscle samples from LGMDR1 patients [155] and *Capn3*$^{-/-}$ mice [185]. Conversely, similar studies performed in the C3KO mouse model fail to detect apoptotic nuclei in muscle fibres [136]. Differences in Ca^{2+} buffer capacity or protective response against oxidative stress may account for the lack of apoptotic nuclei in this LGMDR1mouse model.

In LGMDR1, apoptosis may be triggered through several pathways (see Figure 9). Firstly, CAPN3 activates NFκB in a Ca^{2+} dependent manner, through degradation of the NF-κB inhibitor IκBα [185]. Activation of NF-κB in the skeletal muscle may lead to protein degradation, inflammation, and fibrosis [218], but it also may promote muscle cell survival under certain conditions [219],[220]. This seems to be the case in LGMDR1, since previous works have shown that CAPN3 regulates the expression of NF-κB-dependent survival genes to prevent apoptosis in skeletal muscle, such as c-FLIP [219]. In particular, the expression of c-FLIP, a master anti-apoptotic regulator downstream NF-κB signalling pathway, is downregulated in human myotubes and CAPN3-deficient mouse muscles [135]. Deregulations in the NF-κB pathway could be part of the mechanism responsible for the muscle wasting resulting from CAPN3 deficiency.

Secondly, Cn also plays a significant role in apoptosis through the dephosphorylation of proteins involved in the apoptotic pathway, such as caspase 9. Phosphorylation of caspase 9 by Akt pathway results in caspase 9 inhibition, while Cn triggers caspase activity via dephosphorylation [221]. Thirdly, Cyt-c leakage from mitochondria promotes the generation of the apoptosome in the cytosol, which activates caspase 9 and the downstream caspase cascade, that may result in myoapoptosis [203]. Interestingly, our group has collaborated in a report of the cytosolic Cyt-c localization in LGMDR1 muscle biopsies [155].

Lastly, sustained SR stress, elevated intracellular calcium and oxidative stress, all of which underlie LGMDR1 pathology, may also lead to apoptosis through caspase activation. Therefore, further studies are needed to elucidate the molecular mechanisms that trigger the apoptotic pathway and muscle waste in LGMDR1. These findings may be highly valuable for identification of novel therapeutic candidates.

Muscle atrophy and degradation

Muscle atrophy, the loss of skeletal muscle mass, is due to an imbalance between protein synthesis and protein degradation [222]. Ubiquitin-proteasome (UPS) and the autophagy-lysosome systems are the two most important cell proteolytic processes controlling protein turnover in muscle [223].

In muscle, upon changes in muscle activity, sarcomeric proteins are removed by the UPS [223]. In this process, a cascade of catalytic reactions is essential to tag the targeted proteins by ubiquitin molecules and to drive them to the proteasome, where they will be subsequently degraded. Briefly, E1 enzymes activate ubiquitin, E2 ubiquitin-conjugating enzymes take then the activated ubiquitin, and transfer it to the target substrate by an E3 ubiquitin ligase [224]. Intriguingly, some muscle specific E3 ligases such as atrogin-1, MuRF1, Nedd4-1 or TRIM32, have been suggested to play a crucial role in muscle wasting [225]. Once the labelled protein is recognized by the proteasome, the ubiquitin chains are removed by deubiquitinating enzymes to allow recycling of this ubiquitin for reuse in future conjugation reactions [225].

It has been suggested that in LGMDR1 patients, UPS mediated protein degradation is the main pathway that leads to muscle atrophy, as overexpression of UPS-related genes has been reported in their muscle biopsies [132],[226]. Moreover, previous reports suggest that UPS is under the regulatory effect of CAPN3 since CAPN3 was found to proteolyze the proteasome regulatory subunit RPS6A [227]. Similarly, upregulation of UPS system has been suggested in other muscle dystrophies such as sarcoglycanopathies, dysferlinopathies, and merosin-deficiencies [228]–[233]. Indeed, pharmacological inhibition of this degradation pathway has shown to prevent the removal of mutated proteins, to promote functional recovery and to improve the dystrophic phenotype associated with these disorders [228],[229],[238],[230]–[237].

Autophagy, however, plays a crucial role in the turnover of cell components. Among this pathway, three different mechanisms have been described in mammals for the delivery of the autophagic cargo to lysosomes: macroautophagy, chaperone-mediated autophagy (CMA) and microautophagy [223]. In particular, macroautophagy seems to be also involved in LGMDR1 muscle atrophy, but in a lesser extent [226].

Briefly, in autophagy, ubiquitinated proteins are aggregated and then selectively kidnaped by the phagophore membranes forming autophagosomes, which are double-membrane vesicles. Subsequently, these vesicles merge with lysosomes forming autolysosomes, where proteins will be degraded. The selection of the proteins to be degraded is mediated by p62 protein, which binds ubiquitin and LC3 proteins. During autophagosome formation, LC3 is lipidated into its LC3-II isoform. Interestingly, in LGMDR1 muscle biopsies, increased expression of LC3-II, p62 proteins and up-regulation of *p62* and *Bnip3* (key regulator of cell death/autophagy) have been reported [226].

Therapeutic strategies

Alike other hereditary disorders, there are currently no effective therapies to treat LGMD. Moreover, treatments for these diseases have mostly been symptomatic so far. However, new treatments, both non-disease- and disease-specific, are emerging for LGMD [239]. Among non-disease-specific treatments, both strength and aerobic exercise training are beneficial for LGMD. In particular, strength training improves strength in LGMDR1, although improvement generally seems smaller than with endurance training [240],[241]. One proposed pharmacological approach is to increase muscle mass by enhancing positive regulators of muscle growth, or by inhibiting negative regulators, such as myostatin. In this regard, in the *Capn3*$^{-/-}$ mouse model of LGMDR1, treatment with an adeno-associated virus (AAV) carrying a mutant myostatin pro-peptide with an inactive C-terminal domain has shown increased muscle mass and improved force generation [242]. Strikingly, a Phase I/II trial with MYO-029, a recombinant human antibody that inhibits myostatin activity, has shown good tolerability but minimal improvement in the muscle strength and the pathology of patients with LGMD [243]. More recently, the new pharmacological compound AMBMP has been proposed to activate CaMKII signalling, restoring the phenotype in the C3KO mouse model [244].

To date, although a meaningful effort has been made in all these areas to address the challenge of developing therapies for LGMDR1, most groups are focused on correcting the primary genetic defect through the use of AAV gene therapy, transcriptional modification approaches (exon skipping and induction of stop codon read-through), or cell therapy (stem cells and iPSCs) [245]. In the particular case of LGMDR1, there are currently few ongoing therapeutic approaches, and so far, they are only showing moderate efficacy. Therefore, there is a need for developing new therapeutic strategies directed towards alternative targets of the disease, such as the ones summarized in Figure 4. Until now, transfer of the AAV-mediated *CAPN3* gene has shown safety and efficacy in the LGMDR1 mouse model, resulting in significant myopathology amelioration [246]. Plasmid DNA containing the non-mutated CAPN3 gene injection into the bloodstream has also been suggested in preclinical trials, avoiding viruses for its delivery to muscle fibres [247]. Moreover, gene correction in LGMDR1 patient-specific iPSCs has been successfully achieved. Those genetically corrected iPSCs can be evaluated *in vitro* and *in vivo* once differentiated into skeletal muscle progenitors, in order to address the efficient restoration of full-length *CAPN3* [167]. Finally, Sarepta Therapeutics, in association with Nationwide Children's Hospital, has recently announced a gene therapy program using the AAVrh74 vector, designed to replace *CAPN3* in the skeletal muscle via systemic administration. AAVrh74 has a robust affinity for muscle cells, with a relatively low level of pre-existing immunity [248]. This vector has been previously used in other gene therapy programs targeting DMD and five other LGMDs [249],[250]. All these therapeutic approaches for LGMDR1 are summarized in Table 2.

Table 2. Therapeutic strategies for LGMDR1. Modified from Lasa-Elgarresta J. *et al.* [26]

Therapy	Clinical-pharmacological use	State	Comments	References
Pharmacological therapy				
MYO-029	Myostatin human recombinant neutralizing antibody	Competed for I/II trial	Minimal improvement in muscle strength	[243]
AMBMP	Activator of Wnt signalling without inhibiting GSK-3ß	Preclinical	Reprograming skeletal muscle toward a slow muscle phenotype	[244]
Gene therapy				
AAV-delivered mutant myostatin propeptide	Prevention of the cleavage of myostatin propeptide	Preclinical	Increased muscle mass and force generation in mice	[242]
AAV-mediated transfer of Calpain 3	Increase of Calpain 3 expression and function	Preclinical	Rescue of the contractile force deficits in mice	[246]
Plasmid DNA	Increase of CAPN3 expression and function	Active project		[247]
AAVrh74 vector	Increase of Calpain 3 expression and function	Active project	Systemic delivery to muscle	[251]
Cell therapy				
iPSC	Increase of Calpain 3 expression and function	Active project		[167]

Considering the importance of calcium homeostasis in the pathophysiology of LGMDR1, targeting calcium handling proteins could also conform another therapeutic strategy to ameliorate this calpainopathy outcome. Specifically, restoring the expression or the activity of altered proteins such as RyR, SERCA or CaMKII, should be considered. Actually, since exacerbated degradation of SERCA proteins due to SERCA over-ubiquitination has been suggested previously by our group [134], the inhibition of its degradation could restore its expression contributing to normalize physiological calcium homeostasis.

HYPOTHESIS AND OBJECTIVES

Working hypothesis

Calcium dyshomeostasis is one of the pathophysiologic mechanisms underlying LGMDR1. Therefore, the working hypothesis is that CAPN3 deficiency may trigger calcium handling proteins dysfunction such as Sarco-Endoplasmic Reticulum ATPase pumps (SERCA) by the induction of their abnormal degradation through the Ubiquitin Proteasome System (UPS). Thus, inhibiting this anomalous degradation by pharmacological treatments could improve the deleterious outcome of this muscle dystrophy.

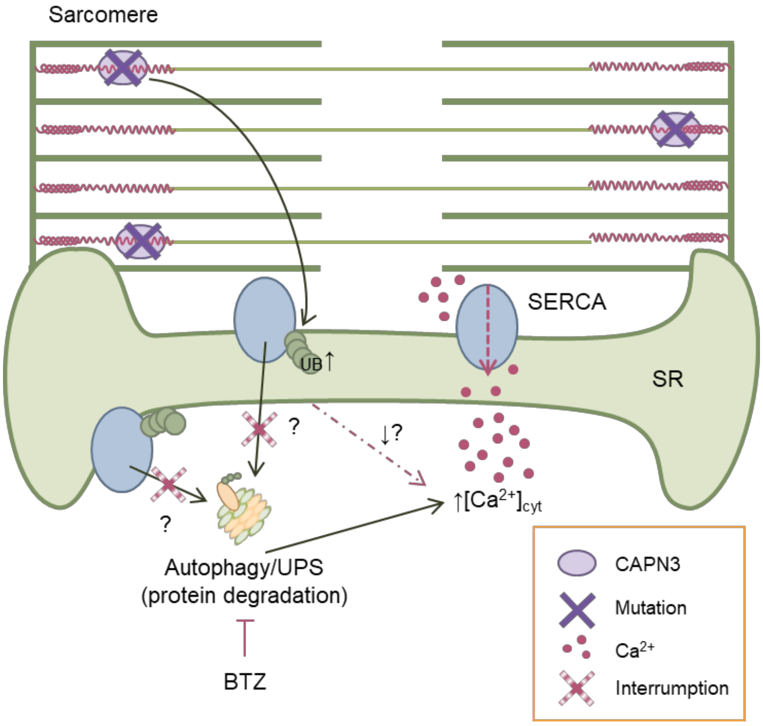

Figure 10. Scheme of the hypothesis. Pathologic mutations in CAPN3 trigger abnormal SERCA ubiquitination (UB) and its consequent exacerbated degradation by Ubiquitin Proteasome System (UPS). SERCA reduction would generate increase cytosolic calcium concentration ($[Ca^{2+}]$). However, inhibition of UPS by Bortezomib (BTZ) treatment, could avoid over-ubiquitinated SERCA protein degradation, and therefore, restoring normal cytosolic $[Ca^{2+}]$.

Aims and objectives

Current knowledge of the implication of calcium dysregulation in LGMDR1 and the lack of efficient therapies for these patients highlight the necessity of the research for new therapeutic approaches. Therefore, the main objective of this thesis is to advance in the finding of pharmacological therapies against this disease. Specifically, this thesis describes the effect of CAPN3 deficiency over SERCA (sarco/endoplasmic reticulum Ca^{2+} ATPase pumps) and the effect of Bortezomib

(BTZ), a specific inhibitor of UPS, in impeding SERCA degradation, which could enhance SERCA activity. Actually, correct calcium re-uptake could restore calcium homeostasis heading this target in LGMRD1.

The specific objectives can be summarized as follows:

1. To characterize calcium handling proteins in CAPN3 deficient human cellular models.
2. To assess the effect of proteasome inhibition on SERCA expression and activity in CAPN3-deficient myotubes *in vitro*.
3. To analyse BTZ treatment in *Capn3*-deficient animal models *in vivo*.

MATERIALS AND METHODS

Cell culture

LHCN-M2 [162] and 8220 [252],[253] control and KM900 and 918 LGMDR1 human immortalized myoblast lines were kindly provided by Dr Vincent Mouly from the Myology Institute in Paris (Table 3). These cells had been previously immortalized by the platform *Immortalization of Human Cells* from the same institution.

For culturing, cells were seeded on 0.5% gelatine-coated dishes and grown in skeletal muscle growth medium (SGM, Promocell) supplemented with 10% FBS, 1X Glutamax and 50µg/ml gentamicin. At confluence, cells were washed with 1X DPBS and then, basic differentiation medium was added (DMEM, 10µg/ml insulin, 100µg/ml apotransferrin and, 50µg/ml gentamicin). Two days after, when fusion of myoblasts was evident, basic differentiation medium was replaced by complete differentiation medium, which is enriched with neurotrofic factors and extracellular matrix components. After 5 days of differentiation, mature myotubes with spontaneous contractile capacity were obtained. In LHCN-M2 myoblast cultures, an overlay of extracellular matrix (ECM Gel from Engelbreth-Holm-Swarm murine, Sigma-Aldrich) was added once confluence was reached before adding basic differentiation medium as previously described [135].

Table 3. Summary of molecular data of the cell lines from LGMDR1 patients.

Cell line	Sex	Mutated site	DNA mutation	Protein mutation
KM900	Male	EX13 EX13	c.1699G>T c.1699G>T	p.(G567W) p.(G567W)
918	Male	EX6 EX13	c.865C>T c.1637G>T	p.(R289W) p.(R546L)

Silencing of CAPN3 with shRNA

LHCN-M2 and 8220 control lines were transduced with lentiviral particles containing shRNAs to knockdown *CAPN3* gene expression. Lentiviral particles were obtained from Viral Vector Unit (ViVU) from The Centro Nacional de Investigaciones Cardiovasculares Carlos III (CNIC). They contained the following plasmids: TRCN0000003494 (human, CAPN3-shRNA) and SHC002 (non-mammalian shRNA control, NS-shRNA) (MISSION® pLKO.1-puro, Sigma-Aldrich).

Human myoblasts were transduced with these particles at a multiplicity of infection (MOI) 5 in proliferation medium with 4µg/ml polybrene for 24h. Afterwards, cells were differentiated to myotubes as described above.

Cell treatment with Bortezomib (BTZ)

Myotubes were treated after 4 days on differentiation, for 24h, with BTZ (Selleckchem), a specific inhibitor of UPS. For treating, complete differentiation medium was removed and replaced by fresh medium containing 5nM BTZ. After treatment, myotubes were washed with 1X DPBS before obtaining the pellet.

Animal models

In this study, two animal models have been employed: C3KO mouse model and the *C3 null* rat. C3KO mouse was generated in a C57BL/6 background using embryonic stem cells disrupted at the C3 locus using a gene trap retroviral vector as previously described [136]. Rat model was generated by Dr. Richard's group using CRIPR/Cas9 technology to delete exon 3 in a CD (Sprague Dawley) rat. Experiments were conducted in accordance with protocols approved by the Institutional Animal Care Ethical Board Committee of Biodonostia (CEEA 17_015) and by Ethical Committee for Animal Experimentation of Généthon (DAP 2017-016-B #14253).

BTZ treatment

C3KO mice were treated with 0.8mg/kg BTZ (Velcade®) in saline by intravenous injection (IV) every 72h for 3 weeks under isoflurane anaesthesia. On the other hand, *C3 null* rats were treated with 0.2mg/kg BTZ (Selleckchem) in saline by intraperitoneal injection (IP) every 72h for 2.5 weeks under isoflurane anaesthesia. However, due to the weight loss observed in treated rats, the dose was reduced to 0.15mg/kg for another 1.5 week.

Protein analysis

Protein extraction and quantification

Cell pellets were homogenized with 50µl lysis buffer (0.125M Tris/HCl, 1% glycerol, 1% SDS, 4M Urea, 5% β-mercaptoethanol, 0.001% bromophenol blue) by pipetting. Samples were boiled for 5min afterwards.

On the other hand, proteins from muscle biopsies were obtained by adding 100µl lysis buffer to each 10mg of muscle. Samples were homogenized with Tissue Lyser (QIAGEN). 3 cycles of 30s at 30Hz were applied in order to get complete tissue disaggregation. Between each cycle, samples were placed on ice for 1min. Later, samples were boiled for 5min and centrifuged at 8,000 rpm for 3min. Finally, the supernatant was recovered.

Protein quantification was performed by Bradford protein assay (Bio-Rad). Protein samples were diluted 1:20 or 1:50 for samples from cell pellet or muscle biopsy, respectively, and then 1:5 dilution of Bradford was added. The absorbance of the unknown samples and the serial of standards was measured at 595nm in a microplate spectrophotometer (Appliscan, Thermo scientific). Finally, protein concentration of the unknown samples was obtained by substitution of the absorbance in the lineal regression obtained from the serial of standards.

Protein homogenization was carried out with a different protocol for CAPN3 detection. In this case, muscle biopsies and cell pellets were homogenized with a different lysis buffer [0.025M Tris/HCl, 25% glycerol, 1.5% SDS, 4M Urea, 1M Thiourea, 0.37M DTT, 0.015% bromophenol blue, 1:200 protease inhibitor (Sigma-Aldrich)] and denaturalized for 10min at 95°C.

Western Blotting

Protein extracts were solved in Min-PROTEAN® TGX™ 4-20% gradient SDS-PAGE precast gels (Bio-Rad). Electrophoresis was carried out in a Miniprotean system (Bio-Rad) in a Tris-glycine buffer (25mM Tris, 200mM glycine, 0.15% SDS) at constant voltage (100V) for 90min. For CAPN3 detection, NuPAGE™ 4 to 12% Bis-Tris precast gels were employed, using a Mini gel talk (Invitrogen) in MOPS buffer (Invitrogen) at 80V for the first 10min, continuing at 130V for another 75min.

Proteins were transferred onto low fluorescence PVDF membranes and blocked with TBS-tween and 5% skim milk powder. After that, membranes were incubated with primary antibodies overnight at 4°C (Table 4).

After washing, membranes were incubated with Alexa Fluor 647- or 488-conjugated secondary antibodies and fluorescence images were acquired with an iBright apparatus (Thermo scientific). For image quantification, Image Studio Lite 4.0 software was used.

Table 4. List of antibodies employed for western blot and immunohistochemistry.

Antibody	Reference	Supplier	Host	Use
Calpain 3 12A2 mAb	MONX10794	Monosan	m	WB (1:100)
Collagen IV pAB	LSL-LB-1403	Antibody BCN	r	IHC (1:1000)
DHPRα2 mAb	ab2864	Abcam	m	WB (1:1000)
Fast MyHC mAB	A4.74	DSHB		IHC (1:25)
Gapdh mAB	MAB374	Millipore	m	WB (1:5000)
MyHC mAb	A4.1025	DSHB	m	WB (1:5000-20000)
MyHC-CFS mAb*	IC4470F	R&D	m	IHC (1:50)
P-CaMKII pAB	PA537833	Invitrogen	r	WB (1:500)
RyR1 mAb	MA3-925	Thermo	m	WB (1:1000)
SERCA1 mAb	MA3-912	Thermo	m	IHC (1:100)/ WB (1:1000)
SERCA2 mAb	sc-376235	Santa Cruz	m	WB (1:250)
SERCA2 pAb	9580	Cell signalling	r	IHC (1:100)
Slow MyHC mAb	A4.840	DSHB	m	IHC (1:25)
SR-actin pAB	ab97378	Abcam	r	WB (1:5000)
ß-CaMKII mAB	13-9800	Invitrogen	m	WB (1:250)

SERCA activity assay

SERCA hydrolyses ATP to re-uptake Ca^{2+} to the SR. Based on a chain of reactions that used the resultant ADP and consume NADH, SERCA activity can be measured by spectrophotometry, as previously described [134]. In fact, decline of NADH absorbance at 340nm is used as the indicator of steady state ATP hydrolysis, and consequently, of SERCA activity (Figure 10).

Muscle biopsies were manually homogenized by a homogenization pestle with reaction buffer (200mM KCl, 20mM HEPES, pH 7.0, 15mM $MgCl_2$, 10mM NaN_3, 10mM phosphoenolpyruvate, 5mM ATP, 1mM EGTA) with 1X Halt™ Protease and Phosphatase Inhibitor Cocktail (ThermoScientific). 200µg protein was diluted in a total volume of 100µl reaction buffer. Right before starting the reaction, 2µl of Pyruvate kinase/Lactate dehydrogenase (PK/LDH) 18 U/ml and 0.53µl of 0.19mM calcimycin (both from Sigma-Aldrich) were added to the reaction buffer, and this last was used as a blank. Addition of 2μl of 100mM NADH (Sigma-Aldrich) triggered the reaction. To determine basal activity once the reaction started, 3 measurements were taken in 1min intervals using a NanoDrop® ND-1000 apparatus. To determine maximal SERCA activity, 4μl of 20mM $CaCl_2$ were added and measurements were recorded every 30s for 5min. SERCA activity was then inhibited by adding 1mM thapsigargin (Sigma-Aldrich) and measurements were repeated for another 5min. The rate of ATP hydrolysis (mmol of ATP/mg of protein/min) was estimated from the equation:

$$\Delta OD340/(\Delta t \cdot \varepsilon \cdot L \cdot [Prot])$$

ΔOD340/Δt: indicates the decrease in absorbance at 340nm during 5min, estimated by linear regression analysis of plotting OD340 vs. time (min)

ε: represents NADH extinction coefficient (6.22×10^{-3} ml/mmol/cm)

L: optical pathlength (0.1 cm)

[Prot]: amount of protein in mg/ml.

For SERCA ATPase specific activity calculation, ATPase activity in the presence of thapsigargin was subtracted from the maximal ATPase activity.

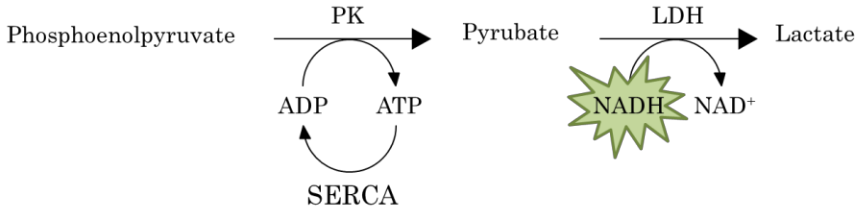

Figure 11. Schematic representation of the enzymatic reactions determining SERCA activity. Phosphoenolpyruvate, ATP, PK (pyruvate-kinase) and LDH (lactate dehydrogenase) are added to the protein homogenates. Then, NADH is added and the decline in its absorbance is used to estimate SERCA enzymatic activity [134].

Real-time quantitative PCR (qPCR)

First, total RNA from cell pellets was extracted by miRNeasy Mini kit (Qiagen), following the instructions supplied by the manufacturer. Optional step with DNase I (Qiagen) was also performed. Once RNA was quantified, 1μg RNA was retrotranscribed into cDNA using SuperScript® Vilo cDNA Synthesis Kit (Thermo Fisher). Finally, qPCR was performed with Power SYBR® Green PCR Master Mix (Thermo Fisher) and with CFX384 apparatus (Bio-Rad). Primers for the genes of study were designed using Primer Express software (Thermo Fisher) and specificity and primer dimers were checked with *in silico* PCR tool from The University of Santa Cruz (California) [254] and Multiple Primer Analyzer tool from Thermo Fisher [255], respectively. Employed primers are collected in Table 5.

Table 5. Sequence of primers used for real-time qPCR analysis.

Gene	Forward primer	Reverse primer	Species
ATP2A1	TACGATGAGATCACAGCCATGAC	ATCCCATGGCAATGCCAAT	Human
ATP2A2	AAAGCTAAAGACATAGTTCCTGGTGAT	AGCAGGAACTTTGTCACCAACA	Human
ATP2A3	CGATACCTGGCTATCGGAGTGTAC	CAGGAAGTTCCTCAGCTGGTAGAA	Human
CAPN3	GAAAAGAGGAACCTCTCTGAGGAA	CGAAGATGATGGGCTTGGTT	Human
Capn3	CTGTTCAAAGGTGAGAAGGTGAAG	AGCTCCAGTCCTTCCAACCAT	Mouse/Rat
c-FLIP	TCCTTCAAATAACTTCAGGCTCCATA	GGATTTCTTCACTGGTTCTTGTTGA	Human
CHOP	CTCCTGGAAATGAAGAGGAAGAAT	TGCTTGTGACCTCTGCTGGT	Human
CK	GAAGCTCTCTGTGGAAGCTCTCA	CCTTCTCCGTCATGCTCTTCA	Human
Ckmt2 [43]	ATAGGCAGAAGGTATCTGCTGATG	GTGTCATCTTGTTTCGGAGTTTGG	Mouse/Rat
DHPRa1	GCCATCTCCGTGGTGAAGAT	CACTGCACCACGTGCTTCA	Human/Mouse
DYST	ACAGGGCAAAAACTGCCAAA	CGCAGTGCCTTGTTGACATT	Human/Mouse
Gapdh	CCTGGCCAAGGTCATCCAT	TGGCATGGACTGTGGTCATG	Mouse
GRP78	AGAAGGTTACCCATGCAGTTGTTACT	CTCATAACATTTAGGCCAGCAATAGTT	Human
HERP	CAAGGTGGCTGAATCCACAGA	GCCTTAAACCATCACTTGAGGAAT	Human
HPRT1	CATGGACTAATTATGGACAGGACTGA	TGAGCACACAGAGGGCTACAA	Human/Mouse
Lpl [43]	TCGTCATCGAGAGGATCCGA	TGTTTGTCCAGTGTCAGCCA	Mouse/Rat
Mmp9[256]	CAATCCTTGCAATGTGGATG	AGTAAGGAAGGGGCCCTGTA	Mouse/Rat
Myl2 [43]	AGTTCAAGGAAGCCTTCACAATC	ATTGGACCTGGAGCCTCTTTGAT	Mouse/Rat
Myo18b [43]	TGAGGTCGTCATGGAAAGGC	CCAGACTTTCTGTGCCTCGT	Mouse/Rat
Myom3 [43]	CGGCAAGTACCGTATCACCA	ATCTCCGAGTCAAAGCCAGC	Mouse
Pnpla2 [43]	CTCACATCTACGGAGCCTCG	CCAGGTTGAAGGAGGGATGC	Mouse/Rat
Ppargc1 [257]	AATCAGACCTGACACAACGC	GCATTCCTCAATTTCACCAA	Mouse/Rat
Tgfb1 [258]	GCGGACTACTATGCTAAAGAGG	GTAGAGTTCCACATGTTGCTCC	Mouse/Rat
XBP1	GCAGGTGCAGGCCCAGTTGTCAC	CCCCACTGACAGAGAAAGGGAGG	Human
XBP1s	GCTGAGTCCGCAGCAGGT	CCCCACTGACAGAGAAAGGGAGG	Human

Human gene expression was normalized by the geometric mean expression of 4 genes as normalization factor: *CK*, *DHPRa1*, *DYST* and *HPRT1*. On the other hand, for mouse and rat gene expression the normalization factor was based on *Dhpra1*, *Dyst, Gapdh* and *Hprt1*.

Calcium imaging

Cytosolic calcium imaging was analysed in human myotubes using ratiometric calcium dye Fura-2AM. First, myotubes were loaded with 4µM Fura-2AM in presence of 0.02% pluronic acid for 30min at 37°C in culture medium. Then, medium with dye was replaced by Ringer solution (125mM NaCl, 5mM KCl, 1.2mM $MgSO_4$, 6mM glucose, 2mM $CaCl_2$ and 25mM HEPES, pH 7.4) for another 30min at 37ºC. This step allows removing extracellular dye and the de-esterification. Experiments were performed in continuous perfusion (2ml/min; 37ºC) with Ringer buffer. Images were obtained with ECLIPSE Ti/L100 microscope (Nikon) equipped with a 20X S-Fluor objective and attached to a lambda-DG4 illumination system coupled to an Orca-Flash 2.8 camera (Hamamatsu). Analysis of the obtained results was performed with Ar NIS elements software (Nikon).

Serum creatine kinase

Blood extracted by intracardiac puncture was collected in BD Microtainer® SST tubes. Samples were centrifuged at 6,000 g for 10min at 4ºC and serum was kept at -80ºC until analysis. Creatine kinase determination was performed by the Biochemistry Service at Donostia University Hospital following a standardized photometric technique. Samples were haemolysis was detected were discarded from data analysis.

Grip Strength test

Forelimb grip strength was performed using a grip strength meter (Bioseb) following the standard procedure [259]. Briefly, mice were lifted by the tail and left to grasp the grid with the forelimbs. Five consecutive measurements were done with a rest of 1min between them. For data analysis, only the three highest measurements were considered. Data were normalized to the body weight.

Fatigue resistance

Mice were subjected to running exhaustion experiment. Before exhaustion test, mice were accustomed to the treadmill (Columbus Instruments) with a 20min run once per day at 10 m/min for 2 days. Based on previously described protocol [43], mice run at 16cm/s for the first 10min (0–10min), at 20 cm/s during 10–30min and 24 cm/s during 30–60min. After that time, the speed was increased by 4 cm/s every

5min until the mouse was unable to continue running. A mouse was considered exhausted when it was not able to continue running on the treadmill for 1min, and when during that time it received 3 or more electrical shocks [260].

Diaphragm strength *in vitro* measurement

Diaphragm strength of C3KO mice has been assessed by a contractility apparatus (Model 1300A, Aurora Scientific Inc, Canada). Once mice have been sacrificed, diaphragms were extracted (including the insertion site of the diaphragm at the ribs) and placed in a dissecting dish with oxygenated cold Ringer Mammalian Buffer (137mM NaCl, 24mM $NaHCO_3$, 11mM glucose, 5mM KCl, 2mM $CaCl_2$, 1mM $MgSO_4$, 1mM NaH_2PO_4 adjusted to pH 7.4). A small strip of the diaphragm from the central tendon to the ribs along the orientation of the fibres in the central portion of the lateral hemidiaphragm was cut. Sutures were tied to the central tendon and then to the ribs. Finally, a large loop was done in each size of the diaphragm tying the sutures.

Diaphragms were placed in the Aurora Scientific apparatus in its *in vitro* set up, which has a bath filled with oxygenated Ringer Mammalian Buffer at room temperature.

First of all, the length of the muscle has been adjusted to make sure the muscle is not slack but is not taut. To establish supramaximal stimulation conditions, single 0.5msec stimulation pulses have been applied to generate a twitch. Unlike in *in vivo* assays, *in vitro* 1A current is applied. The current increases until the force reaches a maximum but steady level. A 10% higher current was applied for the rest of the experiment. Optimum length (L_0) was fixed at the point where maximal force was obtained. Then, the maximal isometric tetanic force was measured applying 10, 30, 50, 80 and 100Hz stimuli for 500msec. Between the stimuli trains, muscle rested for 2min. The following equation was used to obtain the specific force:

$$sP = \frac{P}{\frac{weight}{L_f \; x \; D}}$$

Where weight is obtained after weighing the piece of diaphragm employed in the assay; L_f is the result of multiplying the length of the tissue by length-to-fibre length ratio (the value of this ratio is 1 for diaphragm tissue); and D is the density of the skeletal muscle tissue (1.06g/mm^3) [260].

Finally, eccentric contractions were performed applying a 10% L_0 stretch. 5 stimuli trains were induced at 150Hz with 2min rest between them. Moreover, during each train after the first 500msec 10% L_0 stretch was applied in the final 200msec. These data are represented as %-change from the first measure.

Open field test

Impact of exercise on mice was tested performing treadmill run at 5cm/s for 5min and 25cm/s for another 5min more. Afterwards, their behaviour was recorded in open-field [261]. Mice movements were recorded for 6min in a 45x45x45cm box. Videos were analysed by Smart video tracking software (Panlab, Harvard Apparatus).

Voluntary exercise

Mice were located into a cage with a running wheel (Med Associates Inc.) for 48h to get conditioned. Next, mice performed two 6min walk test in open field, with treadmill running exercise in between. Finally, voluntary exercise data were collected for the next 24h by wheel manager software (Med Associates Inc.).

Histological analysis

At the end of the treatment, mice were sacrificed by cervical dislocation and diaphragm and *soleus* muscles were dissected for histological assays. Right demi-diaphragms were embedded in OCT (Optimal Cutting Temperature Compound) and freeze in liquid nitrogen-cooled isopentane. Similarly, *soleus* muscles were mounted onto a cork slice with OCT and frozen following the same procedure. All muscles were stored at -80°C until sectioning. Cross-sections of 8µm were performed in a Leica CM3050S cryostat.

Haematoxylin & Eosin (HE) and Sirius Red were performed at the Histology service of Généthon (Évry, France). Briefly, for HE, slices were immersed into haematoxylin solution for 1min, and then the excess was removed washing with water. Sections were differentiated with an alcoholic acidic solution, a process that was stopped by returning to an alkaline environment. Then, sections were stained with an alcoholic solution of eosin and they were passed through several changes of increasing alcohol % solutions and dehydrated in several baths with xylene. Finally, sections were mounted with a thin layer of Shandon Consul mounting medium and a coverslip. For Sirius Red, slices were washed in tap water before rinsing them with distilled water. Then, slices were treated in phosphomolybdic acid 0.2% aqueous for 1-5min and stained in Sirius Red 0.1% in saturated picric acid for 90min. Next, sections were washed for 2min in 0.01N HCl before rinsing in 70% ethanol for 45s. Finally, samples were dehydrated, cleared and mounted in Permount. Images were taken at 10X with a Zeiss Axio Scan.Z1 at the Image service (Généthon). A whole section of the diaphragm of each animal has been analysed (approximately 2,000 muscle fibres have been counted).

Analysis of muscle fibres´ phenotype was performed by immunofluorescence. Briefly, sections were fixed in pre-cooled acetone and then blocked for an hour (2% BSA, 1% GS, 0.5% Triton X100 and 0.02% NaN3 in PBS). Then, sections were incubated with primary antibodies overnight at 4°C. After washing, slices were incubated with Alexa Fluor 647- or 555-conjugated secondary antibodies for 1h at room temperature. Subsequently, sections were incubated with FITC-conjugated MyHC antibody or slow MyHC for 1h at 37°C. Sections incubated with slow MyHC were then incubated with IgM Alexa Fluor 488-conjugated secondary antibody for 1h at room temperature. Finally, slices were mounted with Prolong® Gold antifade reagent with DAPI (Life technologies). Images were acquired by an ECLIPSE Ti/L100 microscope (Nikon) equipped with a 10X S-Fluor objective and an Orca-Flash 2.8 camera (Hamamatsu). The analysis was performed using Fiji software (ImageJ, NIH).

Ubiquitin proteasome activity

Ubiquitin proteasome activity was measured in *soleus* muscles from control, untreated and BTZ treated C3KO mice by cleavage of specific fluorogenic substrates modifying ta previously described method [262]. Briefly, muscle samples were homogenised in 50mM HEPES, 100mM NaCl, pH 8.0 and centrifuged. The protein concentration of supernatants was determined by Bradford protein assay (Bio-Rad) as described in the western blot section. 12.5µg protein was incubated for 60min at 37°C in the presence of a specific fluorogenic substrate (LLVY-R110, Sigma-Aldrich). The fluorescent signal was read with Glomax® Discover microplate reader (Promega) at 525nm. Homogenization buffer was employed as negative control and

50μM BTZ was added to the protein sample as a positive control. Unspecific activity from positive control was subtracted from sample signals as well as background signal from the negative control.

Data analysis and statistical procedures

All results are expressed as mean ± standard error of the mean (SEM). After detecting and removing outlier data, distribution data has been analysed by Saphiro wilk's test. When sample number was too small, we considered normal distribution and student's t-test was applied in comparisons of two groups. Paired t-test were applied in infections carried out at the same time while unpaired t-test was used when samples were not matched among them. On the other hand, multiple t-test was performed when multiple measures from samples were analised among two groups. In case of 3 group comparisons, one-way analysis of variance (ANOVA) was used. In all cases, when interaction between two factors was significant, single effects were analysed by one-way ANOVA followed by post-hoc Dunnet's test taking as a reference non-treated CAPN3 deficient group. When multiple measures from samples were analised among three groups repeated one-way ANOVA was employed. The level of significance was set at $p<0.05$ (*) and $p<0.01$ (**), $p<0.001$ (***) and $p<0.0001$ (****). GraphPad Prism version 6.04 was used to perform statistical analysis.

RESULTS

Downregulation of SERCA protein in CAPN3 deficient *in vitro* models

Calcium homeostasis disruption is one of the pathophysiological presented mechanisms in LGMDR1. With the aim of delving into the role that CAPN3 plays on this mechanism, we have generated different *in vitro* models by using lentiviral particles carrying an shRNA to block the translation of mRNA into CAPN3 protein.

Once the myotubes have been obtained, we have analysed the expression of different proteins involved in calcium homeostasis by western blotting. We have seen that the generated CAPN3 deficit causes a clear detriment of the protein expression of SERCA1 and SERCA2 (69% and 86%, respectively; $^{*}p<0.05$). However, we have not observed changes in SERCA expression at the mRNA level. These data together with the greater ubiquitination of SERCAs previously reported by our group [134] indicate that the observed posttransductional changes in SERCA levels are possibly due to a destabilization of SERCA proteins caused by the absence of CAPN3 (Figure 11).

Decreased expression of SERCA, the main calcium transporter from the cytosol to the SR, could generate a severe alteration in intracellular calcium homeostasis. To verify this, we have analysed intracellular calcium levels using the ratiometric calcium fluorochrome Fura-2AM. Myotubes have been treated with this fluorochrome, and the obtained images have been analysed in real-time. Thereby, we observe that dystrophic myotubes show a 41% increase in intracellular calcium levels compared to control myotubes (100 ± 8% in NS-shRNA vs. 142 ± 11% in shCAPN3; $^{**}p<0.01$) (Figure 12).

Furthermore, a decreased expression of SERCA could generate an increase of SR stress due to its reduction in calcium levels in SR lumen. This effect has been evaluated by analysing the expression of different genes related to SR stress such as *CHOP, HERP, GRP78* and the ratio between the isoforms *XBP1s* and *XBP1*, which is commonly used as a marker of activation of the unfolded protein response (UPR), which is related to SR stress [57]. Furthermore, the expression of *c-FLIP*, an antiapoptotic factor whose reduction has been previously described in biopsies of LGMDR1 patients, has been analysed [219]. On the one hand, we have observed that reticulum stress markers are increased in the CAPN3 silencing model in LHCN-M2 myotubes. Additionally, as in patients´ biopsies, we observed that *c-FLIP* factor is decreased in silenced cells, compared to control myotubes. Therefore, we conclude that by silencing CAPN3 in the LHCN-M2 myotubes, we have obtained an *in vitro* model capable of recapitulating the molecular characteristics of LGMDR1 shown by LGMDR1 animal models that still need to be clarified in humans (Figure 13).

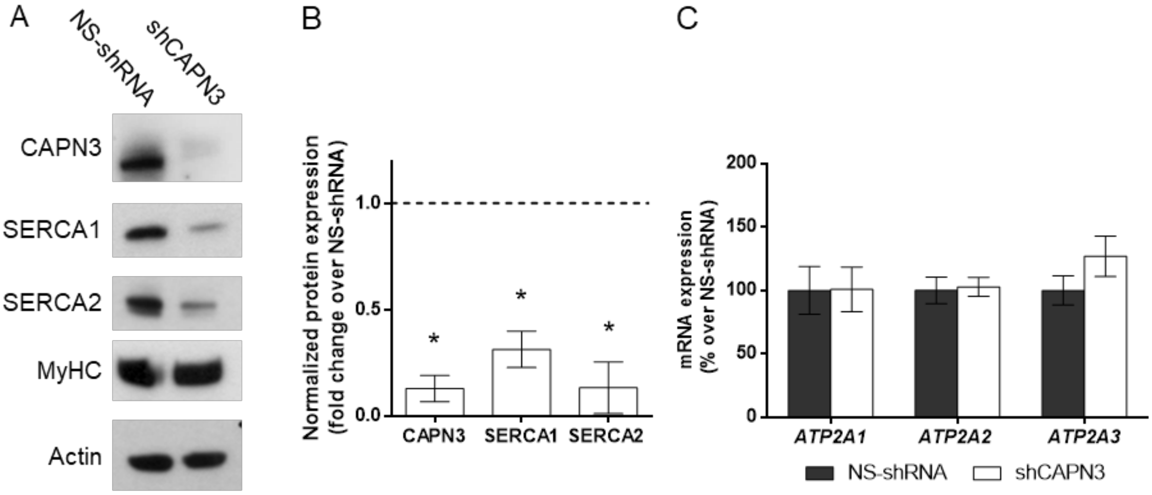

Figure 12. CAPN3-deficiency in human LHCN-M2 myotubes. A) Representative western blot images of CAPN3, SERCA1, SERCA2, MyHC and Actin in human LHCNM-2 control (NS-shRNA) and CAPN3-deficient (shCAPN3) myotubes. B) Quantification of western blotting signals from CAPN3-deficient LHCN-M2 myotubes compared to control myotubes represented as a discontinuous line. N=3 independent experiments. C) Analysis of *ATP2A1, ATP2A2 and ATP2A3* mRNA levels by quantitative PCR (qPCR) in human LHCNM-2 NS-shRNA and shCAPN3 myotubes. Data expressed as mean percentage over Ns-shRNA signal ±SEM. N=3 independent experiments; **p*<0.01 vs. NS-shRNA (paired t-test). No significant differences were observed in C.

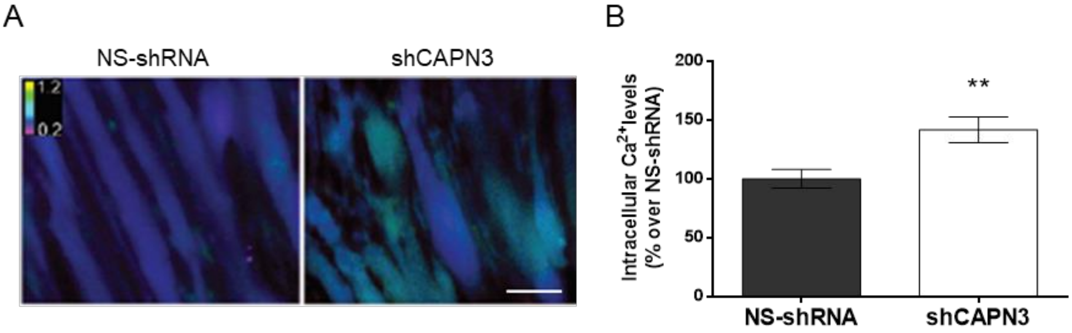

Figure 13. Intracellular Ca^{2+} imaging of human LHCN-M2 myotubes. A) Representative pseudocoloured images of control (NS-shRNA) and CAPN3-deficient (shCAPN3) myotubes loaded by FURA-2AM at basal conditions. Scale bar: 25µm. B) Resting intracellular calcium levels of LHCN-M2 NS-shRNA and shCAPN3 myotubes. Data expressed as mean percentage over NS-shRNA ±SEM. 200–500 myotubes analysed from at least N=3 independent experiments; ***p*<0.01 vs. NS-shRNA (unpaired t-test).

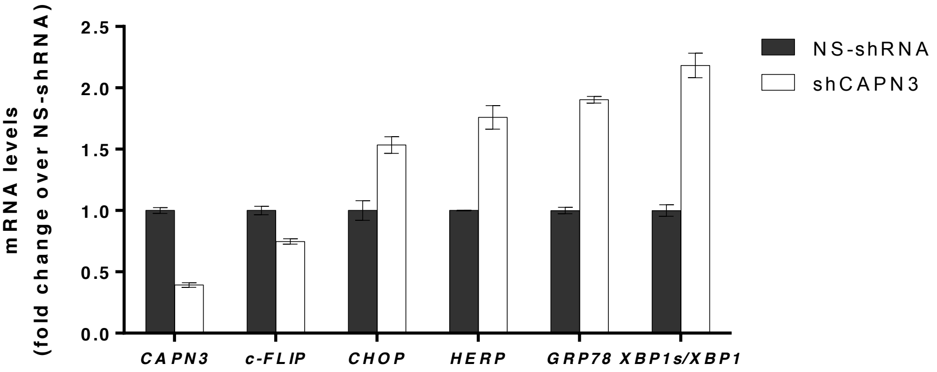

Figure 14. Analysis of mRNA expression in CAPN3 deficient LHCN-M2 myotubes. mRNA expression of *CAPN3, c-FLIP, CHOP, HERP, GRP78*, and the *XBP1s* (spliced) /*XBP1* ratio in human LHCN-M2 NS-shRNA- and shCAPN3-treated myotubes after 14 days in differentiation. Data expressed as mean fold change over NS-shRNA ±SEM of technical replicates. N=1.

To verify the cellular model of LGMDR1 by CAPN3 silencing, we have tried to replicate this strategy in another control line of human myoblasts (8220). In this case, we observe that the 8220 myoblasts are capable of differentiating into mature myotubes showing spontaneous contractility in a shorter time, even without the addition of the upper layer of ECM. As in LHCN-M2, CAPN3 silencing in the 8220 cells is effective, and a significant reduction of 68% in the level of CAPN3 protein is observed with respect to control myotubes ($p<0.05$) (Figure 15). Unlike what it was previously observed in the C3KO murine model, in this silenced model there are no differences in the expression of β-CaMKII or in its phosphorylated form [19]. However, as in CAPN3-deficient LHCN-M2, we observe a concomitant reduction in SERCA proteins. In particular, in 8220 CAPN3-silenced myotubes, SERCA1 and SERCA2 proteins are reduced by 50% and 67%, respectively, although they do not reach statistical significance ($p=0.27$ in SERCA1 and $p=0.22$ in SERCA2) (Figure 15B-C).

According to mRNA levels, the degree of CAPN3 silencing in 8220 myotubes is similar to the observed in LHCN-M2 myotubes. In both cases, a significant reduction of more than 50% is obtained with respect to the control myotubes ($p<0.01$). On the other hand, regarding the expression of SERCA, as in the previous case, no differences are observed in mRNA levels between control and silenced myotubes. One of the major differences that we have observed between both models, LHCN-M2 and 8220, is with respect to the SR stress. In the case of 8220, no significant changes have been observed in the CAPN3-silenced myotubes in terms of SR stress markers and *c-FLIP* expression, compared to control cells (Figure 16).

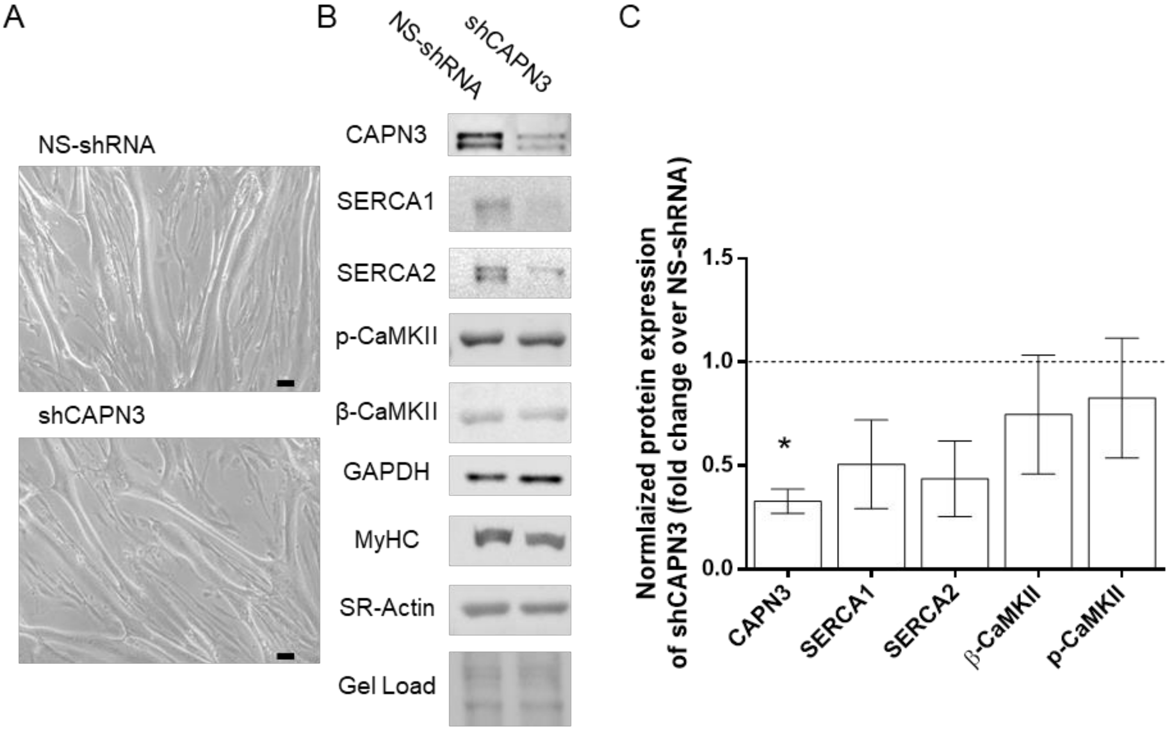

Figure 15. Analysis of Ca^{2+} handling proteins in CAPN3 deficient 8220 myotubes. A) Representative bright-field images of 8220 human myotubes transduced with NS-shRNA and shCAPN3 after 5 days in differentiation. Scale bar: 50µm. B) Representative western blot signals of CAPN3, SERCA1, SERCA2, p-CaMKII, ß-CaMKII, GAPDH, MyHC, SR-Actin and gel load from A). C) Quantification of western blotting signals from CAPN3-deficient 8220 and control myotubes. Expression values from NS-shRNA myotubes are represented as a discontinuous line. Data expressed as mean fold change over NS-shRNA ±SEM. N=3 independent experiments; *p<0.05 vs. NS-shRNA (ratio paired t-test).

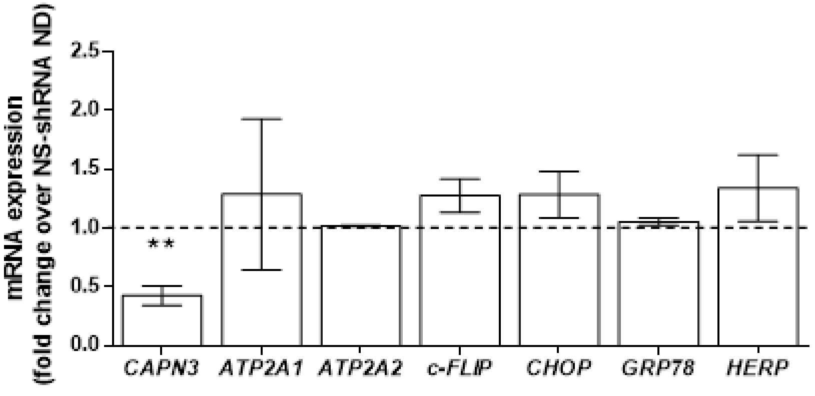

Figure 16. Analysis of mRNA expression in LGMDR1 model based on CAPN3 silencing in 8220 control myotubes. mRNA expression of *CAPN3*, *ATP2A1*, *ATP2A2* and SR stress markers (*c-FLIP*, *CHOP*, *GRP78, HERP*) in CAPN3-silenced human 8220 myotubes. Data from NS-shRNA are represented as a discontinuous line. Data expressed as mean fold-change ±SEM. N=3 independent experiments; **p<0.01 vs. NS-shRNA (ratio paired t-test).

Finally, 8220 CAPN3-silenced myotubes do recapitulate the intracellular calcium increases previously observed in the LHCN-M2 silenced line. In this case, we observe that the CAPN3 deficit and the concomitant reduction of SERCA1 and SERCA2 result in a significant increase in basal intracellular calcium levels of 21% (100 ± 2.88 in NS-shRNA vs. 121.2 ± 5.96 in shCAPN3; $p<0.01$) (Figure 17).

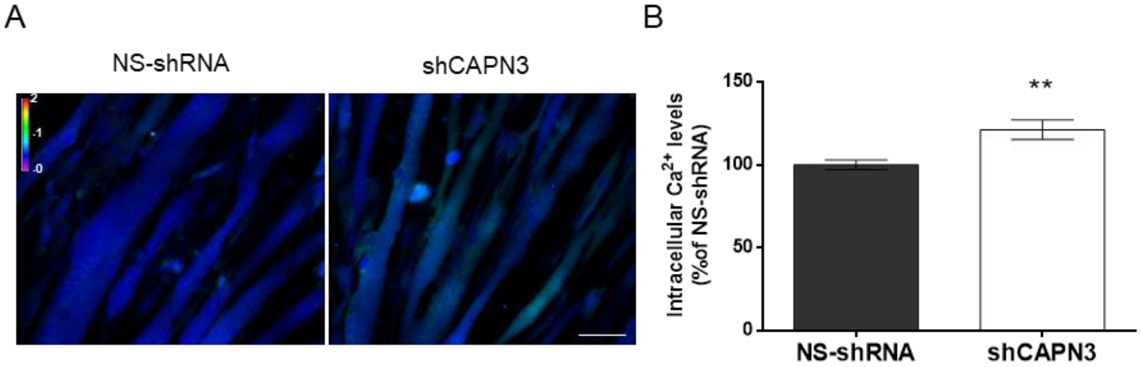

Figure 17. Intracellular Ca^{2+} imaging of 8220 myotubes after being loaded by ratiometric dye Fura 2AM. A) Representative pseudocoloured images of NS-shRNA and shCAPN3-silenced myotubes at basal conditions after being loaded by FURA-2AM. Scale bar: 25μm. B) Resting intracellular calcium levels of 8220 NS-shRNA and shCAPN3 myotubes. Data expressed as mean % over NS-shRNA ±SEM. 120-160 myotubes were analysed; $^{**}p<0.01$ vs. NS-shRNA (unpaired t-test).

Effect of Bortezomib (BTZ) over CAPN3 deficient myotubes

Taking into account that CAPN3-deficient myotubes show decreased levels of SERCA proteins, but maintain mRNA levels similar to those of the control, we hypothesized that SERCA proteins are destabilized in the absence of CAPN3 and consequently, increasing its degradation by the UPS. Indeed, in previous studies developed in our laboratory, we observed an increase in the ubiquitination of SERCA1 and SERCA2 [134], which suggests that the ubiquitin proteasome pathway is involved in the degradation of these proteins. Therefore, we wanted to study the effect of inhibition of this pathway on the expression of CAPN3, SERCA1 and SERCA2. We decided to use Bortezomib (Velcade®) for this study, as it is a specific UPS inhibitor approved by the FDA for the treatment of multiple myeloma [263], which has been previously used in preclinical trials of other muscular dystrophies [230],[262],[264].

First, we have treated the 8220 CAPN3-silenced myotubes with 5nM Bortezomib (BTZ), non-toxic for human myotubes, as previously described [265]. After 24 hours of BTZ treatment, CAPN3-deficient myotubes present a significant increase in 21% SERCA2 protein levels ($p<0.01$), with no changes in SERCA1 levels with respect to untreated myotubes (Figure 18). Strikingly, we also observe a markedly increased of CAPN3 levels in the myotubes treated with BTZ, although they do not reach statistical significance.

Next, we have analysed gene expression at the mRNA level, and we have observed that treatment with BTZ does not alter CAPN3 levels, while it increases the expression of SR *CHOP* stress markers (10.52 ± 5.36 in shCAPN3 BTZ vs. 1.16 ± 0.2 in shCAPN3 ND), *GRP78* (2.47 ± 0.64 in shCAPN3 BTZ vs. 0.96 ± 0.10 in shCAPN3 ND) and *HERP* (1.68 ± 0.47 in shCAPN3 BTZ vs. 1.34 ± 0.28 in shCAPN3 ND; $p<0.05$). Moreover, we have been able to detect an increase in the expression of *c-FLIP* with BTZ treatment (2.436 ± 0.55 in shCAPN3 BTZ vs. 1.187 ± 0.14 in shCAPN3 ND; $p<0.05$) (Figure 19).

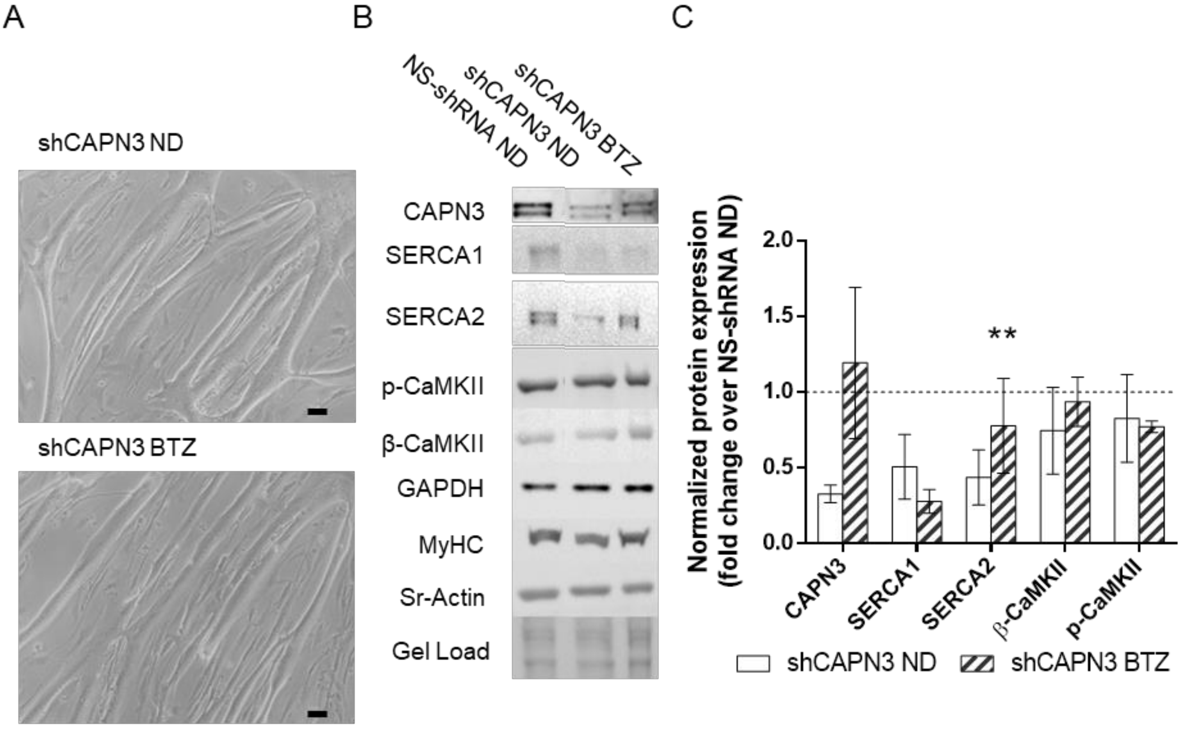

Figure 18. Effect of BTZ treatment over calcium handling proteins in CAPN3-deficient 8220 myotubes. A) Representative bright-field images of 8220 human myotubes differentiated for 5 days, transduced with shCAPN3, non-treated (ND) and after 5nM BTZ treatment for 24h. Scale bar: 50μm. B) Representative western blot signals of CAPN3, SERCA1, SERCA2, p-CaMKII, ß-CaMKII, GAPDH, MyHC, SR-Actin and gel load in NS-shRNA, shCAPN3 and BTZ treated shCAPN3 8220 myotubes. C) Quantification of western blotting signals of BTZ treated and non-treated shCAPN3, normalized by MyHC signal. Reference NS-shRNA shown as a discontinuous line. Data expressed as mean fold change ±SEM. N=3 independent experiments; $^{**}p<0.01$ vs. shCAPN3 ND (ratio paired t-test).

Finally, we have analysed whether the increase in SERCA2 observed in the silenced myotubes treated with BTZ translates into a reduction in intracellular calcium levels. Remarkably, we observe that BTZ is able to significantly normalize intracellular calcium levels, which is increased in CAPN3-silenced myotubes with respect to control (91.70 ± 2.97 in shCAPN3 BTZ vs. 121.2 ± 5.96 in shCAPN3 ND; *p*<0.0001) (Figure 20). This indicates that the SERCA2 transporter has a predominant action on the calcium increase observed in the 8220 CAPN3-deficient myotubes.

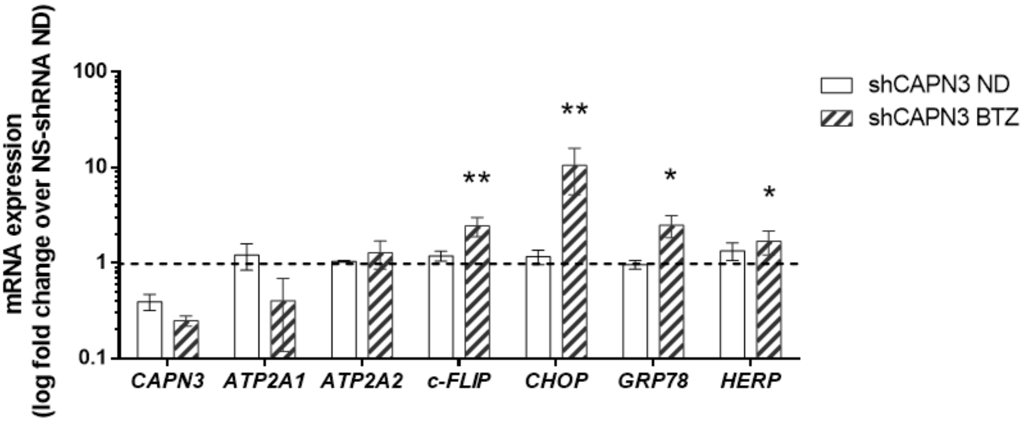

Figure 19. Gene expression analysis in BTZ treated CAPN3-deficient 8220 myotubes. Quantification of the expression of *CAPN3, ATP2A1, ATP2A2, c-FLIP, CHOP, GRP78* and *HERP* in 5nM BTZ treated and non-treated (ND) CAPN3-deficient 8220 myotubes after 5 days in differentiation. Reference NS-shRNA represented by a discontinuous line. Data expressed as log mean fold change ±SEM. N=3 independent experiments; *p<0.05 vs. shCAPN3; **p<0.01 vs. shCAPN3 (ratio paired t-test).

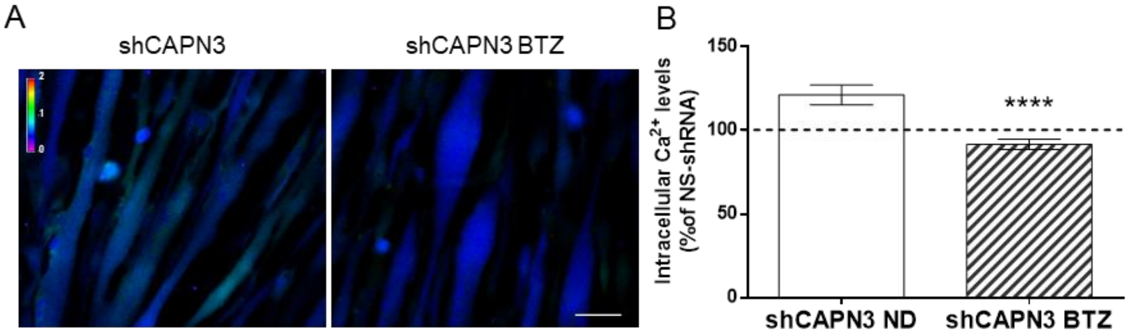

Figure 20. Intercellular Ca2+ imaging of BTZ treated and no-treated CAPN3-deficient 8220 myotubes by loading with ratiometric marker Fura 2AM. A) Representative pseudocoloured images of shCAPN3 ND (non-drug) and 5nM BTZ treated shCAPN3 myotubes at basal conditions. Scale bar: 25µm. B) Resting intracellular calcium levels of non-treated and BTZ treated CAPN3-deficient 8220 myotubes after 5 days in differentiation. Basal level from NS-shRNA is represented by a discontinuous line. Data expressed as mean % ±SEM. 120-160 myotubes analysed; ****p<0.0001 vs. shCAPN3 (unpaired t-test).

SERCA protein deficiency in human primary immortalized myoblasts from LGMDR1 patients and BTZ treatment.

In addition to the control myoblast lines used in the silencing assays, we have been able to obtain 2 samples of immortalized myoblasts from LGMDR1 patients: Km900 (LG1) [266] and 918 (LG2) [266]. Myoblasts have been differentiated following the same protocol as for control myoblasts (8220), obtaining myotubes with similar morphology, as shown in the culture images (Figure 21). The CK activity of the cultures is similar between control and LG myotubes (469.1 in LG1, 460.85 in LG2 vs. 484.23 in control), and no significant differences are observed in the mean width of the myotubes. However, a more detailed analysis shows that LG1 myotubes show a higher percentage of smaller width-myotubes than control and LG2 myotubes ($p<0.05$) (Figure 21).

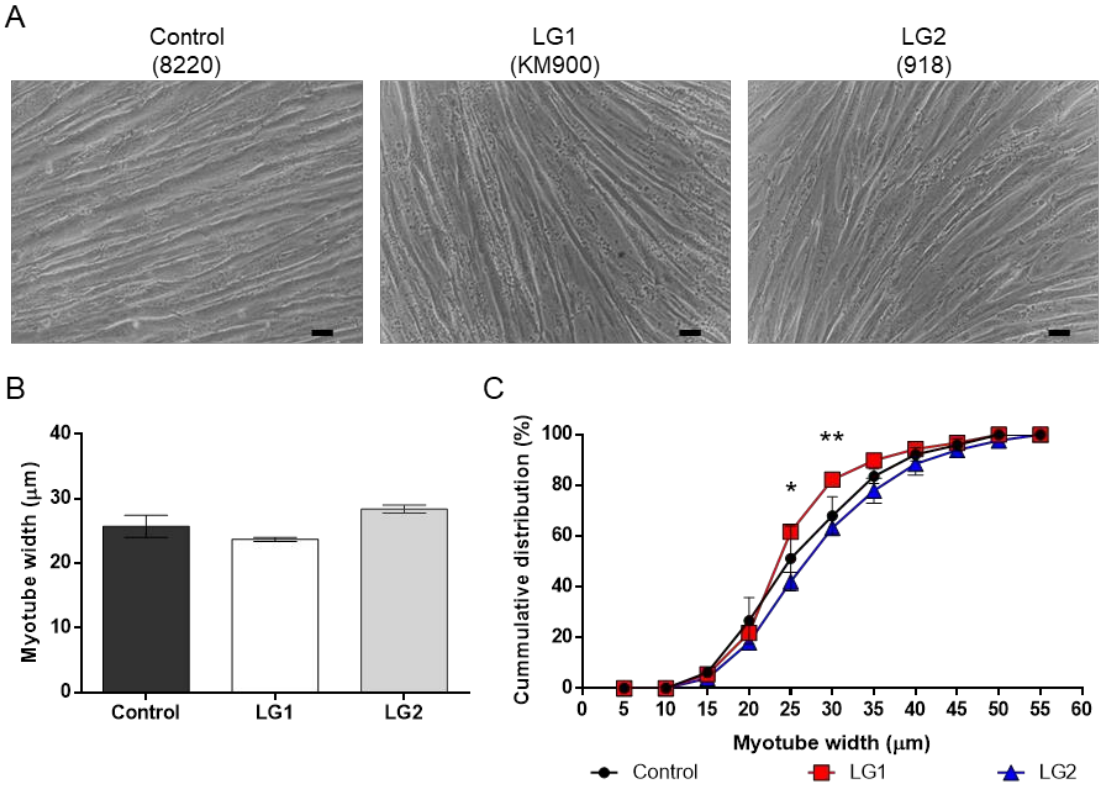

Figure 21. Immortalized human LGMDR1 myotubes. A) Representative bright-field images from immortalized human myotubes from a control and two LGMDR1 samples (LG1 and LG2) after 5 days in differentiation. Scale bar: 50μm. B) Mean and C) cumulative distribution of myotube width from control, LG1 and LG2 myotubes after 5 days in differentiation. 90-170 myotubes analysed from at least N=3 independent experiments. Data are expressed as mean % ±SEM. No significant changes are observed in B. *$p<0.05$ LG1 vs. control; **$p<0.01$ LG1 vs. control in C (one-way ANOVA post hoc Dunnett's test in B; repeated-measures one-way ANOVA post hoc Dunnett's test in C).

Subsequently, we have characterized gene expression of these samples, focusing on the expression of *CAPN3* and *ATP2A1, ATP2A2* genes, which code for SERCA1 and SERCA2, respectively. Furthermore, we have analysed the expression of SR stress markers and *c-FLIP* to compare it with that observed in the CAPN3 silencing models. We have observed that unlike LG1, LG2 myotubes, present lower expression of *CAPN3* compared to control cells (0.29 ± 0.05 in LG2 vs. 1.00 ± 0.24 in control, $p<0.05$). In these myotubes a tendency to a reduced expression of *ATP2A1* is also observed (0.19 ± 0.07 in LG2 vs. 1 ± 0.53 in control, $p=0.46$). In addition, the expression of *ATP2A2* is significantly reduced by 50% in the LG1 and LG2 myotubes with respect to control myotubes (0.43 ± 0.039 in LG1; 0.5 ± 0.035 in LG2 vs. 1 ± 0.12 in control, $p=0.05$). On the other hand, the expression of *RYR* is not altered. Finally, regarding SR stress markers and *c-FLIP*, LGMDR1 myotubes do not present obvious alterations in the expression of these genes in comparison with control myotubes (Figure 22).

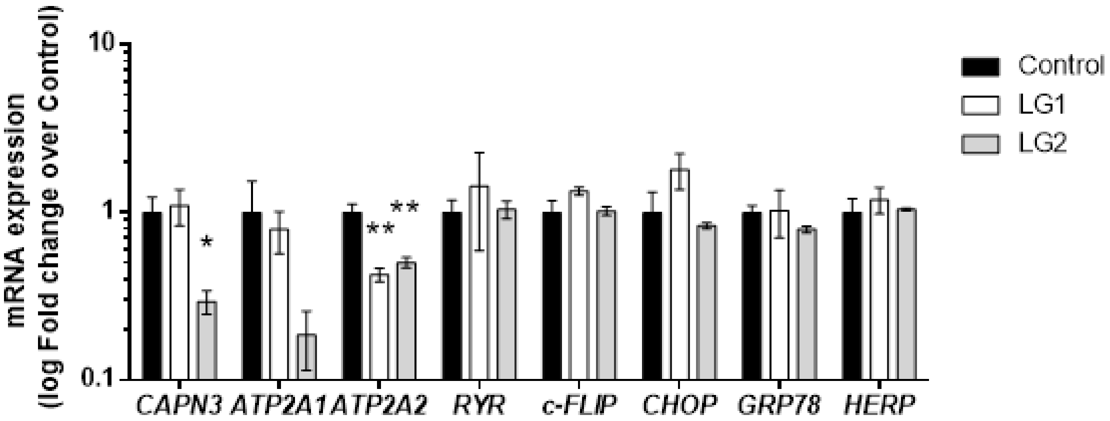

Figure 22. Gene expression analysis in primary immortalized LGMDR1 and control human myotubes. qPCR expression analysis of *CAPN3, ATP2A1, ATP2A2, RYR, c-FLIP, CHOP, GRP78* and *HERP* in control, LG1 and LG2 myotubes after 5 days in differentiation. Data are expressed as mean fold change ±SEM. N=3 independent experiments. *$p<0.05$ vs. control; **$p<0.01$ vs. control (one-way ANOVA post hoc Dunnet's test).

The expression of these genes at the mRNA level shows a high correlation with protein levels. As observed in Figure 23, LG1 myotubes present levels of CAPN3 protein similar to control myotubes (8220), while the expression of CAPN3 protein is barely detected in the LG2 myotubes. Furthermore, we have been able to observe that the levels of SERCA proteins are decreased in patients´ myotubes, especially in the LG2 myotubes, which present very low expression of CAPN3 (Figure 23).

Then, we assessed the effect of BTZ treatment on myotubes derived from LGMDR1 patients. In this case, we have observed an upward trend in CAPN3 expression that carries upregulation in SERCA2 protein expression, but not in SERCA1 (Figure 24A-B).

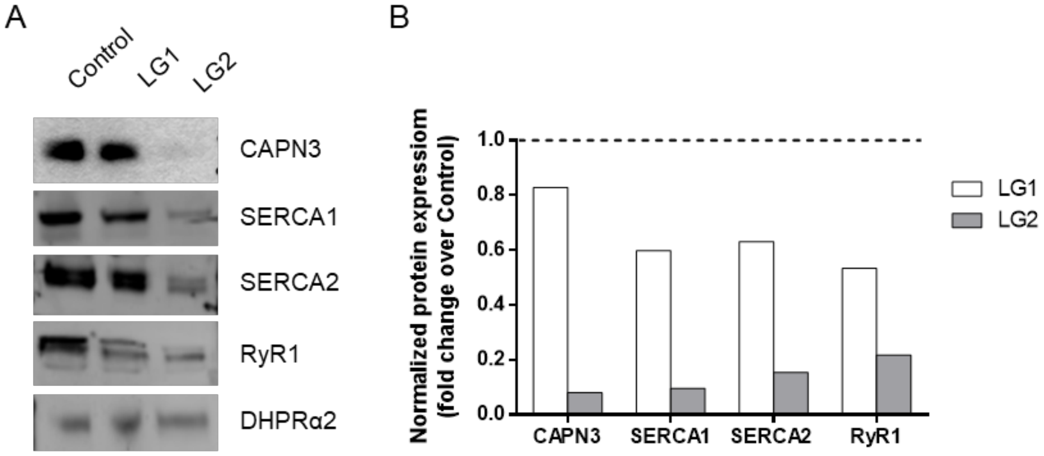

Figure 23. Characterization of human primary immortalized LGMDR1 and control myotubes at the protein level. A) Representative images of western blot signals for CAPN3, SERCA1, SERCA2 and RyR1. B) Quantification of the signals from western blot, normalized by the signal from DHPRα2. Data expressed as mean fold change. N=1.

According to the effect of mRNA levels, after 24h of BTZ treatment, we observe a two-fold increase in SERCA2 protein expression in LG1 and LG2 myotubes, together with a very pronounced decrease in SERCA1 levels, approximately 10 times. Furthermore, in both cell lines, BTZ causes an increase in SR stress markers, especially in the cases of *CHOP* and *GRP78* (Figure 24C). *c-FLIP* levels are also increased in the myotubes of the two patients after BTZ treatment. Overall, the effect of BTZ is very similar in myotubes from patients and CAPN3-silenced myotubes, causing an increase in the levels of SERCA2, *c-FLIP* and SR stress markers, and a reduction in the levels of SERCA1 (Figure 24).

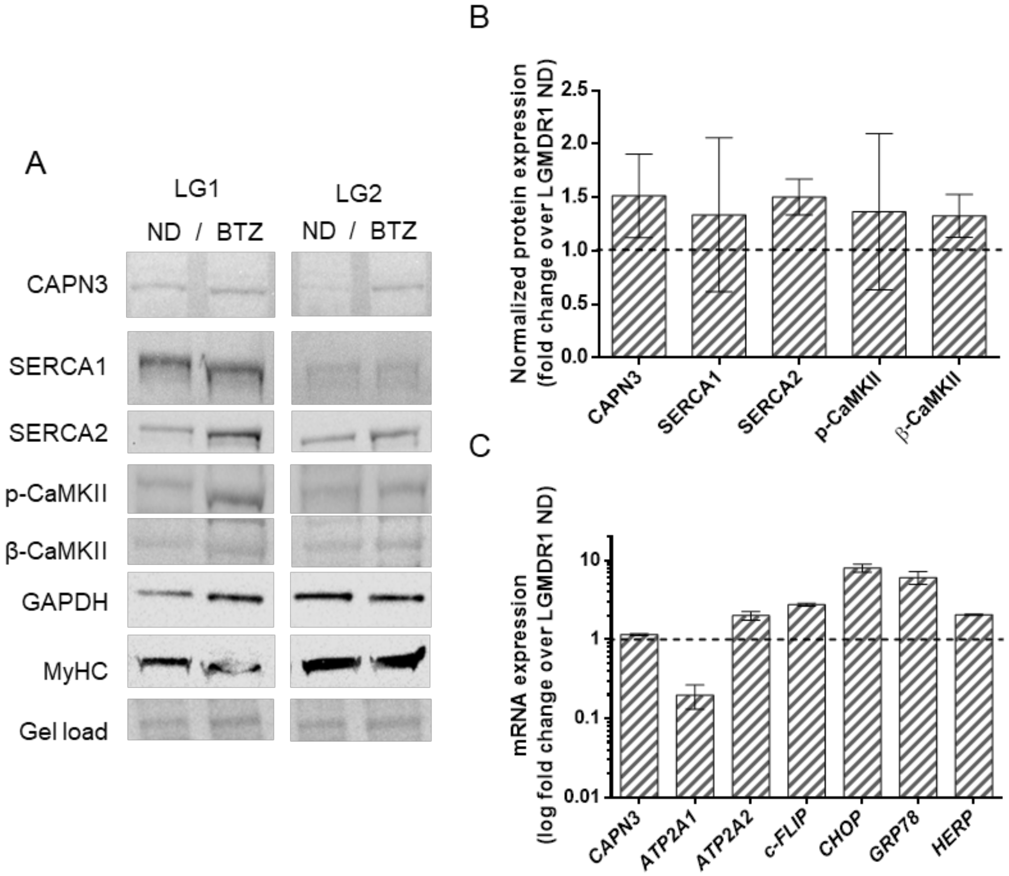

Figure 24. Effect of BTZ treatment on protein and mRNA expression in immortalized human primary LGMDR1 myotubes. A) Representative western blot signals from LG1 and LG2 myotubes treated with 5nM BTZ for 24h after 5 days in differentiation. Signals of CAPN3, SERCA1, SERCA2, p-CaMKII, β-CaMKII, GAPDH, MyHC, and gel load are represented. B) Quantification of western blotting signals of BTZ treated LG myotubes, represented by fold change over non-treated myotubes. Non-treated (ND) LG expression levels are shown as a discontinuous line. C) Gene expression of *CAPN3, ATP2A1, ATP2A2, c-FLIP, CHOP, GRP78* and *HERP* in 5nM BTZ treated LG myotubes. Non-treated LG expression levels are shown as a discontinuous line. Data expressed as mean fold change ±SEM. N=2 LG.

SERCA protein expression in C3KO model

Up to now, several animal models have been generated with the idea of recapitulating the pathophysiological characteristics of LGMDR1. One of the most used models is the C3KO mouse generated by the group led by Dr Melissa J. Spencer, (UCLA, USA). In this model, a premature STOP translational signal is generated in the *Capn3* gene resulting in the absence of the protein. This model has been previously characterized in adulthood. However, we wanted to study its phenotype at an earlier stage of the disease in order to evaluate SERCA levels in preclinical stages. As we expected, when evaluating C3KO mice at 2 months of age, no significant changes have been observed in terms of grip strength (Figure 25) or in terms of resistance to fatigue of the dystrophic mice compared to controls (Figure 26).

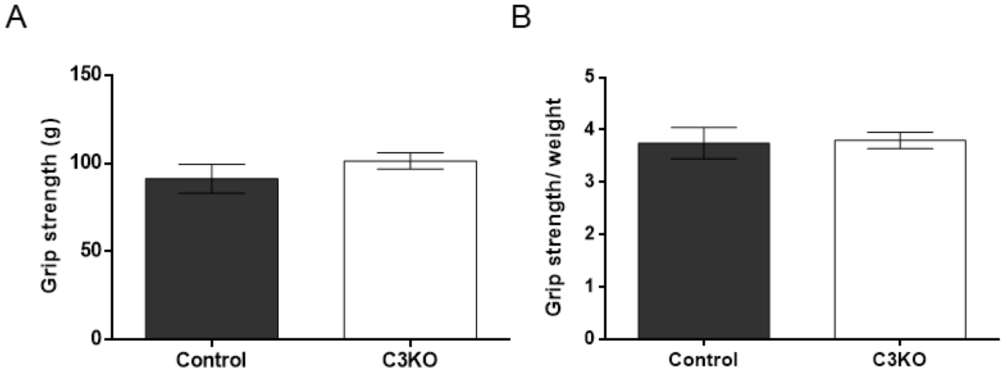

Figure 25. Forelimb grip strength of young control and C3KO mice. A) Non-normalized grip strength data. B) Grip strength normalised to body weight. Data expressed as mean ±SEM. N=8 2-month-old male mice for each genotype. No significant differences were observed (unpaired t-test).

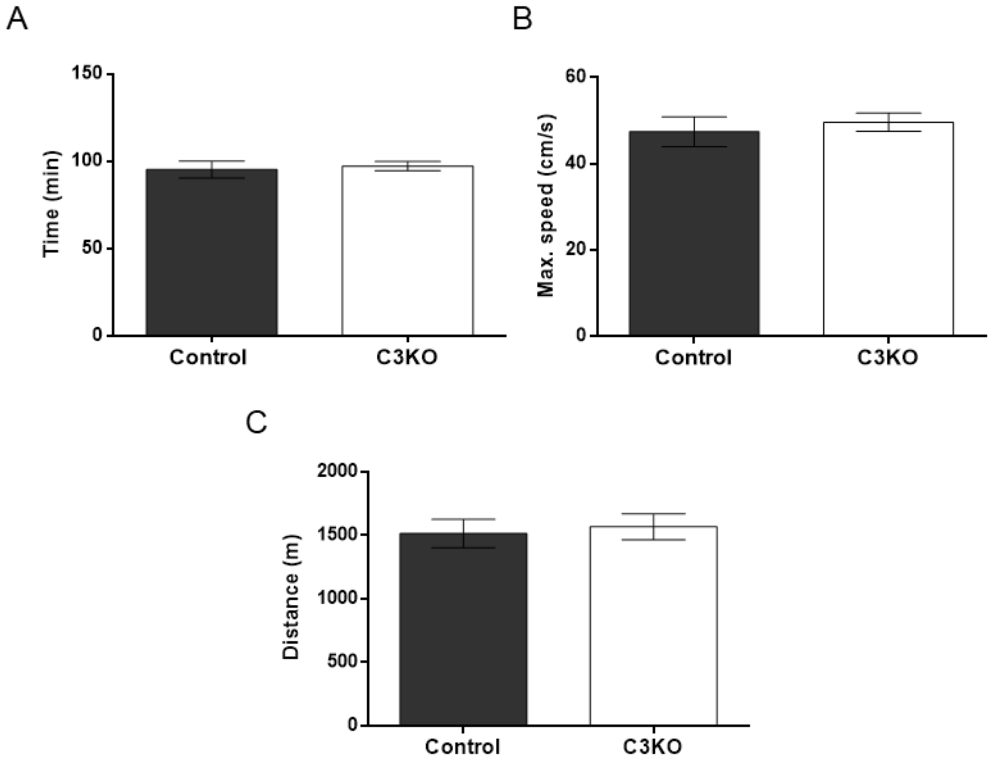

Figure 26. Results of run-to-exhaustion test in young control and C3KO mice. A) Running time; B) speed; and C) distance for control and C3KO mice are shown. Data expressed as mean ±SEM. N=5 2-month-old male mice per group. No significant differences were observed (unpaired t-test).

Soleus and diaphragm are among the most affected muscles in the C3KO model [136]. To date, the expression of SERCA has not been analysed in this model, so we have assessed its expression in the mentioned muscles. Indeed, we have observed that in the *soleus* the expression of SERCA1 in C3KO mice is significantly lower than in controls, decreasing by 23% (0.78 ± 0.043 in C3KO vs. 1 ± 0.055 in control;

p<0.05). However, no changes are observed in SERCA2 expression (Figure 27). Regarding the diaphragm, we observe that the levels of both, SERCA1 and SERCA2, are significantly reduced, by 20% for SERCA1 (0.8 ± 0.056 in C3KO vs. 1.0 ± 0.06 in control; *p*<0.05) and 39% for SERCA2 (0.61 ± 0.052 in C3KO vs. 1.0 ± 0.053 in control; *p*<0.0001) (Figure 28).

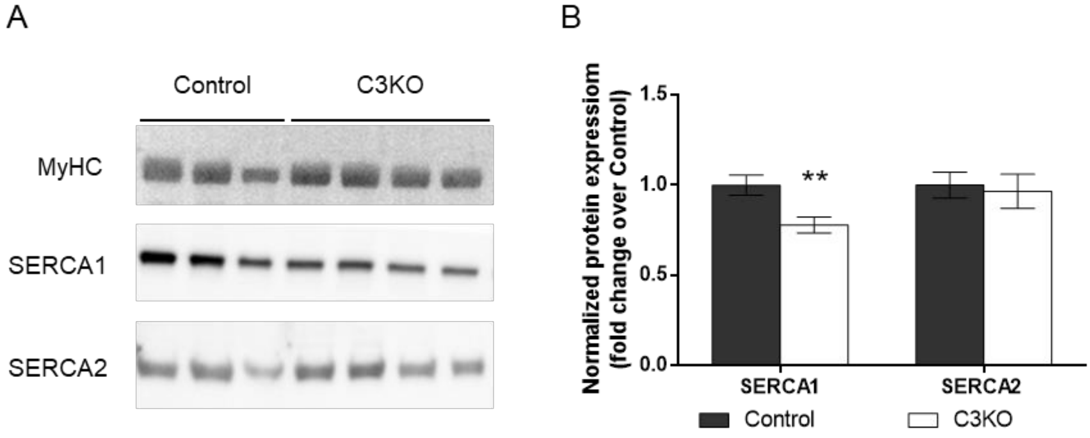

Figure 27. Characterization of SERCA expression in *soleus* muscle of young control and C3KO mice. A) Representation of western blot signals obtained from SERCA1, SERCA2 and MyHC expression. B) Analysis of the western blot signals normalized by maturation marker MyHC signal. Data expression are represented as mean fold change ±SEM. N=8 per each genotype (2-month-old mice). ***p*<0.01 vs. control (unpaired t-test).

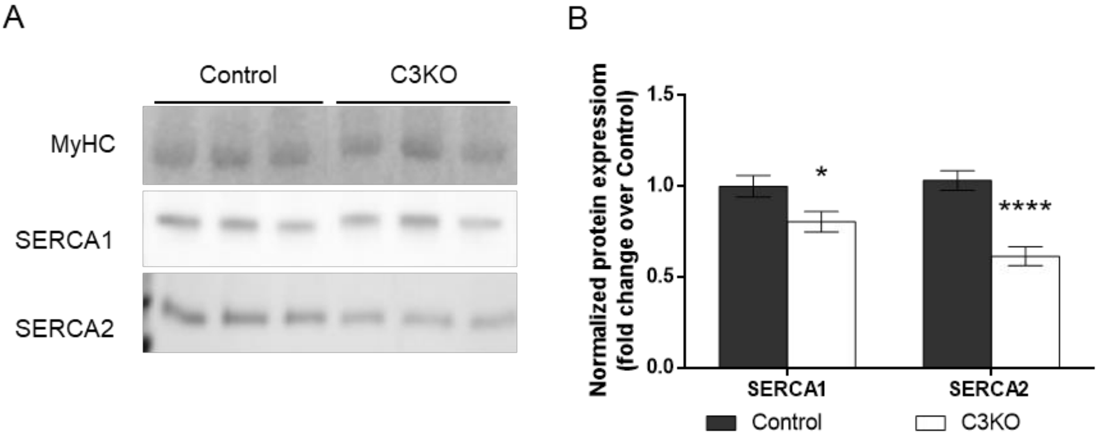

Figure 28. Characterization of SERCA expression in the diaphragm of young control and C3KO mice. A) Representation of the signals obtained from SERCA1, SERCA2 and MyHC expression by western blot. B) Analysis of the western blot signals normalized by MyHC expression and represented as mean ±SEM. N=8 per each genotype (2-month-old mice). **p*<0.05 vs. control; *****p*<0.0001 vs. control (unpaired t-test).

Taking into account the decrease in the expression of SERCAs in the diaphragm, we have analysed whether this phenomenon translates into a lower force of this specific muscle using the *in vitro* set up of the 1300A whole animal system apparatus (Aurora Scientific). In this case, we have observed that the specific twitch force of the diaphragm is 54% lower in C3KO mice compared to the diaphragms of controls ($p<0.05$) (Figure 29A). Moreover, the tetanic isometric force shown is also significantly lower in the case of dystrophic animals, reduced approximately by half ($p<0.05$) (Figure 29B).

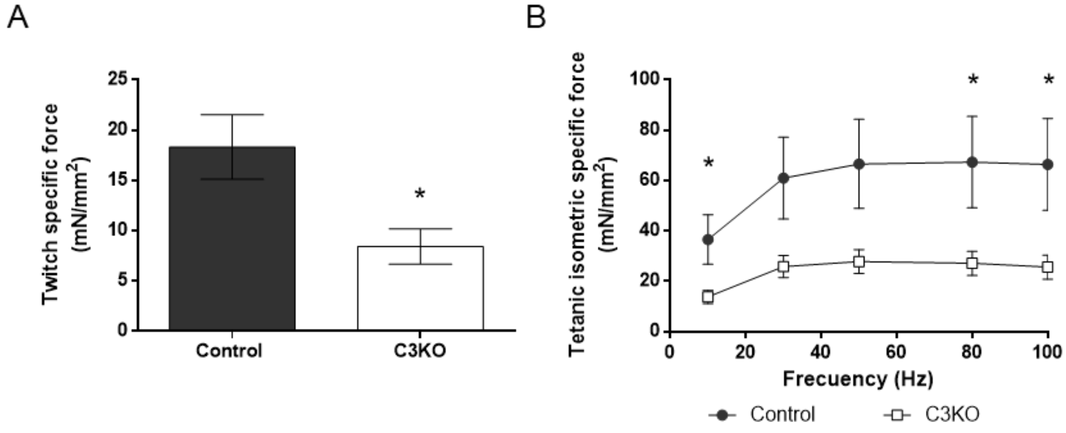

Figure 29. ***In vitro*** **diaphragm force analysis in young control and C3KO mice.** A) Specific force obtained by single 1A isometric stimulation on a 4mm wide diaphragm strip from control and C3KO mice. Data are normalised by diaphragm piece weight. B) Tetanic force of control and C3KO diaphragms. Data are normalised by diaphragm cross-sectional area (CSA). Data expressed as mean ±SEM. N=9 control, N=10 2-month-old C3KO mice. *$p<0.05$ vs. control (unpaired t-test in A; multiple t-test in B).

In addition to the loss of strength, previous studies suggest that hyper-CKemia could be a phenomenon that can occur in humans, in early stages [100],[140]. For this reason, we wanted to check if the C3KO murine model replicates this fact, observing that, at 2 months of age, no significant differences are seen between C3KO and control mice, although there is a slight upward trend (Figure 30).

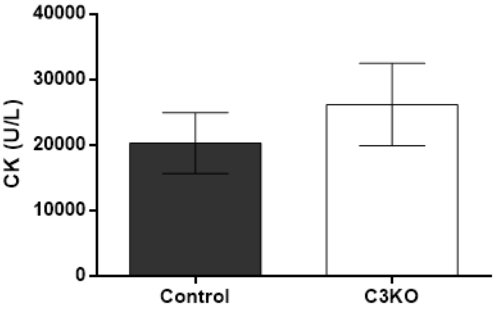

Figure 30. Serum creatine kinase (CK) levels of young control and C3KO mice. Data are expressed as mean ±SEM. N=4 2-month-old mice per each genotype. No significant differences were observed (unpaired t-test).

Another of the pathophysiological mechanisms described in LGMDR1 muscular dystrophy is the dysregulation of calcium homeostasis. Along these lines, Dr Spencer's group has described alterations in calcium homeostasis in adult C3KO mice [153],[267]. In our case, we have observed in the isolated fibres of the *flexor digitorum brevis* (FDB) muscle that C3KO mice do not present differences in basal intracellular calcium levels compared to control mice at 2 months of age (Figure 31). This result wasn´t unexpected, since we previously described that CAPN3-deficient murine myotubes do not present alterations in basal calcium levels in contrast to human myotubes [134]. A possible explanation for this phenomenon could be the greater capacity of murine muscle to buffer intracellular calcium levels, by expressing the protein parvalbumin, which has a great capacity to chelate cytosolic calcium.

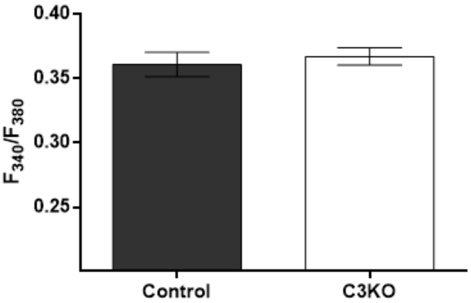

Figure 31. Resting intracellular calcium levels of FDB-isolated myofibres from young control and C3KO mice. Data expressed as mean ±SEM. 115-155 fibres analysed from N=4 2-month-old mice. No significant differences were observed (unpaired t-test). FDB, *flexor digitorum brevis*.

Next, we have evaluated the deficiencies of SERCA in the C3KO model of almost one year of age, since the most severe phenotype is described in adulthood [19],[43],[153]. The evaluation of grip strength concludes that at this age, C3KO mice do not show significant differences with respect to controls. In both, control and C3KO mice, a significant reduction in normalized force is observed with respect to 2-month-old young mice. This decrease in normalized force is probably due to the gain of weight of the mice ($p<0.05$ in controls and $p<0.0008$ in C3KO) (Figure 32).

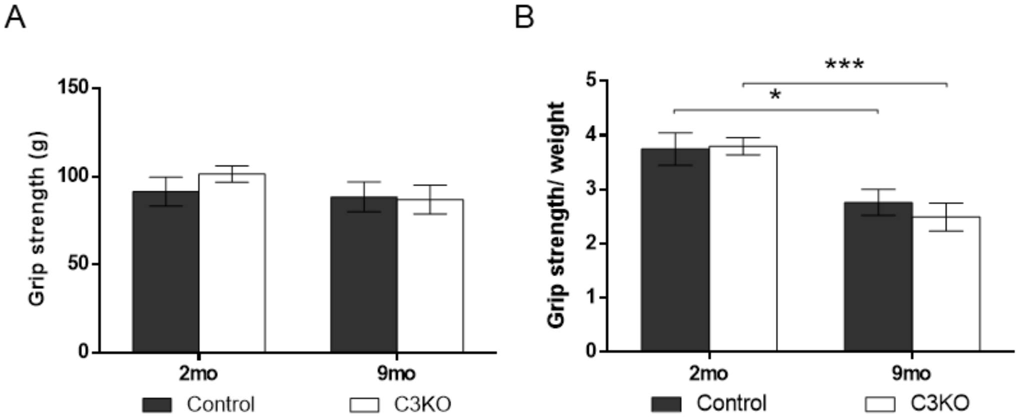

Figure 32. Forelimb grip strength of young and adult control and C3KO mice. A) Non-normalised grip strength. B) Grip-strength data normalised to the body weight. mo, months. Data expressed as mean ±SEM. N=8 mice for young (2mo) mice from each genotype; N=9 mice for adult (9mo) mice from each genotype. No significant differences were observed in A. **p*<0.05 vs. control; *****p*<0.001 vs. C3KO in C (unpaired t-test).

Subsequently, we have evaluated the ability of dystrophic animals to perform voluntary exercise by introducing voluntary wheels installed in individual cages (Med Associates Inc.). This analysis has not previously been performed in C3KO mice, but has been used in other muscular dystrophy models [268]. In our study, we have observed that C3KO mice show a tendency to run a shorter distance in 24h than controls, but none of the parameters evaluated (distance, average speed, maximum speed or exercise time) reached statistical significance (Figure 33).

Moreover, the locomotor function of C3KO mice has been analysed using the six-minute walk test following a protocol previously described in the literature [261]. To do this, we analyzed the distance covered by the mice for 6min in an open field before and after performing a light force training of 13 minutes on the treadmill [261]. However, no differences were observed in terms of the covered distance during the six minutes of open field as well as after performing the forced exercise (Figure 34).

In addition to the aforementioned functional tests, we wanted to analyse the phenotype at the histological level, where it had been previously observed that C3KO mnice had a smaller cross-sectional area (CSA) in both, fast (*gastrocnemius* [136]) and slow (*soleus* [136],[201]) fibres. In this case, we have analysed the CSA of the diaphragm fibres of this model without observing significant differences between dystrophic and control mice (Figure 35). Differences in the percentage of fast and slow fibres have been neither found, although C3KO mice show a small tendency to have greater number of slow fibres compared to controls (Figure 36).

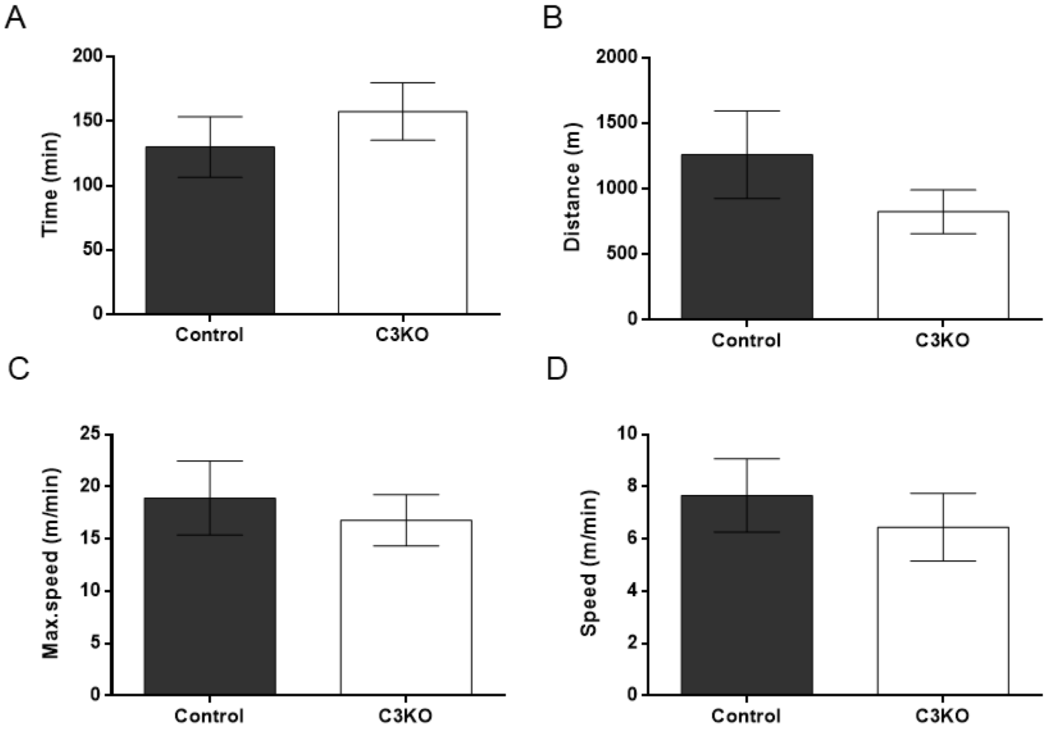

Figure 33. Voluntary exercise performed for 24h by adult control and C3KO mice. A) Running time; B) running distance; C) maximum speed; and D) mean speed. Data expressed as mean ±SEM. N=10 control; N=9 C3KO. Adult, 9-month-old mice. No significant differences were observed (unpaired t-test).

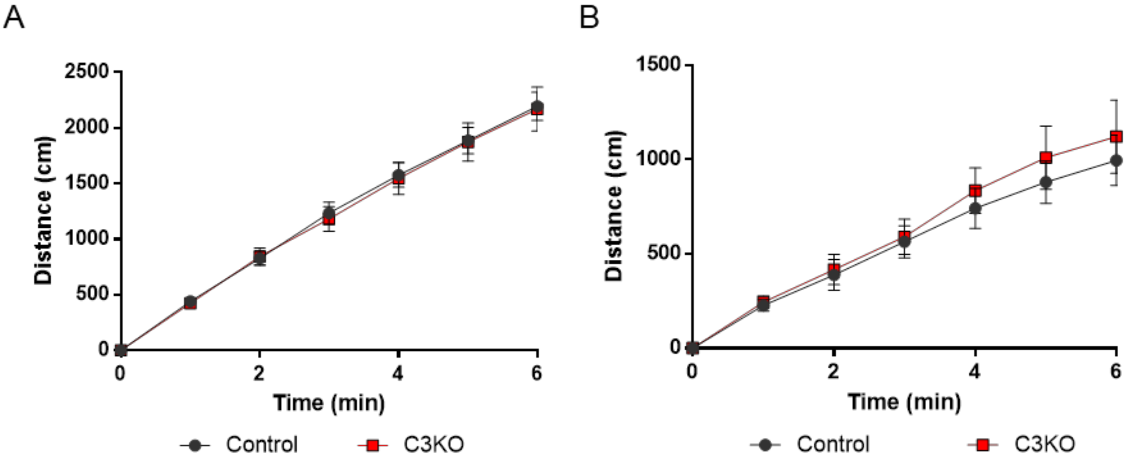

Figure 34. Six-min-walk test in open field of adult control and C3KO mice. A) Walking distance over 6 minutes, before treadmill mild exercise. B) Walking distance over 6 minutes, after treadmill mild exercise. Data presented as mean ±SEM over time. N=10 control; N=9 C3KO. Adult, 9-month-old mice. No significant differences were observed (multiple t-test).

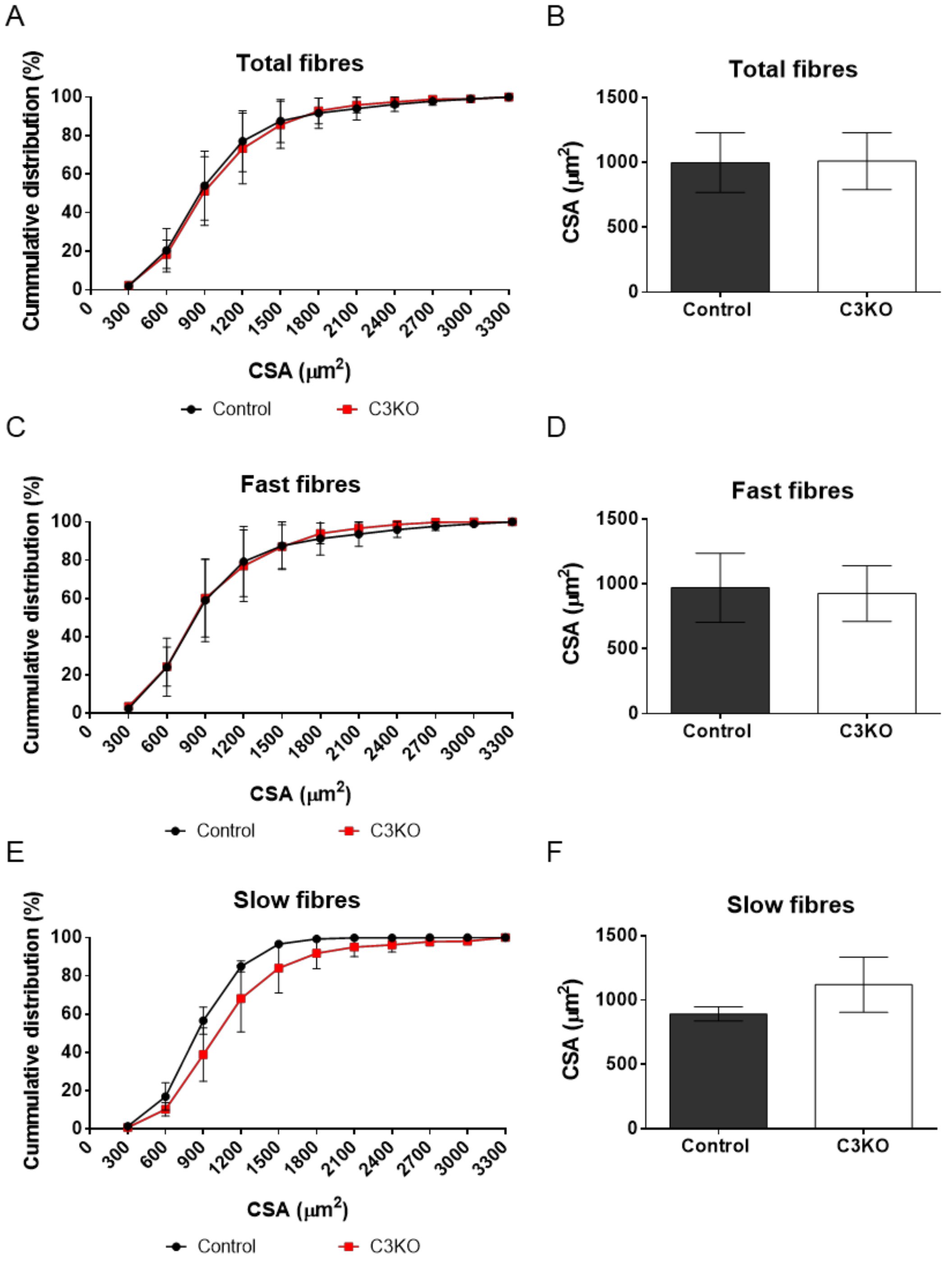

Figure 35. Analysis of muscle fibres CSA of adult control and C3KO mice diaphragms. Cumulative frequency of cross-sectional area (CSA) (left panels) and mean CSA (right panel) of A-B) total fibres, C-D) fast fibres, and E-F) slow fibres. Data are presented as mean ±SEM. N=3 for each genotype (9-month-old mice). No significant differences were observed (multiple t-test in A, C and E; unpaired t-test in B, D and F).

On the other hand, we have analysed the central nucleation present in the fibres, as it is a marker of muscle regeneration, symptom of impair homeostasis [269]. We have been able to verify that in the 9-month-old C3KO mice there is a significant increase in the central nucleation of the fibres compared to the controls (0.74 ± 0.14

in C3KO vs. 0.13 ± 0.88 in control; $p<0.05$), but in less than 1% (Figure 37), much lower than that which occurs in other dystrophic models, such as the *mdx* mouse, with frequencies greater than 40% [270]. In any case, this result corresponds to data previously reported in the *soleus* muscle of 8-week-old C3KO mice, which shows a frequency of fibres with central nuclei of less than 5% [271].

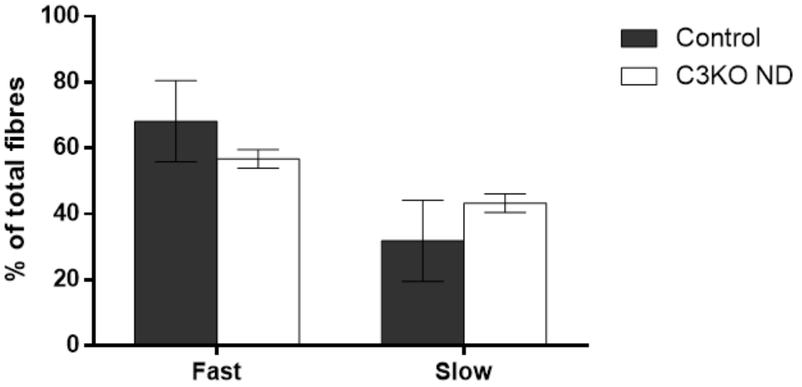

Figure 36. Percentage of fast and slow fibres among total fibres in adult control and C3KO mice diaphragms. Data are presented as mean % ±SEM. N=3 for each genotype (9-month-old mice). No significant differences were observed (unpaired t-test).

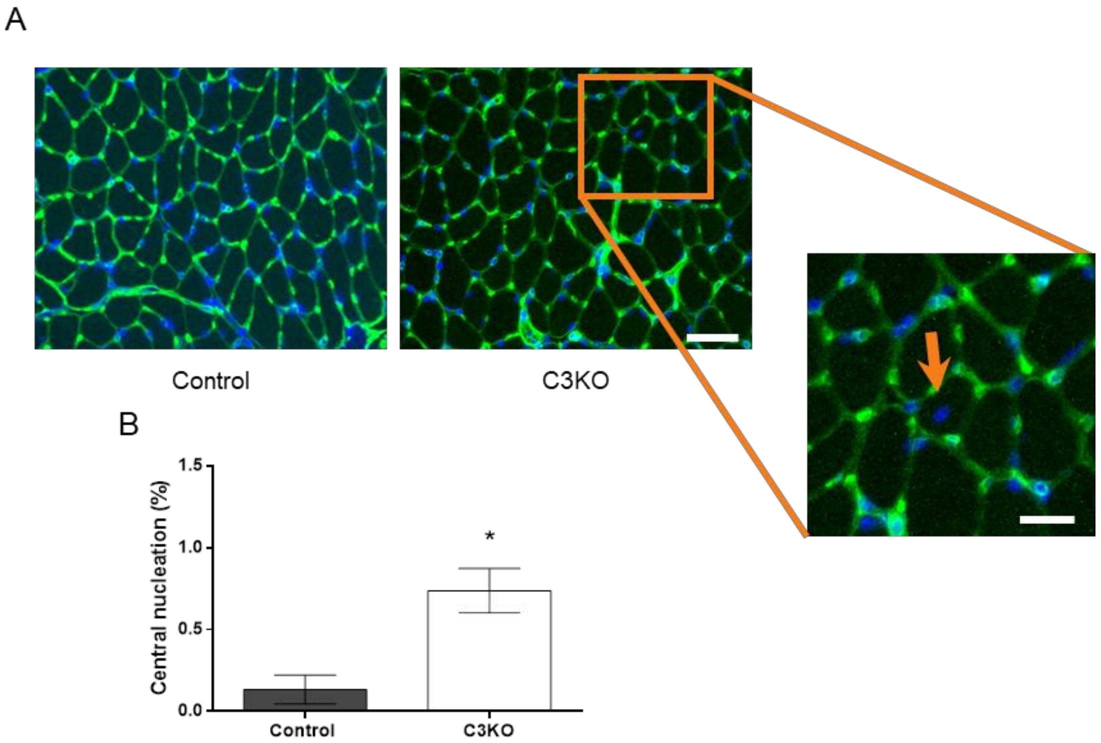

Figure 37. Analysis of central nucleation of control and C3KO adult mouse diaphragm cryosections by immunofluorescence. A) Representative images of immunofluorescent staining of Collagen IV (green) and nuclei (blue). Orange arrow indicate central nuclei. Scale bar: 50µm and 25µm in magnification. B) Quantification of the percentage of nucleated fibres. Data are presented as mean % ±SEM. N=3 for each genotype (9-month-old mice). *$p<0.05$ (unpaired t-test).

Effect of BTZ treatment in C3KO mice

After observing the decrease in SERCA expression in the 2-month-old mice and the tendency to low voluntary mobility of dystrophic mice at 9 months, we decided to analyse the effect of the ubiquitin proteasome inhibition by BTZ on the phenotypic altered factors of the 9-month-old C3KO mice.

To do so, an administration protocol was carried out based on a previous study in the Duchenne animal model, *mdx* mice, with the aim of recovering the expression of dystrophin [262]. 0.8mg/kg BTZ (Velcade®) was administered twice weekly intravenously for 3 weeks. During the treatment, no drastic changes have been observed in the evolution of mice body weight (Figure 38).

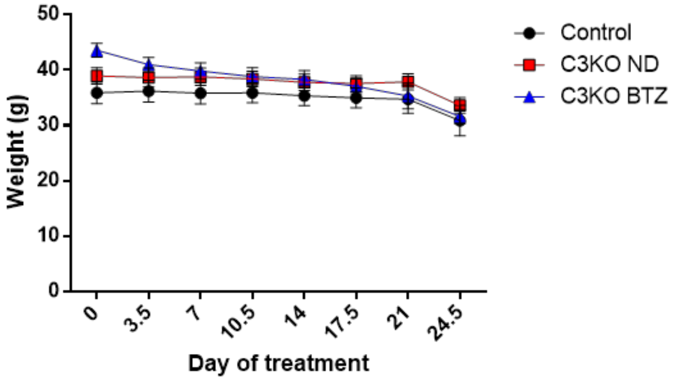

Figure 38. Body weight evolution during BTZ treatment of adult mice. Data are presented as mean ±SEM. N=10 non-treated control, N=9 vehicle-treated (ND) C3KO, N=7 BTZ-treated (0.8 mg/kg) C3KO. Adult, 9-month-old mice. No significant differences were observed (one-way ANOVA post hoc Dunnett's test).

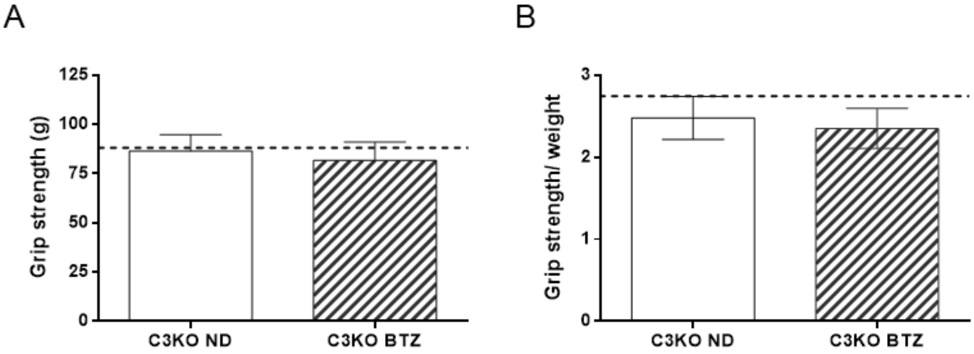

Figure 39. Forelimb grip strength of adult mice after BTZ treatment. A) Non-normalised grip strength. B) Grip strength data normalised to body weight. Non-treated (ND) C3KO control values are represented as a discontinuous line. Data expressed as mean ±SEM. N=9 vehicle-treated C3KO, N=7 BTZ-treated (0.8 mg/kg). C3KO. Adult, 9-month-old mice. No significant differences were observed (one-way ANOVA post hoc Dunnett's test).

Assessing grip strength tests performed prior to sacrifice, no changes have been detected in BTZ treated mice compared to untreated dystrophic mice (Figure

39). Likewise, no changes have been observed in the running distance, the running time, or the speed achieved during voluntary exercise with the BTZ treatment (Figure 40). However, BTZ treated mice show a little trend to have greater mobility in six minute-walk test after treadmill mild exercise (Figure 41).

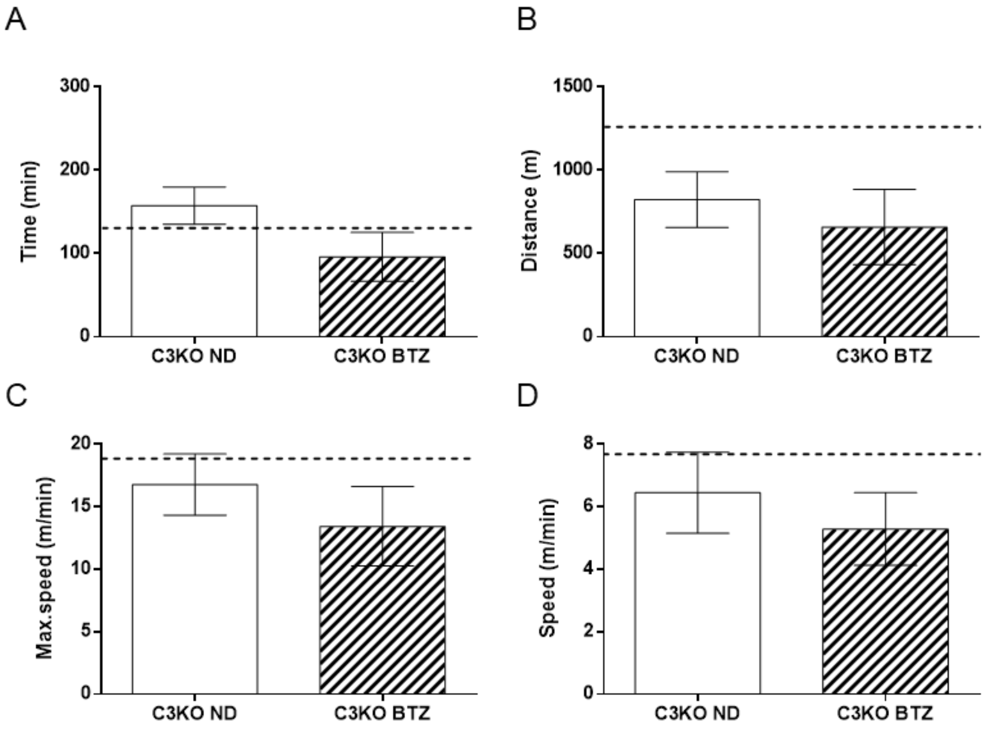

Figure 40. Voluntary exercise of adult mice after BTZ treatment. A) Running time; B) distances; C) maximum speed; and D) mean speed are represented in C3KO BTZ vs. C3KO ND. Non-treated (ND) C3KO control values are represented as a discontinuous line. Data expressed as mean ±SEM. N=9 C3KO ND, N=7 BTZ-treated (0.8 mg/kg) C3KO. Adult, 9-month-old mice. No significant differences were observed (one-way ANOVA post hoc Dunnett's test).

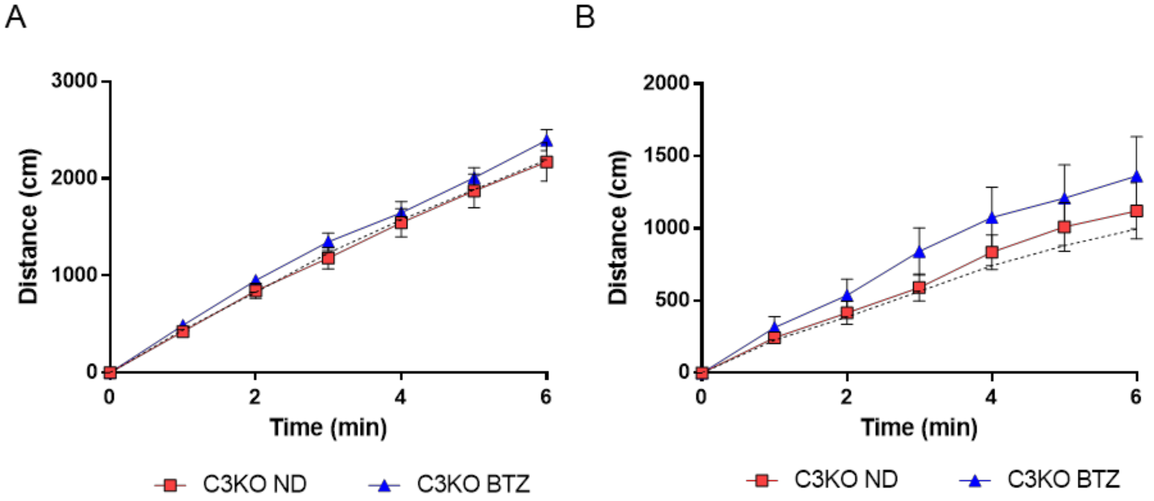

Figure 41. Six-min-walk test in the open-field of adult mice after BTZ treatment. Walking distance of C3KO mice over six minutes A) before and B) after performing treadmill mild exercise. The discontinuous line represents control non-treated (ND) C3KO mice behaviour. Data presented as mean ±SEM over time. N=9 C3KO ND; N=7 BTZ-treated (0.8 mg/kg) C3KO. Adult, 9-month-old mice. No significant differences were observed (one-way ANOVA post hoc Dunnett's test).

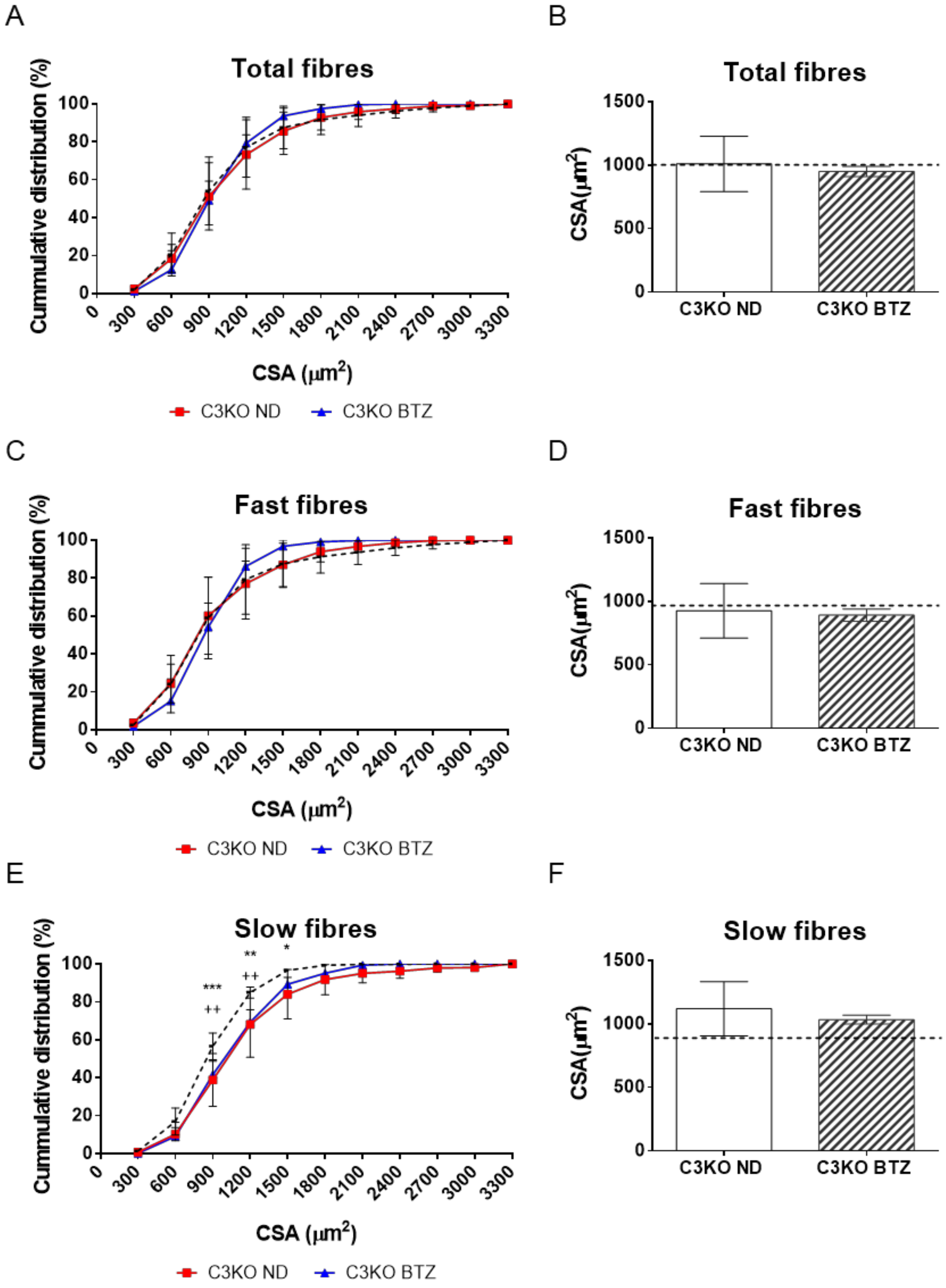

Figure 42. Analysis of muscle fibres CSA in adult mice after BTZ treatment. Cumulative frequency of cross-sectional area (CSA) (left panels) and mean CSA (right panel) of A-B) total fibres, C-D) fast fibres, and E-F) slow fibres. Control values are represented as a discontinuous line. Data are presented as mean ±SEM. N=3 for each genotype (9-month-old mice). No significant differences were observed in A, B, C, D and F. *$p<0.05$; **$p<0.01$; ***$p<0.001$ C3KO ND vs. control; ++ $p<0.01$ C3KO BTZ vs. control (Repeated-measures one-way ANOVA post hoc Dunnett's test in A, C and E; one-way ANOVA post hoc Dunnett's test in B, D and F).

According to histological analysis, the inhibition of UPS did not significantly affect the percentage of fibres with central nuclei, nor did it affect the proportion of fast and slow fibres observed in the diaphragms of C3KO mice or their size. (Figures 42-44).

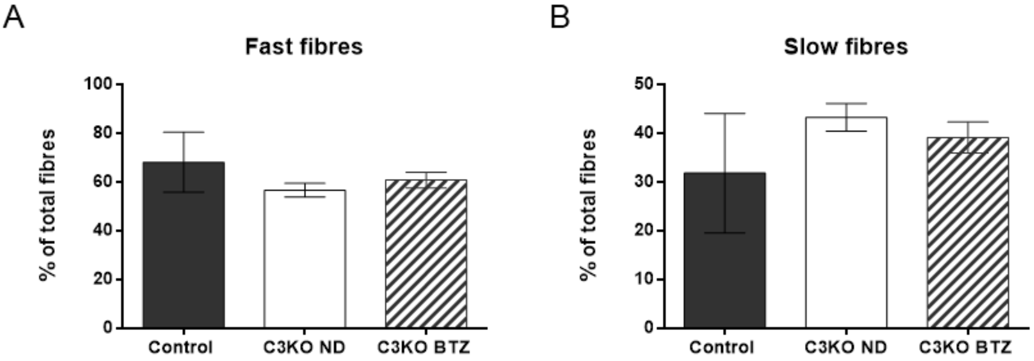

Figure 43. Proportion of fast and slow fibres in *soleus* from adult mice after BTZ treatment. A) Fast fibres percentage over total fibres. B) Slow fibres percentage over total fibres from non-treated (ND) C3KO and BTZ-treated (0.8 mg/kg each 3.5 days) C3KO mice. Data are presented as mean % ±SEM. N=3 for each genotype (9-month-old mice). No significant differences were observed (one-way ANOVA post hoc Dunnett's test).

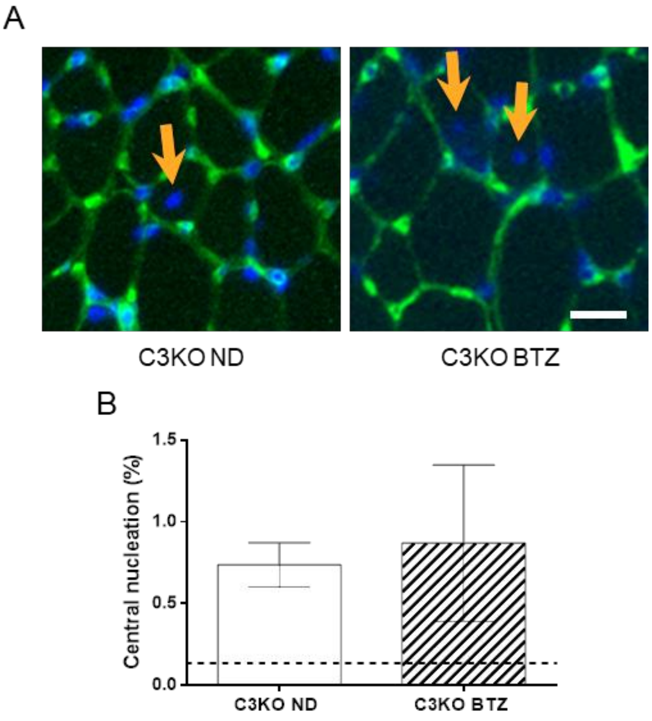

Figure 44. Analysis of central nucleation of adult mouse diaphragms after BTZ treatment. A) Representative images of immunofluorescent staining of Collagen IV (green) and nuclei (blue). Orange arrows indicate central nuclei. Scale bar: 25µm. B) Quantification of the percentage of centrally nucleated fibres. A discontinuous line shows data from control diaphragms. Data are presented as mean % ±SEM. N=3 for each genotype (9-month-old mice). No significant differences were observed (unpaired t-test). ND, non-drug. BTZ, 0.8 mg/kg.

At the molecular level, the effect of BTZ treatment on the expression of different genes whose expression has been previously altered in this same model has been analysed [43]. At the same time, we have evaluated the expression of genes whose transcription is affected by the activation of CaMKII, which are myofibrils genes such as *Myl2, Myom3, Ckmt2* and *Myo18b*, or which are related to lipid metabolism, such as *Lpl* and *Pnpla2*. Our results indicate that there is a global trend to increase the expression of these genes in C3KO mice. Strikingly, its expression is downregulated with BTZ treatment even beneath control levels (Figure 45). We have also checked the expression of *Mmp9,* an activator of fibrosis inductor *Tgfb1,* which remains unchanged in untreated dystrophic mice. These data suggest that the slow fibre myogenic program is unaffected in non-exercised mice while supporting the absence of changes in slow fibre ratio and area shown in figures 35-36 and 42-43.

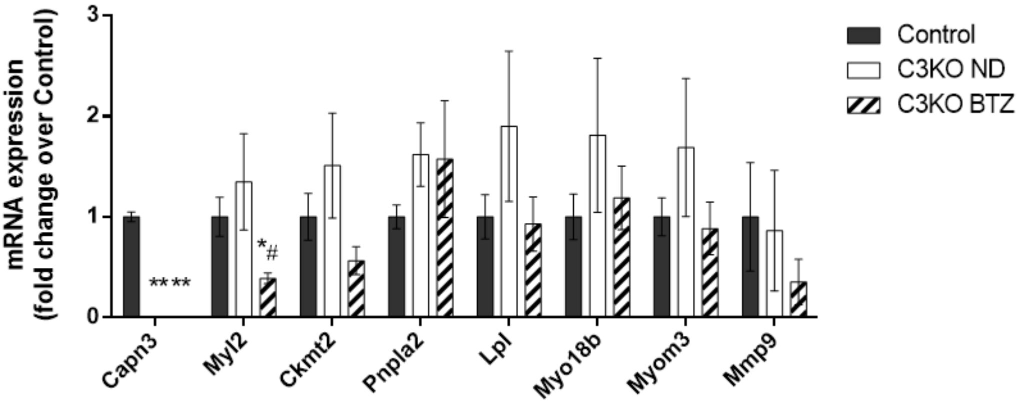

Figure 45. Gene expression analysis of adult mouse diaphragms after BTZ treatment. Among the genes activated by CaMKII signalling, *Myl2, Ckmt2, Pnpla2, Lpl, Myo18b* and *Myom3* are shown. Data are expressed as mean fold change ±SEM. N=6-9 mice per group (9-months-old mice). *$p<0.05$; **$p<0.01$ vs. control; # $p<0.05$ vs. C3KO ND (non-drug) (one-way ANOVA post hoc Tukey's test). BTZ, 0.8 mg/kg.

Muscle regeneration upon muscle injury has been suggested to be another of the affected processes in C3KO mice. For the correct performance of the process, the activation of different genes is necessary, among them, *Ppargc1* and *Tgfb1* [138]. *Ppargc1* is the gene that encodes the PGC1α protein, being a key regulator of mitochondrial biosynthesis. Previous studies suggested that *Ppargc1* expression is slightly decreased in *Capn3*-deficient mice due to low signalling of the CaMKII pathway [43]. In control mice, the expression of this gene increases during the muscle regeneration process; however, C3KO mice fail in its induction. In our study, on the contrary, we have detected that in the diaphragm of dystrophic mice the expression of *Ppargc1* tends to increase (Figure 46). Furthermore, BTZ treatment restores the expression, reaching the expression observed in control mice (Figure 46).

On the other hand, *Tgfb1* is a potent inhibitor of myogenic differentiation that increases after muscle damage, participating in the early transitory inflammatory process, which, if persisting, contributes to the formation of fibrotic tissue [272]. Previously, it had been observed that undamaged C3KO mice did not show altered expression of *Tgfb1* [138]. However, our data show a clear increase in its expression in the diaphragm. Moreover, BTZ treatment decreases *Tgfb1* levels, an effect that could be beneficial as previously described for other myopathies [273]–[278] (Figure 46).

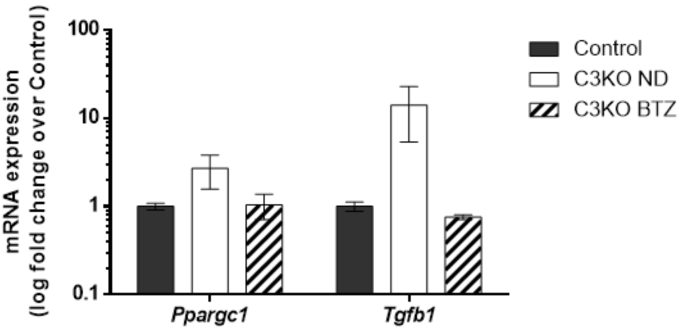

Figure 46. Gene expression analysis of mitochondrial biosynthesis marker Ppargc1 and myogenic inhibitor *Tgfb1* of adult mouse diaphragm. Data are expressed as mean fold change ±SEM. N=3-7 mice per group (9-months-old mice). No significant differences were observed (one-way ANOVA post hoc Dunnett's test). ND, non-drug. BTZ, 0.8 mg/kg.

Finally, the effect of BTZ treatment on SERCA expression has been assessed with no effects on its expression. Besides, CaMKII activation also did not undergo any modification (Figure 47).

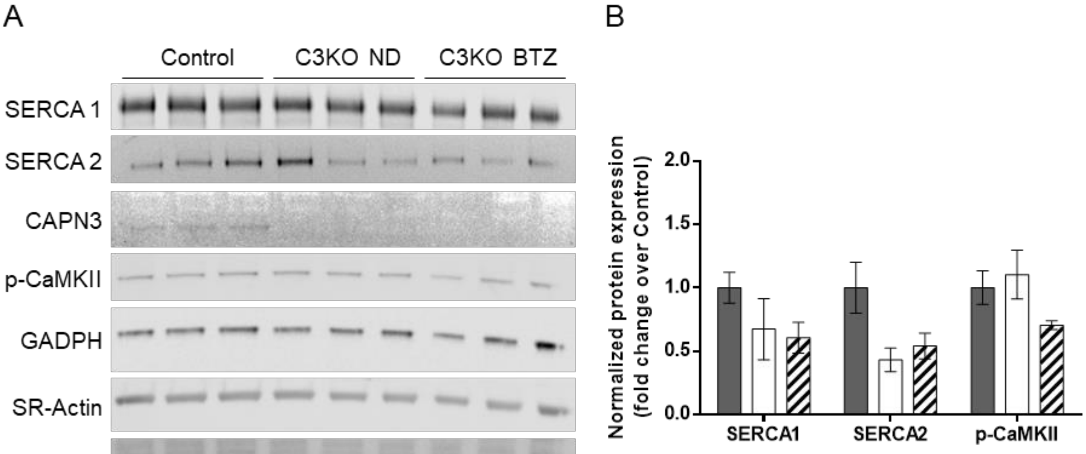

Figure 47. Characterization of SERCAs and p-CaMKII expression in diaphragms from adult BTZ-treated mice. A) Representation of the signals obtained by western blot for SERCA1, SERCA2, CAPN3, p-CaMKII, MyHC, GAPDH, SR-actin and gel load of non-treated (ND) control, non-treated C3KO and BTZ-treated (0.8 mg/kg) C3KO mice. B) Analysis of western blot signals from SERCA1, SERCA2, and p-CaMKII normalized by gel load signal. Data expressed as mean fold-change ±SEM. N=5-9 per each group (9-month-old mice). No significant differences were observed (one-way ANOVA post hoc Dunnett's test).

Since SERCA expression was not significantly modified by BTZ treatment, we assessed the activity of the UPS degradation pathway in non-treated and BTZ treated mice, observing inefficient inhibition of UPS with the employed BTZ dose (Figure 48). Therefore, BTZ treatment could trigger little molecular modifications but without effective big changes.

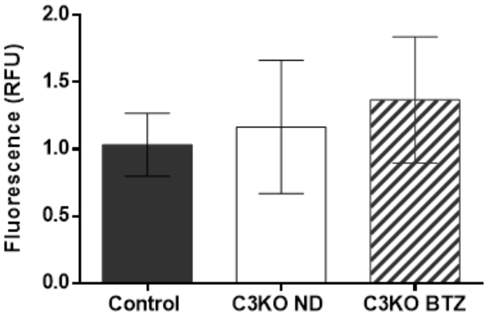

Figure 48. Ubiquitin proteasome activity in *soleus* muscle of adult mice after BTZ treatment. UPS activity measured by fluorometric enzymatic assay in non-treated (ND control, non-treated C3KO and BTZ-treated (0.8 mg/kg) C3KO mice. Data represented as mean ±SEM. N=6 control; N=3 C3KO ND; N=3 BTZ-treated C3KO. Adult, 9-month-old mice. No significant differences were observed (one-way ANOVA post hoc Dunnett's test).

SERCA protein expression in *C3 null* rat model and the effect of UPS inhibition.

DISCUSSION

CAPN3 deficiency generates SERCA deficiency in human *in vitro* myotubes

CAPN3 deficiency leads to alteration in calcium homeostasis in murine models where the structural function is absent [152]. Additionally, as part of the triad, CAPN3 may play a role stabilizing RyR, AldoA, and CaMKII within this structure, in addition to interacting with SERCA1 [19],[152],[153]. Due to the high homology among SERCA1 and SERCA2, it has been suggested that CAPN3 could interact with SERCA2 as well [134]. Recently, we have found reduced SERCA protein expression in muscle biopsies from LGMDR1 patients [134], which could prompt higher resting cytosolic [Ca^{2+}] in human myotubes [134], and lower SR Ca^{2+} content, as observed in *C3*$^{-/-}$ mice myotubes [154]. Therefore, our first objective focused on analysing the effect of CAPN3 deficiency over SERCA expression and function in human *in vitro* LGMDR1 models.

To delve in the role of CAPN3 deficiency in calcium homeostasis, we have generated new human *in vitro* models based on downregulating *CAPN3* gene expression. For this purpose, we have used immortalized human myotubes from two healthy donors, confirming that induced CAPN3 deficiency triggers concomitant decrease of SERCA1 and SERCA2 proteins. However, the expression levels of *ATP2A1* (SERCA1) and *ATP2A2* (SERCA2) mRNAs remain unaltered, indicating possible post-trascriptional or post-traslational modifications on SERCA that could affect its protein expression and/or function. Therefore, SERCA expression might be reduced by lower SERCA protein synthesis or by an exacerbated degradation of the protein. Interestingly, in our previous studies, higher ubiquitination of SERCA was observed, suggesting that greater degradation may underlay this misbalance [134].

In addition to increased basal [Ca^{2+}], inhibition of SERCA activity can lead to reduced [Ca^{2+}] in the SR, driving the activation of the Unfolded Protein Response (UPR) [282] in the reticulum. Indeed, our results in CAPN3-deficient LHCN-M2 myotubes have shown upregulation of different SR stress markers, such as *CHOP, HERP*, *GRP78* and the ratio of *XBP1* spliced and *XBP1*, in highly mature CAPN3-deficient myotubes. Moreover, we have observed that mRNA expression of the antiapoptotic protein c-FLIP is reduced. According to these data, it should be noted that persistent induction of ER stress promotes pro-apoptotic signalling, activating NF-κB pathway, whose activity is actually increased in LGMDR1 muscles [132],[155]. In physiologic conditions, upon NF-κB activation, *c-FLIP* expression is induced, promoting cell survival and cell resistance to apoptosis [283]. However, this compensatory mechanism fails to be induced in LGMDR1 patients [219].

Evidence for enhanced SR stress and UPR has been reported in several other neurodegenerative diseases as in Parkinson's disease, Huntington's disease, amyotrophic lateral sclerosis, sporadic inclusion body myositis, myotonic dystrophy type 1, and dysferlin-deficient muscular dystrophy [49],[50],[284]–[286]. In fact, FDA approved chemical chaperons, IRE1, PERK, ATF6α inhibitors, and AAV-based gene therapies, which are reviewed in [49],[287], have been proposed as different therapeutic strategies for targeting SR stress and UPR.

It is worth mentioning that neither increased SR stress or UPR nor c-FLIP deficiency have been detected in CAPN3-deficient 8220 myotubes, implying that these features could depend on different factors related to muscle sample origin or the employed differentiation protocol. Certainly, despite both healthy donors were male, LHCN-M2 myoblasts are derived from *pectoralis major* from a 41-year-old man while 8220 cells were obtained from an unknown muscle from a 12 years-old boy. On the other hand, while 8220 myoblasts were able to differentiate into mature myotubes in absence of ECM in culture, LHCN-M2 myoblasts needed the addition of an ECM overlay to improve differentiation into mature myotubes. This supplemental component confers myotubes a richer microenvironment as interactions between molecules present in ECM and their receptors play essential roles in muscle development and maintenance, hence, promoting higher mature level [288].

Besides human myoblasts immortalization from healthy donors, Dr Mouly's group has generated immortalized myoblasts from dystrophic patients [289]. Due to the dual function of CAPN3 that comprises the catalytic and the structural function, unlike the silencing method, this strategy lets us analyse the role of specific mutations of *CAPN3* over the pathophysiological features previously described in the literature. In particular, we have had access to two LGMDR1 samples (LG1 and LG2) carrying different pathogenic missense variants, which in contrast to the abnormal morphology previously observed when differentiating primary myoblasts from LGMDR1 patients [196], these myotubes present similar appearance to control myotubes.

On the one hand, LG1 has homozygous c.1699G>T mutation that was described for the first time in 1997 [95] with no report about a possible modulation of CAPN3 expression. Thus, we first analysed this sample, detecting that CAPN3 expression in myotubes was not affected. On the other hand, the LG2 sample carries two mutations: c.1637G>T and c.865C>T. c.1637G>T mutation is not included in the CAPN3 transcript variants database of Leiden [121]. However, c.865C>T mutation has been previously described in combination with c.550delA mutation, to severely reduce CAPN3 expression and delete its catalytic activity [290]. Actually, we have verified that in LG2 myotubes, with combined c.865C>T and c.1637G>T mutations, CAPN3 expression is almost lost. Thereby, we have used two patient samples with different CAPN3 outcomes. In one case CAPN3 is expressed (LG1), though mutated, while in the other sample CAPN3 is absent (LG2).

According to SERCA gene expression in these LG immortalized myotubes, we have observed a significant decrease in *ATP2A2* in both samples. However, this mRNA downregulation is only translated into lower SERCA2 levels when CAPN3 expression is reduced (LG2 myotubes). Moreover, the detriment of SERCA1 at protein and mRNA levels is only detected in this sample. These data suggest that despite having lower gene expression of *ATP2A1* and *ATP2A2*, the non-proteolytic function of CAPN3 plays an essential role maintaining correct SERCA protein expression. Noteworthily, in general, patient carrying two null mutations in their *CAPN3* alleles develop a more severe phenotype with an earlier onset, compared to patients that port at least one missense mutation [83],[84],[96],[97],[291],[292]. Thus, if missense mutations generate CAPN3 catalytic deficiency while maintaining its structural function, SERCA expression could be stabilized and thus, calcium flux into SR may be restored inducing milder muscle phenotype. Actually, studies performed in LGMDR1 mouse models with inactive *Capn3* expression or *Capn3* knockout mice, suggest calcium dyshomeostasis as a feature present only in the absence of CAPN3 [152].

Similar to CAPN3-deficient 8220 myotubes, we have not detected upregulation of SR stress or UPS markers nor the *c-FLIP* decrease observed in the LHCN-M2-silenced model. The reasons for that may be also the different origin of the muscle biopsies and the lack of ECM in the differentiation process.

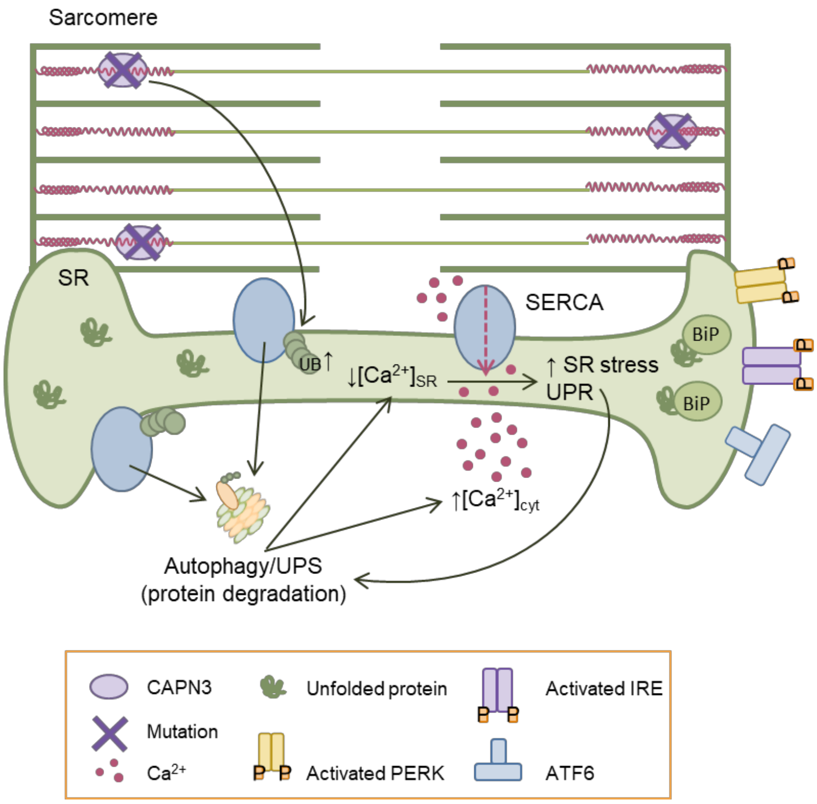

Figure 60. Hypothetic model of SERCA deficiency upon CAPN3 reduction in SR network. CAPN3 deficiency triggers abnormal SERCA ubiquitination (UB) and its consequent exacerbated degradation by Ubiquitin Proteasome System (UPS). SERCA reduction generates increase cytosolic calcium concentration ($[Ca^{2+}]$) whereas $[Ca^{2+}]$ in sarcoplasmic reticulum (SR) may be downregulated. Depleted SR $[Ca^{2+}]$ induces the expression of SR stress and Unfolded Protein Response (UPR) markers such as BiP/GRP78, ATF6, ATF4 or XBP1s. In turn, elevated SR stress/UPR induce greater UPS activation.

Bortezomib treatment can restore SERCA2 expression and functionality in CAPN3-deficient *in vitro* human myotubes but induces SR stress

In agreement with our data from the characterization of *in vitro* models and the higher SERCA ubiquitination previously described by our group [134], reduction of CAPN3 may generate the greater degradation of SERCA by the proteolytic pathways Ubiquitin Proteasome System (UPS) or autophagy. Actually, it has been suggested that the activation of atrophy in LGMDR1 seems to relay mainly on the induction of UPS and not so much on autophagy [226]. In addition, previous studies have shown the potential of UPS inhibition by Bortezomib (BTZ) or MG132 treatments to restore the expression of mutated SERCA1 in Chianina cattle congenital pseudomyotonia, suggesting it as a therapeutic approach for Brody disease, which is caused by mutations in *ATP2A1* gene [293]. Therefore, we have hypothesized that UPS inhibition could restore SERCA protein expression in our LGMDR1 *in vitro* models.

Unlike the proteasome inhibitor MG-132, which also inhibits the calpain system, BTZ has selectivity and high affinity for the proteasome. This means that this compound would be optimal to test its therapeutic capacity in muscular dystrophies [262]. Strikingly, BTZ has shown a potent antitumoral effect in several tumour types [294],[295], being approved by the US Food and Drug Administration (FDA) for the treatment of multiple myeloma (plasma cells cancer) [263]56] and for the treatment of mantle cell lymphoma (lymph nodes cancer) [296].

BTZ treatment in LGMDR1 *in vitro* models showed partial restoring of SERCA2 in CAPN3-deficient 8220 myotubes, as well as in the two immortalized LG samples. However, the effect over SERCA1 protein expression is inconclusive, although its gene expression tends to decrease by the treatment. Remarkably, the recovery of SERCA2 expression in 8220 dystrophic myotubes by 5nM BTZ, which is its IC50 and the range of plasma concentration following administration of 1.3 mg/m^2 in patients [297]–[299], is accompanied by a decrease in basal intracellular calcium levels.

Furthermore, BTZ treatment increased mutated CAPN3 expression without affecting its mRNA in myotubes derived from the two LGMDR1 patients, so preserving its structural function. On the other hand, in silenced myotubes, a slight increment is observed, as the residual expression of CAPN3 after silencing could not undergo its physiological degradation due to the UPS inhibition. These data, together with the observed recovery of SERCA2, suggest that recovering the non-proteolytic function of CAPN3 could stabilize SERCA2. Furthermore, considering the significant increase in SERCA in silenced 8220 myotubes, the treatment could also directly inhibit SERCA2 degradation. Together, these results indicate that by avoiding abnormal degradation of SERCA2 by UPS inhibition, SERCA function could be recovered, and consequently, calcium homeostasis may be partially restored in CAPN3-deficient myotubes, although further studies are needed.

Noteworthily, the mechanism of inhibiting the proteasome by BTZ has its limitations due to possible side effects [300]. For instance, the most common dose limiting side effect of BTZ in multiple myeloma is peripheral neuropathy, which is characterized by burning sensation, paraesthesia, numbness and/or neuropathic pain [301],[302]. BTZ is usually administered as a short intravenous (IV) infusion at 1.3 mg/m^2 starting dose on days 1, 4, 8, 11 of a 3 weekly cycle [297],[303], and patients usually receive up to eight cycles [263],[296]. This posology becomes really important as cells must recover the normal proteasome inhibition in order to prevent excessive side effects. Notably, due to BTZ posology in multiple myeloma, neuropathy improves or resolves once treatment is completed over an average of 3 months [302]. In addition to peripheral neuropathy, metabolic myopathy has also been suggested as another effect of BTZ administration, characterized by excessive storage of lipid droplets together with mitochondrial abnormalities [265]. Indeed, high concentrations of BTZ (10-20nM) or long periods of treatment may generated metabolic symptoms and cytotoxic effect [265]. Despite no cytotoxic effects were observed after treating LGMDR1 *in vitro* models with 5nM BTZ for 24h, SR stress and the UPR markers are increased at the mRNA level. Moreover, upon BTZ treatment *c-FLIP* expression is increased, which could imply a compensatory mechanism upon greater UPR.

To overcome the undesired effect of BTZ over SR stress and UPR, additional complementary therapeutic strategies could be considered such as FDA approved chemical chaperons, IRE1, PERK, ATF6α inhibitors, and AAV-based gene therapies, which are reviewed in [49],[287],

Together, these observations suggest that inhibition of UPS by BTZ treatment may restore the structural function of mutated CAPN3 as well as SERCA2 expression by preventing their degradation, restoring calcium homeostasis in LGMDR1. However, chronic generalized UPS inhibition may be ineffective or even potentially deleterious, because of undesirable accumulation of mutated proteins and unsustainable perturbation of cellular protein homeostasis. Therefore, special attention should be paid over BTZ administration protocol design for *in vivo* studies.

LGMDR1 animal models show mild LGMDR1 phenotype though SERCA deficiency is observed.

C3KO

Often, due to its easy accessibility and less invasiveness, we use *in* vitro models in order to decipher different mechanisms affecting a specific scenario, disease or homeostasis. However, *in vitro* results are really difficult to translate into human condition, especially when exploring future treatments. Thus, a more physiological system is necessary to understand the disease in its complexity to favour translational approaches when searching for therapies. Therefore, the generation of animal models that recapitulate the different human diseases is essential. Mouse and human share 90% of their genes [304], thus, mouse models have been developed for years as an approximation for whole system research.

Up to now, different LGMDR1 mouse models have been generated, covering different possible Capn3 deficiency scenarios that may take place. On the one hand, similarly to LG1 human sample, in *Capn3* knockin models [181],[183],[184], endogenous CAPN3 is replaced by CAPN3:C129S, a protease-inactive mutant, to abolish CAPN3 protease activity. On the other hand, knockout (KO) models do not express *Capn3* at all [136],[185], therefore losing all its functions, including catalytic and structural activities. In fact, the development of these two scenarios has let the characterization of the non-proteolytic function of CAPN3 [152].

Among these models, the KOs are the most widely used, especially the C3KO. Most of the tests carried out for the functional characterization of the C3KO mice have been developed in adult animals. Interestingly, it has been recently shown that calcium dyshomeostasis may be an early phenomenon in this model [267]. Therefore, we decided to analyse different functional characteristics in young C3KO mice.

First, we assessed grip strength of the forelimbs and their resistance to fatigue in young male mice. Unlike the observation in these two functional tests of 4-6 month-old male mice reported by Dr Spencer's group [43],[184],[244], 2 month-old C3KO mice behave similar to control mice, suggesting that at this age C3KO are pre-symptomatic. However, we have not observed grip strength difference even in 9 month-old C3KO mice.

Additionally, Hyper-CKemia has been previously described in the early stages of the disease [140],[305], as creatine kinase (CK) constitutes the most sensitive indicator of muscle damage, being the most used enzyme in the diagnosis and monitoring of muscle diseases [306]. However, in our young C3KO mice no significant differences have been observed compared to controls, suggesting that in this pre-symptomatic stage muscle damage is not evident.

Considering previous findings, altered calcium homeostasis in C3KO corresponds to the aberrant calcium exit from the reticulum to the cytosol in animals older than 2 months [153]. In this line, *flexor digitorum brevis* (FDB) muscle did not show alterations in basal calcium levels in 2-month-old mice. This fact may be due to the higher expression of proteins capable of buffering calcium in murine muscles compared to humans, such as parvalbumin [194],[307]. Yet, we did not stimulate muscle fibres in order to asses Ca^{2+} release and re-uptake flux in these muscles fibres as it was reported.

As alteration of calcium homeostasis has been described as an early feature, we wanted to check if SERCA deficiency could underlay this early phenomenon, assessing SERCA expression in young C3KO mice. Specifically, we have analysed the expression of SERCA in the *soleus* and diaphragm, as they are the most affected muscles in this model [136]. In fact, these muscles are made up of a significant proportion of slow fibres and are the most similar to human skeletal muscles [308]. Interestingly, despite *soleus* is mainly build up by slow twitch fibres [309], previous reports suggest greater decrease in the cross sectional area of fast fibres (28%) than in slow fibres (21%) in C3KO mice compared to controls [136],[184]. SERCA1 is mainly express in fast fibres, and accordingly, SERCA1 but not SERCA2 is significantly downregulated in *soleus*; however, in diaphragm, a mixed fibre-type skeletal muscle[310], both isoforms are affected, with a more prominent decrease in SERCA2. Together, these data suggest that Capn3 deficiency affects these muscles differently depending on the proportion of fast / slow fibres and on the affection of each phenotype in different muscles; nonetheless, SERCA affection is evident in both. Strikingly, SERCA proteins deficit in mice muscles is not as evident as the observed in human samples. This effect could follow the same trend of the buffered intracellular calcium levels observed in mice myofibres due to parvalbumin expression. Normalized calcium homeostasis could prevent the prolonged UPR activation, and therefore, the greater UPS activation, which in turn could increase polyubiquitinated SERCA protein degradation.

Furthermore, downregulation of SERCA and its consequent activity loss can affect calcium homeostasis in the diaphragm myofibres. Therefore, the strength of this muscle can be affected in C3KO mice, as we have demonstrated in diaphragms response to an isolated electrical stimulus. Moreover, the tetanic isometric force is significantly lower in young C3KO mice. However, this effect is not reflected in the resistance to endurance exercise on the treadmill, where different muscle groups are also involved and might compensate lower diaphragm force.

All in all, as well as RyR and αDHPR decrease previously observed in young C3KO [267], SERCA protein reduction at this age might be independent of the degenerative processes occurring in the pathogenesis of C3KO muscles during disease progression. The consequent Ca^{2+} reduction in skeletal muscle can affect several downstream signalling pathways involved in different processes such as muscle adaptation or muscle regeneration for instance. During disease progression, consequences of abnormal Ca^{2+} fluxes may become more evident, since possible compensatory mechanisms may be reduced, triggering a cumulative effect of altered Ca^{2+} homeostasis. However, further protocol optimization and analysis are required to test this hypothesis.

Certainly, since LGMDR1 is a muscular dystrophy characterized by progressive strength loss, adult C3KO mice had been characterized in greater depth. Previous reports suggested reduced forelimb grip strength in 4-6-month-old C3KO mice. Moreover, skeletal muscle adaptation upon physiological and environmental changes has been studied in these mice [199]. On the one hand, it has been shown that muscle fibre area in *soleus* is reduced as well as slow fibre area in *gastrocnemius* muscle [19]. Additionally, lower proportion of slow myofibres has been observed [19]. On the other hand, it has been suggested that upon muscle damage, the C3KO model does not have the ability to induce the expression of genes related to slow myogenic program as *Myl2, Ckmt2 Pnpla2 Lpl, Myo18b*, and *Myom3*, due to lower activation of CaMKII-dependent pathway in *plantaris* muscle, leading to muscle dysfunction [39],[311]. Furthermore, according to induced gene expression during muscle regeneration, an impaired activation of *Ppargc1* and *Tgfb1* genes had been suggested [138]. *Ppargc1*, which encodes the PGC1α protein, a key regulator of mitochondrial biosynthesis, has been suggested to be slightly downregulated in *Capn3*-deficient mice due to low signalling of the CaMKII pathway [43]. On the other hand, although undamaged C3KO mice did not show altered expression of *Tgfb1* [138], upon muscle damage, C3KO mice had been reported to fail in the induction of *Tgfb1* expression, a potent inhibitor of myogenic differentiation which participates in the early transitory inflammatory process, and contributes to the formation of fibrotic tissue [272].

In our study, we couldn´t recapitulate the loss of grip strength in 9 month-old mice previously reported in Ermolova N. *et al.* [184] with 6 moth-old mice, probably due to a smaller experimental group (N=9 vs. N=31). Moreover, we did not observe large differences in the mobility of dystrophic mice by voluntary exercise or 6-min walk test. According to histological features, due to SERCA deficiency in young C3KO diaphragms, we focused on analysing this muscle, were no differences neither in the proportion nor in the Cross-Sectional Area (CSA) of fast or slow fibres were observed. However, compared to control mice, only a little increase in central nucleation was detected.

In terms of muscle adaptation and slow program gene expression, in basal stage, *Myl2, Ckmt2 Pnpla2 Lpl, Myo18b*, and *Myom3* genes have shown a tendency to increase their expression in C3KO diaphragms, despite the high variability among mice. In contrast, no changes of this genes have been previously described, but after forced exercise in treadmill[43]. Furthermore, we have not detected modification of CaMKII phosphorylation in C3KO diaphragms. Considering the preferential affection of slow fibres suggested in this C3KO mice model [19], upregulation of these genes could act as a compensatory mechanism trying to maintain the correct fibre proportion.

In the same line, our results indicate an upregulation of *Ppargc1* expression in adult C3KO mice, suggesting greater mitochondrial biosynthesis, which a trend to increase PGC1α expression in sedentary C3KO mice [43]. Since mitochondrial dysfunction had been previously reported in these mice [139], *Ppargc1* upregulation may also be part of the compensatory mechanisms in C3KO mice. However, further analyses are needed in order to check that, upon muscle damage, induction of *Ppargc1* expression fails also in the diaphragm. In addition, in the C3KO diaphragms, we have observed a clear increase of *Tgfb1* expression in contrast to the undamaged *gastrocnemius* [138], suggesting that muscle fibrosis could be more prominent in the diaphragm.

Considering the observed SERCA downregulation in diaphragms of dystrophic mice and that, as in the *in vitro* models, its decrease could be a consequence of abnormal degradation by UPS, BTZ treatment could be a therapeutic strategy to try to recover SERCA expression in C3KO mice. Consequently, the cumulative effect of abnormal calcium homeostasis may be ameliorated.

BTZ treatment has previously been tested in dystrophic models showing significant improvements on its phenotype [230],[236],[238],[262],[264], in addition of proving the safety of treatment posology. Moreover, this treatment has reached phase I clinical trials for LGMDR2 treatment (NCT01863004) [312]. However, applying the dosage previously described by Gazzerro E. *et al.* [262], we could not observe a large inhibition of UPS activity. Therefore, we have not been able to see significant differences regarding histological features. Furthermore, BTZ shows little SERCA2 protein expression increase as well as partial restoration of several of the studied genes. This can be explained as compensation to the possible accumulation of their coded proteins due to UPS inhibition. Remarkably, MYL2, which has been previously reported to be degraded by UPS [313], is significantly downregulated upon BTZ treatment. Nonetheless, this effect has not been detected at histological level. On the other hand, reduced *Tgfb1* expression after BTZ treatment may suggest lower fibrotic tissue in treated C3KO diaphragms.

Together, in this study, we have focused in the characterization of adult C3KO diaphragm, which despite being one of the affected muscles, not much data has been published about it so far. According to our results and previously reported features, these mice show really mild phenotype compared to LGMDR1 patients, hindering phenotypic improvements with any treatment. Therefore, although BTZ dose protocol should be optimized to efficiently inhibit UPS activity, other LGMDR1 animal models with more severe and closer to human dystrophic phenotype should be employed to obtain more conclusive data about this therapeutic approach.

C3 null rat

Given that rats show more precise motor coordination and a more enriched behaviour compared to mice [314], rats have been considered a very useful specie for the development of drugs, testing of pharmacological effects, and the evaluation of toxicity. Interestingly, rat models have been generated for the study of muscular dystrophies as DMD, which display severe muscle phenotype than the widely used *mdx* mice [315]. For instance, fibrosis is more marked, lower strength has been reported as well as locomotion impairment [315]. Thus, considering the mild phenotype presented by C3KO mouse model, the group led by Dr Isabelle Richard has generated a LGMRD1 rat model, which has higher number of affected muscles compared to mouse models (unpublished data). This fact makes LGMDR1 rat a more promising model than those in mice.

Similar to C3KO mouse model, one of the most affected muscles in the rat is the diaphragm, where through a preliminary study of 4-month-old rats, we have verified the tendency to reduce SERCA1 and SERCA2 expression in early stages. Likewise, these data corroborate that the recovery of SERCA expression may be a therapeutic strategy to be addressed in this dystrophy. Therefore, as well as in the

C3KO model, BTZ treatment has been conducted in older rats. In this case, due to availability, female rats have been used and the dose of BTZ has been determined taking into account the clinical dose and adapting it to rats tolerance [279]. However, during the experiment, rats lost their weight as possible sign of compound toxicity and, consequently, the dose was readjusted stabilizing the weight of the animals.

Noteworthily, due to the low number of animals available for the experiment, we have obtained trends but no significant differences when evaluating phenotypic aspects of the model, such as the forelimbs grip strength. In fact, this dystrophic model seems to have lower strength, which seems to be recovered by BTZ treatment. However, force restoration due to BTZ treatment may be affected by the toxic effect of BTZ on rats, since it has clearly affected its weight.

On the other hand, unlike the mouse model but similar to humans, hyper-CKemia was detected in dystrophic rats serum as a sign of muscle damage [140],[305]. Interestingly, BTZ treatment seems to restore CK levels. Moreover, according to the greater central nucleation observed in *soleus* histological sections, muscle degeneration-regeneration process seems to be more pronounced than in control rats. However, BTZ do not affect overtly this feature. Besides, contrary to previous findings in C3KO *soleus* [136], we have neither observed differences in myofibres area nor the proportion of each of them.

In the rat model, as in the mouse C3KO, the *soleus* and the diaphragm are two of the most affected muscles, as previously mentioned. Therefore, we have analysed the expression of SERCA1 and SERCA2 in both muscles, observing that, as in the C3KO, there is a differential expression between both muscles, being the diaphragm the most affected muscle. Actually, the expression of SERCAs correlates with their specific activity. In this case, BTZ treatment seems to affect the expression of SERCA1 but not SERCA2. Strikingly, this small increase in SERCA1 was translated into the increased SERCA activity after treatment.

Muscle adaptation has not been characterized in the rat model so far. Therefore, we characterized the expression of genes related to the slow myogenic program as previously done in the C3KO mouse model. As in C3KO mice, expression of these genes shows a tendency to increase in *Capn3*-deficient rats. Moreover, BTZ treatment also shows a tendency to restore the expression of these genes.

Nonetheless, unlike in C3KO mice, *Capn3*-deficient rats show decreased *Ppargc1* expression, that BTZ treatment was unable to restore.

Moreover, fibrosis mediator *Tgfb1* is increased in *C3 null* rats, as observed in C3KO and the *mdx* dystrophic model [316],[317]. Furthermore, its activator *Mmp9* [281] is also elevated in the diaphragm of *Capn3*-deficient rats. In both cases, BTZ treatment manages to slightly reduce its expression, suggesting that this model may display lower fibrosis areas in muscle, as occurs in *mdx* mice when *Mmp9* expression is reduced [318]. Interestingly Sirius Red staining showed greater fibrosis proportion in *C3*null rats which is reduced with BTZ treatment as well. This reduction in fibrosis is accompanied by a reduction in serum CK levels in *mdx* mice [318], a phenomenon that also takes place in *C3 null* rats with BTZ treatment.

In conclusion, both, the functional and molecular data obtained from the *C3 null* rat, suggest that this LGMDR1 model recapitulates more severely the studied features compared to C3KO mouse model. However, due to rats' sensitivity to BTZ, it is not the best model for testing BTZ effectiveness.

Future direction

According to the role of Ca^{2+} dysregulation as a pathological mechanism underlying LGMDR1, it would be interesting to test different compounds as well as other therapeutic approaches targeting Ca^{2+}-handling proteins compromised in LGMDR1 such as SERCA.

We have tried to restore SERCA protein expression and its consequent activity by UPS inhibition, observing some beneficial features *in vitro* as restoration of intracellular calcium levels. However, *in vivo*, we have not been able to observe significant differences after BTZ treatment. On the one hand, C3KO mouse model shows no big functional differences compared to wild type according to the tests we have performed, making it difficult to obtain phenotypic improvements with any treatment. On the other hand, LGMDR1 rat model presents a more severe phenotype than C3KO mice, making it a better model to test therapeutic strategies although it remains still far from recapitulating human pathophysiological features. Due to the sensitivity to BTZ observed in rats, we couldn´t observe very clear beneficial effects after treatment. Therefore, BTZ treatment posology should be redesign in rats, lowering the dose or expanding the treatment time, but considering the addition of treatment-free periods in order to avoid the possible side effects previously mentioned. Nevertheless, this posology changes can imply the ineffectiveness of the treatment.

Considering the narrow therapeutic window between effectiveness and toxicity of BTZ treatment, other therapeutic strategies should be considered. For instance, SERCA overexpression by AAV-mediated gene therapy [319],[320] or the use of drugs which could increase SERCA expression or function, including adrenoceptor blockers, adrenergic agonists, hormones, glucocorticoids, natural antioxidants, and small molecule SERCA activators such as CDN1163 [194],[321],[322], could be assessed.

Actually, further studies should focus on the generation of new animal models with human-like *CAPN3* mutations and a dystrophic phenotype more similar to the one observed in human patients. However, in this project, we propose a therapeutic target to ameliorate the dystrophic phenotype in this illness as well as new LGMDR1 *in vitro* models as preclinical tools. These models would also help understand the different pathophysiological mechanisms underlying this disease and move forward towards the development of new therapies for LGMDR1

CONCLUSIONS

1) CAPN3-silencing in healthy human myotubes results in a reduction of SERCA proteins, but not mRNA expression, resulting in a significant increase of the resting cytosolic Ca^{2+} levels. Moreover, evidence of sarcoplasmic reticulum stress was found in LHCN-M2 but not in the 8220 silenced-myotubes.

2) Immortalized myotubes from two LGMDR1 patients present normal differentiation and maturation levels. KM900 (G567T mutation) myotubes express CAPN3 while 918 (R289W/R546L mutations) myotubes present reduced levels. Both lines present lower SERCA2 mRNA levels compared to control myotubes. SERCA proteins are mostly affected when CAPN3 expression is severely reduced.

3) CAPN3-silenced human myotubes treated with the proteasome inhibitor Bortezomib significantly increases SERCA2 protein levels and normalizes resting cytosolic Ca^{2+} levels to control levels. Bortezomib treatment seems to reduce *SERCA1* mRNA levels without affecting protein levels.

4) Bortezomib treatment increases the expression of CAPN3 and SERCA2 in immortalized myotubes from two LGMDR1 patients. This indicates that inhibiting UPS activity may stabilize CAPN3 and SERCA2 protein expression. The effect of Bortezomib on SERCA1 expression is inconclusive.

5) In all analysed cellular models, Bortezomib treatment upregulates sarcoplasmic reticulum stress markers such as *CHOP, GRP78* and *HERP*, and *c-FLIP*, the antiapoptotic factor found reduced in LGMDR1 muscle biopsies.

6) Young C3KO mice present very mild dystrophic phenotype, with no significant differences in the grip strength, endurance resistance, and voluntary exercise tests. At the histological level, C3KO mice present more central nucleation and reduced cross-sectional area of the muscle fibres. At the protein level, SERCA expression is downregulated particularly in the diaphragm.

7) Bortezomib treatment did not affect muscle histology or function in C3KO dystrophic mice. Bortezomib does not rescue SERCA protein expression in

C3KO diaphragms. The unchanged ubiquitin-proteasome activity observed in these muscles suggests that a higher dose may be needed to analyse efficacy.

8) Adult *C3 null* rats present more severe dystrophic phenotype than C3KO mice, with reduced grip strength test, higher number of centrally nucleated muscle fibres and increased fibrosis. Several genes downstream CaMKII pathway, such as *Pnpla2, Lpl* and *Myo18b* are upregulated in *C3 null* rats, which is indicative of abnormal muscle adaptation.

9) *C3 null* rats are more sensitive to Bortezomib treatment than C3KO mice, with major weight loss, compelling a reduction of the dose. This renders the LGMDR1 rat model unsuitable for testing Bortezomib efficacy.

10) Bortezomib treatment is not able to restore SERCA2 downregulation in *C3 null* rat diaphragms. No other negative effect of Bortezomib has been observed over the skeletal muscle.

The extremely mild phenotype of C3KO mice, together with the high susceptibility of the rat model to Bortezomib treatment, have been major limitations to this study. In any case, our results support SERCA2 as a promising molecular target for Calpainopathy therapies, given that this protein is reduced in the analysed cellular models, as well as in the LGMDR1 mouse and rat models. In fact, SERCA2 deficiency was found in young C3KO mouse model. Further studies should focus on using other approaches to stabilize SERCA2 protein in the skeletal muscle. Ideally, this approach may also target stabilization of mutant CAPN3. Generation of new animal models with human-like CAPN3 mutations may be needed to analyse stabilization of mutant CAPN3. Moreover, these models would also help understand the different pathophysiological mechanisms underlying this disease to pave the way for the development of new therapies.

REFERENCES

1. OpenStax. Muscle Tissue and Motion. In *Anatomy and Physiology*; 2016; OpenStax CNX, 2016.
2. Standring, S. *Gray's Anatomy*, 41st ed.er ed.; Standring, S., Ed.; 2016;
3. Frontera, W. R.; Ochala, J. Skeletal Muscle: A Brief Review of Structure and Function. *Calcif. Tissue Int.* **2015**, *96*, 183–195. https://doi.org/10.1007/s00223-014-9915-y.
4. U.S. National Insitutes of Health, N. C. I. SEER Training Modules, Structure of skeletal muscle. Avaiable online: https://training.seer.cancer.gov/ (accessed on8 December, 2020).
5. Relaix, F.; Zammit, P. S. Satellite Cells Are Essential for Skeletal Muscle Regeneration: The Cell on the Edge Returns Centre Stage. *Development* **2012**, *139*, 2845–2856. https://doi.org/10.1242/dev.069088.
6. Karalaki, M.; Fili, S.; Philippou, A.; Koutsilieris, M. Muscle Regeneration: Cellular and Molecular Events. *In Vivo* **2009**, *23*, 779–796.
7. Glaser, J.; Suzuki, M. Skeletal Muscle Fiber Types in Neuromuscular Diseases; 2018; 2018. https://doi.org/10.5772/intechopen.79474.
8. Rode, C.; Siebert, T.; Tomalka, A.; Blickhan, R. Myosin Filament Sliding through the Z-Disc Relates Striated Muscle Fibre Structure to Function. *Proceedings. Biol. Sci.* **2016**, *283*, 20153030. https://doi.org/10.1098/rspb.2015.3030.
9. Henderson, C. A.; Gomez, C. G.; Novak, S. M.; Mi-Mi, L.; Gregorio, C. C. Overview of the Muscle Cytoskeleton. *Compr. Physiol.* **2017**, *7*, 891–944. https://doi.org/10.1002/cphy.c160033.
10. Peter, A. K.; Cheng, H.; Ross, R. S.; Knowlton, K. U.; Chen, J. The Costamere Bridges Sarcomeres to the Sarcolemma in Striated Muscle. *Prog. Pediatr. Cardiol.* **2011**, *31*, 83–88. https://doi.org/10.1016/j.ppedcard.2011.02.003.
11. Herzog, W. The Role of Titin in Eccentric Muscle Contraction. *J. Exp. Biol.* **2014**, *217*, 2825–2833. https://doi.org/10.1242/jeb.099127.
12. Kuo, I. Y.; Ehrlich, B. E. Signaling in Muscle Contraction. *Cold Spring Harb. Perspect. Biol.* **2015**, *7*, a006023. https://doi.org/10.1101/cshperspect.a006023.
13. Dowling, J. J.; Lawlor, M. W.; Dirksen, R. T. Triadopathies: An Emerging Class of Skeletal Muscle Diseases. *Neurother. J. Am. Soc. Exp. Neurother.* **2014**, *11*, 773–785. https://doi.org/10.1007/s13311-014-0300-3.
14. Talbot, J.; Mavez, L. Resistance To Muscle Disease. *Wiley Interdiscip. Rev. Dev. Biol.* **2016**, *5*, 518–534. https://doi.org/10.1002/wdev.230.
15. Tellis, C. M.; Rosen, C.; Thekdi, A.; Sciote, J. J. Anatomy and Fiber Type Composition of Human Interarytenoid Muscle. *Ann. Otol. Rhinol. Laryngol.* **2004**, *113*, 97–107. https://doi.org/10.1177/000348940411300203.
16. Nguyen-Tran, D.-H.; Hait, N. C.; Sperber, H.; Qi, J.; Fischer, K.; Ieronimakis, N.; Pantoja, M.; Hays, A.; Allegood, J.; Reyes, M.; et al. Molecular Mechanism of Sphingosine-1-Phosphate Action in Duchenne Muscular Dystrophy. *Dis. Model. Mech.* **2014**, *7*, 41–54. https://doi.org/10.1242/dmm.013631.
17. Schneider, J. S.; Shanmugam, M.; Gonzalez, J. P.; Lopez, H.; Gordan, R.; Fraidenraich, D.; Babu, G. J. Increased Sarcolipin Expression and Decreased Sarco(Endo)Plasmic Reticulum Ca^{2+} Uptake in Skeletal Muscles of Mouse Models of Duchenne Muscular Dystrophy. *J. Muscle Res. Cell Motil.* **2013**, *34*, 349–356. https://doi.org/10.1007/s10974-013-9350-0.
18. Ohlendieck, K. Proteomic Profiling of Fast-To-Slow Muscle Transitions during Aging. *Front. Physiol.* **2011**, *2*, 105. https://doi.org/10.3389/fphys.2011.00105.

19. Kramerova, I.; Kudryashova, E.; Ermolova, N.; Saenz, A.; Jaka, O.; López de munain, A.; Spencer, M. J.; Lopez de Munain, A.; Spencer, M. J. Impaired Calcium Calmodulin Kinase Signaling and Muscle Adaptation Response in the Absence of Calpain 3. *Hum. Mol. Genet.* **2012**, *21*, 3193–3204. https://doi.org/10.1093/hmg/dds144.

20. Berridge, M. J.; Lipp, P.; Bootman, M. D. The Versatility and Universality of Calcium Signalling. *Nat. Rev. Mol. Cell.* **2000**, *1*, 11–21. https://doi.org/10.1038/35036035.

21. Cheng, X.; Zhang, X.; Yu, L.; Xu, H. Calcium Signaling in Membrane Repair. *Semin. Cell Dev. Biol.* **2015**, *45*, 24–31. https://doi.org/10.1016/j.semcdb.2015.10.031.

22. Gehlert, S.; Bloch, W.; Suhr, F. Ca^{2+}-Dependent Regulations and Signaling in Skeletal Muscle: From Electro-Mechanical Coupling to Adaptation. *Int. J. Mol. Sci.* **2015**, *16*, 1066–1095. https://doi.org/10.3390/ijms16011066.

23. Protasi, F. Structural Interaction between RyRs and DHPRs in Calcium Release Units of Cardiac and Skeletal Muscle Cells. *Front. Biosci.* **2002**, *7*, 650–658.

24. Santulli, G.; Lewis, D. R.; Marks, A. R. Physiology and Pathophysiology of Excitation-Contraction Coupling: The Functional Role of Ryanodine Receptor. *J. Muscle Res. Cell Motil.* **2017**, *38*, 37–45. https://doi.org/10.1183/09031936.00063810.The.

25. Lanner, J. T.; Georgiou, D. K.; Joshi, A. D.; Hamilton, S. L. Ryanodine Receptors: Structure, Expression, Molecular Details, and Function in Calcium Release. *Cold Spring Harb. Perspect Biol* **2010**, *2*, a003996. https://doi.org/10.1101/cshperspect.a003996.

26. Capes, E. M.; Loaiza, R.; Valdivia, H. H. Ryanodine Receptors. *Skelet. Muscle* **2011**, *1*, 18. https://doi.org/10.1201/9781420038231.

27. Lasa-Elgarresta, J.; Mosqueira-Martin, L.; Naldaiz-Gastesi, N.; Saenz, A.; Lopez de Munain, A.; Vallejo-Illarramendi, A. Calcium Mechanisms in Limb-Girdle Muscular Dystrophy with CAPN3 Mutations. *Int. J. Mol. Sci.* **2019**, *20*. https://doi.org/10.3390/ijms20184548.

28. Rossi, A. E.; Dirksen, R. T. Sarcoplasmic Reticulum: The Dynamic Calcium Governor of Muscle. *Muscle and Nerve* **2006**, *33*, 715–731. https://doi.org/10.1002/mus.20512.

29. Rodney, G. G.; Williams, B. Y.; Strasburg, G. M.; Beckingham, K.; Hamilton, S. L. Regulation of RYR1 Activity by Ca^{2+} and Calmodulin. *Biochemistry* **2000**, *39*, 7807–7812. https://doi.org/10.1021/bi0005660.

30. Beard, N. A.; Wei, L.; Dulhunty, A. F. Ca^{2+} Signaling in Striated Muscle: The Elusive Roles of Triadin, Junctin, and Calsequestrin. *Eur. Biophys. J.* **2009**, *39*, 27–36. https://doi.org/10.1007/s00249-009-0449-6.

31. Novák, P.; Soukup, T. Calsequestrin Distribution, Structure and Function, Its Role in Normal and Pathological Situations and the Effect of Thyroid Hormones. *Physiol. Res.* **2011**, *60*, 439–452.

32. Calderón, J. C.; Bolaños, P.; Caputo, C. The Excitation-Contraction Coupling Mechanism in Skeletal Muscle. *Biophys. Rev.* **2014**, *6*, 133–160. https://doi.org/10.1007/s12551-013-0135-x.

33. Periasamy, M.; Kalyanasundaram, A. SERCA Pump Isoforms: Their Role in Calcium Transport and Disease. *Muscle Nerve* **2007**, *35*, 430–442. https://doi.org/10.1002/mus.20745.

34. Dulhunty, A. F.; Wei-LaPierre, L.; Casarotto, M. G.; Beard, N. A. Core Skeletal Muscle Ryanodine Receptor Calcium Release Complex. *Clin. Exp. Pharmacol. Physiol.* **2017**, *44*, 3–12. https://doi.org/10.1111/1440-1681.12676.

35. Avila, G.; O'Brien, J. J.; Dirksen, R. T. Excitation-Contraction Uncoupling by a Human Central

Core Disease Mutation in the Ryanodine Receptor. *Proc. Natl. Acad. Sci. U. S. A.* **2001**, *98*, 4215–4220. https://doi.org/10.1073/pnas.071048198.

36. Periasamy, M.; Maurya, S. K.; Sahoo, S. K.; Singh, S.; Sahoo, S. K.; Reis, F. C. G.; Bal, N. C. Role of SERCA Pump in Muscle Thermogenesis and Metabolism. *Compr. Physiol.* **2017**, *7*, 879–890. https://doi.org/10.1002/cphy.c160030.
37. Murphy, R. M.; Larkins, N. T.; Mollica, J. P.; Beard, N. A.; Lamb, G. D. Calsequestrin Content and SERCA Determine Normal and Maximal Ca $^{2+}$ Storage Levels in Sarcoplasmic Reticulum of Fast- and Slow-Twitch Fibres of Rat. *J. Physiol.* **2009**, *587*, 443–460. https://doi.org/10.1113/jphysiol.2008.163162.
38. Toyoshima, C.; Inesi, G. Structural Basis of Ion Pumping by Ca^{2+}-ATPase of the Sarcoplasmic Reticulum. *Annu. Rev. Biochem.* **2004**, *73*, 269–292. https://doi.org/10.1146/annurev.biochem.73.011303.073700.
39. Anderson, D. M.; Anderson, K. M.; Chang, C.-L. L.; Makarewich, C. A.; Nelson, B. R.; McAnally, J. R.; Kasaragod, P.; Shelton, J. M.; Liou, J.; Bassel-Duby, R.; et al. A Micropeptide Encoded by a Putative Long Noncoding RNA Regulates Muscle Performance. *Cell* **2015**, *160*, 595–606. https://doi.org/10.1016/j.cell.2015.01.009.
40. MacLennan, D. H.; Kranias, E. G. Phospholamban: A Crucial Regulator of Cardiac Contractility. *Nat. Rev. Mol. Cell Biol.* **2003**, *4*, 566–577. https://doi.org/10.1038/nrm1151.
41. Nelson, B. R.; Makarewich, C. A.; Anderson, D. M.; Winders, B. R.; Troupes, C. D.; Wu, F.; Reese, A. L.; McAnally, J. R.; Chen, X.; Kavalali, E. T.; et al. A Peptide Encoded by a Transcript Annotated as Long Noncoding RNA Enhances SERCA Activity in Muscle. *Science* **2016**, *351*, 271–275. https://doi.org/10.1126/science.aad4076.
42. Shaikh, S. A.; Sahoo, S. K.; Periasamy, M. Phospholamban and Sarcolipin: Are They Functionally Redundant or Distinct Regulators of the Sarco(Endo)Plasmic Reticulum Calcium ATPase? *J. Mol. Cell. Cardiol.* **2016**, *91*, 81–91. https://doi.org/10.1016/j.yjmcc.2015.12.030.
43. Kramerova, I.; Ermolova, N.; Eskin, A.; Hevener, A.; Quehenberger, O.; Armando, A. M.; Haller, R.; Romain, N.; Nelson, S. F.; Spencer, M. J. Failure to Up-Regulate Transcription of Genes Necessary for Muscle Adaptation Underlies Limb Girdle Muscular Dystrophy 2A (Calpainopathy). *Hum. Mol. Genet.* **2016**, *25*, 2194–2207. https://doi.org/10.1093/hmg/ddw086.
44. Koss, K. L.; Kranias, E. G. Phospholamban: A Prominent Regulator of Myocardial Contractility. *Circ. Res.* **1996**, *79*, 1059–1063. https://doi.org/10.1161/01.res.79.6.1059.
45. Luo, W.; Grupp, I. L.; Harrer, J.; Ponniah, S.; Grupp, G.; Duffy, J. J.; Doetschman, T.; Kranias, E. G. Targeted Ablation of the Phospholamban Gene Is Associated with Markedly Enhanced Myocardial Contractility and Loss of Beta-Agonist Stimulation. *Circ. Res.* **1994**, *75*, 401–409. https://doi.org/10.1161/01.res.75.3.401.
46. Babu, G. J.; Bhupathy, P.; Carnes, C. A.; Billman, G. E.; Periasamy, M. Differential Expression of Sarcolipin Protein during Muscle Development and Cardiac Pathophysiology. *J. Mol. Cell. Cardiol.* **2007**, *43*, 215–222. https://doi.org/10.1016/j.yjmcc.2007.05.009.
47. Lancel, S.; Qin, F.; Lennon, S. L.; Zhang, J.; Tong, X. Y.; Mazzini, M. J.; Kang, Y. J.; Siwik, D. A.; Cohen, R. A.; Colucci, W. S. Oxidative Posttranslational Modifications Mediate Decreased SERCA Activity and Myocyte Dysfunction in Gαq-Overexpressing Mice. *Circ. Res.* **2010**, *107*, 228–232. https://doi.org/10.1161/CIRCRESAHA.110.217570.Oxidative.
48. Michalak, M.; Robert Parker, J. M.; Opas, M. Ca^{2+} Signaling and Calcium Binding Chaperones

of the Endoplasmic Reticulum. *Cell Calcium* **2002**, *32*, 269–278.

49. Hetz, C.; Chevet, E.; Oakes, S. A. Proteostasis Control by the Unfolded Protein Response. *Nat. Cell Biol.* **2015**, *17*, 829–838. https://doi.org/10.1038/ncb3184.

50. Vattemi, G.; Engel, W. K.; McFerrin, J.; Askanas, V. Endoplasmic Reticulum Stress and Unfolded Protein Response in Inclusion Body Myositis Muscle. *Am. J. Pathol.* **2004**, *164*, 1–7. https://doi.org/10.1016/S0002-9440(10)63089-1.

51. Wu, J.; Kaufman, R. J. From Acute ER Stress to Physiological Roles of the Unfolded Protein Response. *Cell Death Differ.* **2006**, *13*, 374–384. https://doi.org/10.1038/sj.cdd.4401840.

52. Bohnert, K. R.; McMillan, J. D.; Kumar, A. Emerging Roles of ER Stress and Unfolded Protein Response Pathways in Skeletal Muscle Health and Disease. *J. Cell. Physiol.* **2018**, *233*, 67–78. https://doi.org/10.1002/jcp.25852.

53. Hetz, C. The Unfolded Protein Response: Controlling Cell Fate Decisions under ER Stress and Beyond. *Nat. Rev. Mol. Cell Biol.* **2012**, *13*, 89–102. https://doi.org/10.1038/nrm3270.

54. Wang, M.; Wey, S.; Zhang, Y.; Ye, R.; Lee, A. S. Role of the Unfolded Protein Response Regulator GRP78/BiP in Development, Cancer, and Neurological Disorders. *Antioxid. Redox Signal.* **2009**, *11*, 2307–2316. https://doi.org/10.1089/ars.2009.2485.

55. Mekahli, D.; Bultynck, G.; Parys, J. B.; De Smedt, H.; Missiaen, L. Endoplasmic-Reticulum Calcium Depletion and Disease. *Cold Spring Harb. Perspect. Biol.* **2011**, *3*, 131–154. https://doi.org/10.1016/j.cell.2013.02.012.Long.

56. Wang, X. Z.; Harding, H. P.; Zhang, Y.; Jolicoeur, E. M.; Kuroda, M.; Ron, D. Cloning of Mammalian Ire1 Reveals Diversity in the ER Stress Responses. *EMBO J.* **1998**, *17*, 5708–5717. https://doi.org/10.1093/emboj/17.19.5708.

57. Yoshida, H.; Matsui, T.; Hosokawa, N.; Kaufman, R. J.; Nagata, K.; Mori, K. A Time-Dependent Phase Shift in the Mammalian Unfolded Protein Response. *Dev. Cell* **2003**, *4*, 265–271.

58. Sommer, T.; Jentsch, S. A Protein Translocation Defect Linked to Ubiquitin Conjugation at the Endoplasmic Reticulum. *Nature* **1993**, *365*, 176–179. https://doi.org/10.1038/365176a0.

59. Deegan, S.; Saveljeva, S.; Gorman, A. M.; Samali, A. Stress-Induced Self-Cannibalism: On the Regulation of Autophagy by Endoplasmic Reticulum Stress. *Cell. Mol. Life Sci.* **2013**, *70*, 2425–2441. https://doi.org/10.1007/s00018-012-1173-4.

60. Tavi, P.; Westerblad, H. The Role of in Vivo Ca^{2+} Signals Acting on Ca^{2+}-Calmodulin-Dependent Proteins for Skeletal Muscle Plasticity. *J. Physiol.* **2011**, *589*, 5021–5031. https://doi.org/10.1113/jphysiol.2011.212860.

61. Chin, E. R.; Olson, E. N.; Richardson, J. A.; Yang, Q.; Humphries, C.; Shelton, J. M.; Wu, H.; Zhu, W.; Bassel-Duby, R.; Williams, R. S. A Calcineurin-Dependent Transcriptional Pathway Controls Skeletal Muscle Fiber Type. *Genes Dev.* **1998**, *12*, 2499–2509. https://doi.org/10.1101/gad.12.16.2499.

62. Alzuherri, H.; Chang, K. C. Calcineurin Activates NF-Kβ in Skeletal Muscle C2C12 Cells. *Cell. Signal.* **2003**, *15*, 471–478. https://doi.org/10.1016/S0898-6568(02)00120-1.

63. Valdés, J. A.; Gaggero, E.; Hidalgo, J.; Leal, N.; Jaimovich, E.; Carrasco, M. A. NFAT Activation by Membrane Potential Follows a Calcium Pathway Distinct from Other Activity-Related Transcription Factors in Skeletal Muscle Cells. *Am. J. Physiol. Physiol.* **2008**, *294*, C715–C725. https://doi.org/10.1152/ajpcell.00195.2007.

64. McCullagh, K. J. A.; Calabria, E.; Pallafacchina, G.; Ciciliot, S.; Serrano, A. L.; Argentini, C.;

Kalhovde, J. M.; Lomo, T.; Schiaffino, S. NFAT Is a Nerve Activity Sensor in Skeletal Muscle and Controls Activity-Dependent Myosin Switching. *Proc. Natl. Acad. Sci.* **2004**, *101*, 10590–10595. https://doi.org/10.1073/pnas.0308035101.

65. Peterson, J. M.; Bakkar, N.; Guttridge, D. C. *NF-Kβ Signaling in Skeletal Muscle Health and Disease*, 1st ed.er ed.; Cambridge, United States,; 2011; https://doi.org/10.1016/B978-0-12-385940-2.00004-8.

66. Kaltschmidt, B.; Kaltschmidt, C.; Hofmann, T. G.; Hehner, S. P.; Dröge, W.; Schmitz, M. L. The Pro- or Anti-Apoptotic Function of NF-Kβ Is Determined by the Nature of the Apoptotic Stimulus. *Eur. J. Biochem.* **2000**, *267*, 3828–3835. https://doi.org/10.1046/j.1432-1327.2000.01421.x.

67. Eilers, W.; Jaspers, R. T.; De Haan, A.; Ferri, C.; Valdivieso, P.; Flück, M. CaMKII Content Affects Contractile, but Not Mitochondrial, Characteristics in Regenerating Skeletal Muscle. *BMC Physiol.* **2014**, *14*. https://doi.org/10.1186/s12899-014-0007-z.

68. Potthoff, M. J.; Wu, H.; Arnold, M. A.; Shelton, J. M.; Backs, J.; Mcanally, J.; Richardson, J. A.; Bassel-duby, R.; Olson, E. N. Histone Deacetylase Degradation and MEF2 Activation Promote the Formation of Slow-Twitch Myofibers. *J. Clin. Invest.* **2007**, *117*, 2459–2467. https://doi.org/10.1172/JCI31960DS1.

69. Kramerova, I.; Torres, J. A.; Eskin, A.; Nelson, S. F.; Spencer, M. J. Calpain 3 and CaMKIIβ Signaling Are Required to Induce HSP70 Necessary for Adaptive Muscle Growth after Atrophy. *Hum. Mol. Genet.* **2018**, *27*, 1642–1653. https://doi.org/10.1093/hmg/ddy071.

70. Chin, E. R. Role of Ca^{2+} /Calmodulin-Dependent Kinases in Skeletal Muscle Plasticity. *J. Appl. Physiol.* **2005**, *99*, 414–423. https://doi.org/10.1152/japplphysiol.00015.2005.

71. Glick, D.; Barth, S.; Macleod, K. F. Autophagy: Cellular and Molecular Mechanisms. *J. Pathol.* **2010**, *221*, 3–12. https://doi.org/10.1002/path.2697.

72. Mihaylova, M. M.; Shaw, R. J. The AMPK Signalling Pathway Coordinates Cell Growth, Autophagy and Metabolism. *Nat. Cell Biol.* **2011**, *13*, 1016–1023. https://doi.org/10.1038/ncb2329.

73. Zhou, J.; Dhakal, K.; Yi, J. Mitochondrial Ca^{2+} Uptake in Skeletal Muscle Health and Disease. *Sci China Life Sci.* **2016**, *59*, 770–776. https://doi.org/10.1007/s10741-014-9462-7.Natural.

74. Eisner, V.; Csordas, G.; Hajnoczky, G. Interactions between Sarco-Endoplasmic Reticulum and Mitochondria in Cardiac and Skeletal Muscle - Pivotal Roles in Ca^{2+} and Reactive Oxygen Species Signaling. *J. Cell Sci.* **2013**, *126*, 2965–2978. https://doi.org/10.1242/jcs.093609.

75. Fraysse, B.; Nagi, S. M.; Boher, B.; Ragot, H.; Lainé, J.; Salmon, A.; Fiszman, M. Y.; Toussaint, M.; Fromes, Y. Ca^{2+} Overload and Mitochondrial Permeability Transition Pore Activation in Living δ-Sarcoglycan-Deficient Cardiomyocytes. *Am. J. Physiol. Physiol.* **2010**, *299*, C706–C713. https://doi.org/10.1152/ajpcell.00545.2009.

76. Celsi, F.; Pizzo, P.; Brini, M.; Leo, S.; Fotino, C.; Pinton, P.; Rizzuto, R. Mitochondria, Calcium and Cell Death: A Deadly Triad in Neurodegeneration. *Biochim. Biophys. Acta - Bioenerg.* **2009**, *1787*, 335–344. https://doi.org/10.1016/j.bbabio.2009.02.021.

77. Yi, M.; Weaver, D.; Hajnóczky, G. Control of Mitochondrial Motility and Distribution by the Calcium Signal: A Homeostatic Circuit. *J. Cell Biol.* **2004**, *167*, 661–672. https://doi.org/10.1083/jcb.200406038.

78. Rossi, A. E.; Boncompagni, S.; Dirksen, R. T. Sarcoplasmic Reticulum-Mitochondrial Symbiosis:

Bidirectional Signaling in Skeletal Muscle. *Exerc. Sport Sci. Rev.* **2009**, *37*, 29–35. https://doi.org/10.1097/JES.0b013e3181911fa4.

79. Giorgi, C.; Baldassari, F.; Bononi, A.; Bonora, M.; De Marchi, E.; Marchi, S.; Missiroli, S.; Patergnani, S.; Rimessi, A.; Suski, J. M.; et al. Mitochondrial Ca^{2+} and Apoptosis. *Cell Calcium* **2012**, *52*, 36–43. https://doi.org/10.1016/j.ceca.2012.02.008.

80. Bernardi, P.; von Stockum, S. The Permeability Transition Pore as a Ca^{2+} Release Channel: New Answers to an Old Question. *Cell Calcium* **2012**, *52*, 22–27. https://doi.org/10.1016/j.ceca.2012.03.004.

81. Wright, D. C. Mechanisms of Calcium-Induced Mitochondrial Biogenesis and GLUT4 Synthesis. *Appl. Physiol. Nutr. Metab.* **2008**, *32*, 840–845. https://doi.org/10.1139/h07-062.

82. Richard, I.; Broux, O.; Allamand, V.; Fougerousse, F.; Chiannilkulchai, N.; Bourg, N.; Brenguier, L.; Devaud, C.; Pasturaud, P.; Roudaut, C.; et al. Mutations in the Proteolytic Enzyme Calpain 3 Cause Limb-Girdle Muscular Dystrophy Type 2A. *Cell* **1995**, *81*, 27–40. https://doi.org/10.1016/0092-8674(95)90368-2.

83. Fardeau, M.; Eymard, B.; Mignard, C.; Tome, F. M.; Richard, I.; Beckmann, J. S.; Tomé, F. M. S.; Richard, I.; Beckmann, J. S. Chromosome 15-Linked Limb-Girdle Muscular Dystrophy: Clinical Phenotypes in Reunion Island and French Metropolitan Communities. *Neuromuscul. Disord.* **1996**, *6*, 447–453. https://doi.org/10.1016/S0960-8966(96)00387-2.

84. Fardeau, M.; Hillaire, D.; Mignard, C.; Feingold, N.; Feingold, J.; Mignard, D.; de Ubeda, B.; Collin, H.; Tome, F. M.; Richard, I.; et al. Juvenile Limb-Girdle Muscular Dystrophy. Clinical, Histopathological and Genetic Data from a Small Community Living in the Reunion Island. *Brain* **1996**, *119 (Pt 1*, 295–308. https://doi.org/10.1093/brain/119.1.295.

85. Kawai, H.; Akaike, M.; Kunishige, M.; Inui, T.; Adachi, K.; Kimura, C.; Kawajiri, M.; Nishida, Y.; Endo, I.; Kashiwagi, S.; et al. Clinical, Pathological, and Genetic Features of Limb-Girdle Muscular Dystrophy Type 2A with New Calpain 3 Gene Mutations in Seven Patients from Three Japanese Families. *Muscle Nerve* **1998**, *21*, 1493–1501. https://doi.org/10.1002/(sici)1097-4598(199811)21:11<1493::aid-mus19>3.0.co;2-1.

86. Vissing, J.; Barresi, R.; Witting, N.; Van Ghelue, M.; Gammelgaard, L.; Bindoff, L. A.; Straub, V.; Lochmüller, H.; Hudson, J.; Wahl, C. M.; et al. A Heterozygous 21-Bp Deletion in CAPN3 Causes Dominantly Inherited Limb Girdle Muscular Dystrophy. *Brain* **2016**, *139*, 2154–2163. https://doi.org/10.1093/brain/aww133.

87. Martinez-Thompson, J. M.; Niu, Z.; Tracy, J. A.; Moore, S. A.; Swenson, A.; Wieben, E. D.; Milone, M. Autosomal Dominant Calpainopathy Due to Heterozygous CAPN3 C.643_663del21. *Muscle and Nerve* **2018**, *57*, 679–683. https://doi.org/10.1002/mus.25970.

88. Vissing, J.; Dahlqvist, J. R.; Roudaut, C.; Poupiot, J.; Richard, I.; Duno, M.; Krag, T. A Single c.1715G>C Calpain 3 Gene Variant Causes Dominant Calpainopathy with Loss of Calpain 3 Expression and Activity. *Hum. Mutat.* **2020**, *41*, 1507–1513. https://doi.org/10.1002/humu.24066.

89. Cerino, M.; Bartoli, M.; Riccardi, F.; Le Goanvic, B.; Blanck, V.; Salvi, A.; Lévy, N.; Krahn, M.; Choumert, A. Autosomal Dominant Segregation of CAPN3 c.598_612del15 Associated with a Mild Form of Calpainopathy. *Ann. Clin. Transl. Neurol.* **2020**, *n/a*. https://doi.org/10.1002/acn3.51193.

90. Nallamilli, B. R. R.; Chakravorty, S.; Kesari, A.; Tanner, A.; Ankala, A.; Schneider, T.; da Silva,

C.; Beadling, R.; Alexander, J. J.; Askree, S. H.; et al. Genetic Landscape and Novel Disease Mechanisms from a Large LGMD Cohort of 4656 Patients. *Ann. Clin. Transl. Neurol.* **2018**, *5*, 1574–1587. https://doi.org/10.1002/acn3.649.

91. González-Mera, L.; Ravenscroft, G.; Cabrera-Serrano, M.; Ermolova, N.; Domínguez-González, C.; Arteche-López, A.; Soltanzadeh, P.; Evesson, F.; Navas, C.; Mavillard, F.; et al. Heterozygous CAPN3 Missense Variants Causing Autosomal-Dominant Calpainopathy in Seven Unrelated Families. *Neuropathol. Appl. Neurobiol.* **2020**, *n/a*. https://doi.org/10.1111/nan.12663.
92. Sáenz, A.; López de Munain, A. Dominant LGMD2A: Alternative Diagnosis or Hidden Digenism? *Brain* **2017**, *140*, e7. https://doi.org/10.1093/brain/aww281.
93. Dincer, P.; Leturcq, F.; Richard, I.; Piccolo, F.; Yalnizoglu, D.; de Toma, C.; Akcoren, Z.; Broux, O.; Deburgrave, N.; Brenguier, L.; et al. A Biochemical, Genetic, and Clinical Survey of Autosomal Recessive Limb Girdle Muscular Dystrophies in Turkey. *Ann. Neurol.* **1997**, *42*, 222–229. https://doi.org/10.1002/ana.410420214.
94. Topaloğlu, H.; Dincer, P.; Richard, I.; Akçören, Z.; Alehan, D.; Ozme, S.; Caglar, M.; Karaduman, A.; Urtizberea, J. A.; Beckmann, J. Calpain-3 Deficiency Causes a Mild Muscular Dystrophy in Childhood. *Neuropediatrics* **1997**, *28*, 212–216.
95. Richard, I.; Brenguier, L.; Dincer, P.; Roudaut, C.; Bady, B.; Burgunder, J.; Chemaly, R.; Garcia, C.; Halaby, G.; Jackson, C.; et al. Multiple Independent Molecular Etiology for Limb-Girdle Muscular Dystrophy Type 2A Patients from Various Geographical Origins. *Am J Hum Genet* **1997**, *60*, 1128–1138.
96. Chae, J.; Minami, N.; Jin, Y.; Nakagawa, M.; Murayama, K.; Igarashi, F.; Nonaka, I. Calpain 3 Gene Mutations: Genetic and Clinico-Pathologic Findings in Limb-Girdle Muscular Dystrophy. *Neuromuscul. Disord.* **2001**, *11*, 547–555. https://doi.org/10.1016/S0960-8966(01)00197-3.
97. de Paula, F. F. F.; Vainzof, M.; Passos-Bueno, M. R.; M Pavanello, R. de C.; Matioli, S. R.; V B Anderson, L.; Nigro, V.; Zatz, M.; de Cassia M Pavanello, R.; Matioli, S. R.; et al. Clinical Variability in Calpainopathy: What Makes the Difference? *Eur. J. Hum. Genet.* **2002**, *10*, 825–832. https://doi.org/10.1038/sj.ejhg.5200888.
98. Zatz, M.; Starling, A. Calpains and Disease. *N. Engl. J. Med.* **2005**, *352*, 2413–2423. https://doi.org/10.1056/nejmra043361.
99. Orphanet. Avaiable online: https://www.orpha.net/consor/cgi-bin/Disease_Search.php?lng=ES&data_id=870&Disease_Disease_Search_diseaseGroup=LGMD2A&Disease_Disease_Search_diseaseType=Pat&Enfermedad(es)/grupo de enfermedades=Distrofia-muscular-de-cinturas-autos-mica-recesiva-tipo-2 (accessed on2 September, 2019).
100. Urtasun, M.; Saenz, A.; Roudaut, C.; Poza, J. J.; Urtizberea, J. A.; Cobo, A. M.; Richard, I.; Garcia Bragado, F.; Leturcq, F.; Kaplan, J. C.; et al. Limb-Girdle Muscular Dystrophy in Guipuzcoa (Basque Country, Spain). *Brain* **1998**, *121 (Pt 9*, 1735–1747. https://doi.org/10.1093/brain/121.9.1735.
101. Allamand, V.; Broux, O.; Bourg, N.; Richard, I.; Tischfield, J. A.; Hodes, M. E.; Conneally, P. M.; Fardeau, M.; Jackson, C. E.; Beckmann, J. S. Genetic Heterogeneity of Autosomal Recessive Limb-Girdle Muscular Dystrophy in a Genetic Isolate (Amish) and Evidence for a New Locus. *Hum. Mol. Genet.* **1995**, *4*, 459–463.
102. Pantoja-Melendez, C. A.; Miranda-Duarte, A.; Roque-Ramirez, B.; Zenteno, J. C.

Epidemiological and Molecular Characterization of a Mexican Population Isolate with High Prevalence of Limb-Girdle Muscular Dystrophy Type 2A Due to a Novel Calpain-3 Mutation. *PLoS One* **2017**, *12*, e0170280. https://doi.org/10.1371/journal.pone.0170280.

103. Fanin, M.; Benedicenti, F.; Fritegotto, C.; Nascimbeni, A. C.; Peterle, E.; Stanzial, F.; Cristofoletti, A.; Castellan, C.; Angelini, C. An Intronic Mutation Causes Severe LGMD2A in a Large Inbred Family Belonging to a Genetic Isolate in the Alps. *Clin. Genet.* **2012**, *82*, 601–602. https://doi.org/10.1111/j.1399-0004.2012.01873.x.
104. Young, K.; Foroud, T.; Williams, P.; Jackson, C. E.; Beckmann, J. S.; Cohen, D.; Conneally, P. M.; Tischfield, J.; Hodes, M. E. Confirmation of Linkage of Limb-Girdle Muscular Dystrophy, Type 2, to Chromosome 15. *Genomics* **1992**, *13*, 1370–1371. https://doi.org/10.1016/0888-7543(92)90074-3.
105. Richard, I.; Beckmann, J. S. How Neutral Are Synonymous Codon Mutations? *Nature genetics*. United States July 1995, pp.p 259. https://doi.org/10.1038/ng0795-259.
106. Pogoda, T. V; Krakhmaleva, I. N.; Lipatova, N. A.; Shakhovskaya, N. I.; Shishkin, S. S.; Limborska, S. A. High Incidence of 550delA Mutation of CAPN3 in LGMD2 Patients from Russia. *Hum. Mutat.* **2000**, *15*, 295. https://doi.org/10.1002/(SICI)1098-1004(200003)15:3<295::AID-HUMU15>3.0.CO;2-8.
107. Canki-Klain, N.; Milic, A.; Kovac, B.; Trlaja, A.; Grgicevic, D.; Zurak, N.; Fardeau, M.; Leturcq, F.; Kaplan, J.-C.; Urtizberea, J. A.; et al. Prevalence of the 550delA Mutation in Calpainopathy (LGMD 2A) in Croatia. *Am. J. Med. Genet. A* **2004**, *125A*, 152–156. https://doi.org/10.1002/ajmg.a.20408.
108. Chrobakova, T.; Hermanova, M.; Kroupova, I.; Vondracek, P.; Marikova, T.; Mazanec, R.; Zamecnik, J.; Stanek, J.; Havlova, M.; Fajkusova, L. Mutations in Czech LGMD2A Patients Revealed by Analysis of Calpain3 MRNA and Their Phenotypic Outcome. *Neuromuscul. Disord.* **2004**, *14*, 659–665. https://doi.org/10.1016/j.nmd.2004.05.005.
109. Fanin, M.; Nascimbeni, A. C.; Fulizio, L.; Angelini, C. The Frequency of Limb Girdle Muscular Dystrophy 2A in Northeastern Italy. *Neuromuscul. Disord.* **2005**, *15*, 218–224. https://doi.org/10.1016/j.nmd.2004.11.003.
110. Milic, A.; Canki-Klain, N. Calpainopathy (LGMD2A) in Croatia: Molecular and Haplotype Analysis. *Croat. Med. J.* **2005**, *46*, 657–663.
111. Balci, B.; Aurino, S.; Haliloglu, G.; Talim, B.; Erdem, S.; Akcoren, Z.; Tan, E.; Caglar, M.; Richard, I.; Nigro, V.; et al. Calpain-3 Mutations in Turkey. *Eur. J. Pediatr.* **2006**, *165*, 293–298. https://doi.org/10.1007/s00431-005-0046-3.
112. Hanisch, F.; Muller, C. R.; Grimm, D.; Xue, L.; Traufeller, K.; Merkenschlager, A.; Zierz, S.; Deschauer, M. Frequency of Calpain-3 c.550delA Mutation in Limb Girdle Muscular Dystrophy Type 2 and Isolated HyperCKemia in German Patients. *Clin. Neuropathol.* **2007**, *26*, 157–163.
113. Todorova, A.; Georgieva, B.; Tournev, I.; Todorov, T.; Bogdanova, N.; Mitev, V.; Mueller, C. R.; Kremensky, I.; Horst, J. A Large Deletion and Novel Point Mutations in the Calpain 3 Gene (CAPN3) in Bulgarian LGMD2A Patients. *Neurogenetics* **2007**, *8*, 225–229. https://doi.org/10.1007/s10048-007-0083-3.
114. Stehlikova, K.; Skalova, D.; Zidkova, J.; Mrazova, L.; Vondracek, P.; Mazanec, R.; Vohanka, S.; Haberlova, J.; Hermanova, M.; Zamecnik, J.; et al. Autosomal Recessive Limb-Girdle Muscular Dystrophies in the Czech Republic. *BMC Neurol.* **2014**, *14*, 154. https://doi.org/10.1186/s12883-

014-0154-7.

115. Dorobek, M.; Ryniewicz, B.; Kabzinska, D.; Fidzianska, A.; Styczynska, M.; Hausmanowa-Petrusewicz, I. The Frequency of c.550delA Mutation of the CANP3 Gene in the Polish LGMD2A Population. *Genet. Test. Mol. Biomarkers* **2015**, *19*, 637–640. https://doi.org/10.1089/gtmb.2015.0131.

116. Ankala, A.; Kohn, J. N.; Dastur, R.; Gaitonde, P.; Khadilkar, S. V; Hegde, M. R. Ancestral Founder Mutations in Calpain-3 in the Indian Agarwal Community: Historical, Clinical, and Molecular Perspective. *Muscle Nerve* **2013**, *47*, 931–937. https://doi.org/10.1002/mus.23763.

117. Khadilkar, S. V; Chaudhari, C. R.; Dastur, R. S.; Gaitonde, P. S.; Yadav, J. G. Limb-Girdle Muscular Dystrophy in the Agarwals: Utility of Founder Mutations in CAPN3 Gene. *Ann. Indian Acad. Neurol.* **2016**, *19*, 108–111. https://doi.org/10.4103/0972-2327.175435.

118. Cerino, M.; Campana-Salort, E.; Salvi, A.; Cintas, P.; Renard, D.; Juntas Morales, R.; Tard, C.; Leturcq, F.; Stojkovic, T.; Bonello-Palot, N.; et al. Novel CAPN3 Variant Associated with an Autosomal Dominant Calpainopathy. *Neuropathol. Appl. Neurobiol.* **2020**, *46*, 564–578. https://doi.org/10.1111/nan.12624.

119. Herasse, M.; Ono, Y.; Fougerousse, F.; Kimura, E.; Stockholm, D.; Beley, C.; Montarras, D.; Pinset, C.; Sorimachi, H.; Suzuki, K.; et al. Expression and Functional Characteristics of Calpain 3 Isoforms Generated through Tissue-Specific Transcriptional and Posttranscriptional Events. *Mol. Cell. Biol.* **1999**, *19*, 4047–4055. https://doi.org/10.1128/mcb.19.6.4047.

120. Kawabata, Y.; Hata, S.; Ono, Y.; Ito, Y.; Suzuki, K.; Abe, K.; Sorimachi, H. Newly Identified Exons Encoding Novel Variants of P94/Calpain 3 Are Expressed Ubiquitously and Overlap the Alpha-Glucosidase C Gene. *FEBS Lett.* **2003**, *555*, 623–630. https://doi.org/10.1016/s0014-5793(03)01324-3.

121. Leiden database. Avaiable online: https://databases.lovd.nl/shared/genes/CAPN3 (accessed on1 December, 2020).

122. Blazquez, L.; Azpitarte, M.; Saenz, A.; Goicoechea, M.; Otaegui, D.; Ferrer, X.; Illa, I.; Gutierrez-Rivas, E.; Vilchez, J. J.; Lopez de Munain, A.; et al. Characterization of Novel CAPN3 Isoforms in White Blood Cells: An Alternative Approach for Limb-Girdle Muscular Dystrophy 2A Diagnosis. *Neurogenetics* **2008**, *9*, 173–182. https://doi.org/10.1007/s10048-008-0129-1.

123. Richard, I.; Hogrel, J.-Y.; Stockholm, D.; Payan, C. A. M.; Fougerousse, F.; Eymard, B.; Mignard, C.; Lopez de Munain, A.; Fardeau, M.; Urtizberea, J. A. Natural History of LGMD2A for Delineating Outcome Measures in Clinical Trials. *Ann. Clin. Transl. Neurol.* **2016**, *3*, 248–265. https://doi.org/10.1002/acn3.287.

124. Gallardo, E.; Saenz, A.; Illa, I. *Limb-Girdle Muscular Dystrophy 2A*, 1st ed.er ed.; Amsterdam, Netherlands,; Aminoff, M. J., Boller, F., Swaab, D. F., Eds.; 2011; https://doi.org/10.1016/b978-0-08-045031-5.00006-2.

125. Baird, M. F.; Graham, S. M.; Baker, J. S.; Bickerstaff, G. F. Creatine-Kinase- and Exercise-Related Muscle Damage Implications for Muscle Performance and Recovery. *J. Nutr. Metab.* **2012**, *2012*, 960363. https://doi.org/10.1155/2012/960363.

126. Sáenz, A.; Ono, Y.; Sorimachi, H.; Goicoechea, M.; Leturcq, F.; Blázquez, L.; García-Bragado, F.; Marina, A.; Poza, J. J.; Azpitarte, M.; et al. Does the Severity of the LGMD2A Phenotype in Compound Heterozygotes Depend on the Combination of Mutations? *Muscle and Nerve* **2011**, *44*, 710–714. https://doi.org/10.1002/mus.22194.

127. Ono, Y.; Shindo, M.; Doi, N.; Kitamura, F.; Gregorio, C. C.; Sorimachi, H. The N- and C-Terminal Autolytic Fragments of CAPN3/P94/Calpain-3 Restore Proteolytic Activity by Intermolecular Complementation. *Proc. Natl. Acad. Sci.* **2014**, *111*, E5527–E5536. https://doi.org/10.1073/pnas.1411959111.

128. Schessl, J.; Walter, M. C.; Schreiber, G.; Schara, U.; Müller, C. R.; Lochmüller, H.; Bönnemann, C. G.; Korinthenberg, R.; Kirschner, J. Phenotypic Variability in Siblings with Calpainopathy (LGMD2A). *Acta Myol.* **2008**, *27*, 54–58.

129. Mercuri, E.; Bushby, K.; Ricci, E.; Birchall, D.; Pane, M.; Kinali, M.; Allsop, J.; Nigro, V.; Saenz, A.; Nascimbeni, A.; et al. Muscle MRI Findings in Patients with Limb Girdle Muscular Dystrophy with Calpain 3 Deficiency (LGMD2A) and Early Contractures. *Neuromuscul. Disord.* **2005**, *15*, 164–171. https://doi.org/10.1016/j.nmd.2004.10.008.

130. Bushby, K. M. Making Sense of the Limb-Girdle Muscular Dystrophies. *Brain* **1999**, *122 (Pt 8*, 1403–1420. https://doi.org/10.1093/brain/122.8.1403.

131. Pollitt, C.; Anderson, L. V; Pogue, R.; Davison, K.; Pyle, A.; Bushby, K. M. The Phenotype of Calpainopathy: Diagnosis Based on a Multidisciplinary Approach. *Neuromuscul. Disord.* **2001**, *11*, 287–296.

132. Rajakumar, D.; Alexander, M.; Oommen, A. Oxidative Stress, NF-Kß and the Ubiquitin Proteasomal Pathway in the Pathology of Calpainopathy. *Neurochem. Res.* **2013**, *38*, 2009–2018. https://doi.org/10.1007/s11064-013-1107-z.

133. Nilsson, M. I.; Macneil, L. G.; Kitaoka, Y.; Alqarni, F.; Suri, R.; Akhtar, M.; Haikalis, M. E.; Dhaliwal, P.; Saeed, M.; Tarnopolsky, M. a. Redox State and Mitochondrial Respiratory Chain Function in Skeletal Muscle of LGMD2A Patients. *PLoS One* **2014**, *9*, e102549. https://doi.org/10.1371/journal.pone.0102549.

134. Toral-Ojeda, I.; Aldanondo, G.; Lasa-Elgarresta, J.; Lasa-Fernández, H.; Fernández-Torrón, R.; López de Munain, A.; Vallejo-Illarramendi, A.; Lasa-Fernandez, H.; Fernandez-Torron, R.; Lopez de Munain, A.; et al. Calpain 3 Deficiency Affects SERCA Expression and Function in the Skeletal Muscle. *Expert Rev. Mol. Med.* **2016**, *18*, e7. https://doi.org/10.1017/erm.2016.9.

135. Toral-Ojeda, I.; Aldanondo, G.; Lasa-Elgarresta, J.; Lasa-Fernandez, H.; Vesga-Castro, C.; Mouly, V.; Munain, A. L. de; Vallejo-Illarramendi, A. A Novel Functional *In Vitro* Model That Recapitulates Human Muscle Disorders. In *Muscle Cell and Tissue - Current Status of Research Field*; Kuala Lumpur, Malaysia,; Sakuma, K., Ed.; 2018; IntechOpen: Kuala Lumpur, Malaysia, 2018; pp.pp 133–153. https://doi.org/10.5772/intechopen.75903.

136. Kramerova, I.; Kudryashova, E.; Tidball, J. G.; Spencer, M. J. Null Mutation of Calpain 3 (P94) in Mice Causes Abnormal Sarcomere Formation *in Vivo* and in Vitro. *Hum. Mol. Genet.* **2004**, *13*, 1373–1388. https://doi.org/10.1093/hmg/ddh153.

137. El-Khoury, R.; Traboulsi, S.; Hamad, T.; Lamaa, M.; Sawaya, R.; Ahdab-Barmada, M. Divergent Features of Mitochondrial Deficiencies in LGMD2A Associated With Novel Calpain-3 Mutations. *J. Neuropathol. Exp. Neurol.* **2019**, *78*, 88–98. https://doi.org/10.1093/jnen/nly113.

138. Yalvac, M. E.; Amornvit, J.; Braganza, C.; Chen, L.; Hussain, S. R. A.; Shontz, K. M.; Montgomery, C. L.; Flanigan, K. M.; Lewis, S.; Sahenk, Z. Impaired Regeneration in Calpain-3 Null Muscle Is Associated with Perturbations in MTORC1 Signaling and Defective Mitochondrial Biogenesis. *Skelet. Muscle* **2017**, *7*, 1–18. https://doi.org/10.1186/s13395-017-0146-6.

139. Kramerova, I.; Kudryashova, E.; Wu, B.; Germain, S.; Vandenborne, K.; Romain, N.; Haller, R. G.; Verity, M. A.; Spencer, M. J. Mitochondrial Abnormalities, Energy Deficit and Oxidative Stress Are Features of Calpain 3 Deficiency in Skeletal Muscle. *Hum. Mol. Genet.* **2009**, *18*, 3194–3205. https://doi.org/10.1093/hmg/ddp257.

140. Fanin, M.; Angelini, C. Protein and Genetic Diagnosis of Limb Girdle Muscular Dystrophy Type 2A: The Yield and the Pitfalls. *Muscle and Nerve* **2015**, *52*, 163–173. https://doi.org/10.1002/mus.24682.

141. Krahn, M.; Goicoechea, M.; Hanisch, F.; Groen, E.; Bartoli, M.; Pécheux, C.; Garcia-Bragado, F.; Leturcq, F.; Jeannet, P. Y.; Lobrinus, J. A.; et al. Eosinophilic Infiltration Related to CAPN3 Mutations: A Pathophysiological Component of Primary Calpainopathy? *Clin. Genet.* **2011**, *80*, 398–402. https://doi.org/10.1111/j.1399-0004.2010.01620.x.

142. Carafoli, E.; Molinari, M. Calpain: A Protease in Search of a Function? *Biochem. Biophys. Res. Commun.* **1998**, *247*, 193–203. https://doi.org/10.1006/bbrc.1998.8378.

143. Santella, L.; Kyozuka, K.; De Riso, L.; Carafoli, E. Calcium, Protease Action, and the Regulation of the Cell Cycle. *Cell Calcium* **1998**, *23*, 123–130. https://doi.org/10.1016/S0143-4160(98)90110-5.

144. Wang, K. K. W. Calpain and Caspase: Can You Tell the Difference? *Trends Neurosci.* **2000**, *23*, 20–26. https://doi.org/10.1016/S0166-2236(99)01479-4.

145. Glading, A.; Lauffenburger, D. A.; Wells, A. Cutting to the Chase: Calpain Proteases in Cell Motility. *Trends Cell Biol.* **2002**, *12*, 46–54. https://doi.org/10.1016/S0962-8924(01)02179-1.

146. Ono, Y.; Ojima, K.; Shinkai-Ouchi, F.; Hata, S.; Sorimachi, H. An Eccentric Calpain, CAPN3/P94/Calpain-3. *Biochimie* **2016**, *122*, 169–187. https://doi.org/10.1016/j.biochi.2015.09.010.

147. Ye, Q.; Campbell, R. L.; Davies, P. L. Structures of Human Calpain-3 Protease Core with and without Bound Inhibitor Reveal Mechanisms of Calpain Activation. *J. Biol. Chem.* **2018**, *293*, 4056–4070. https://doi.org/10.1074/jbc.RA117.001097.

148. Sorimachi, H.; Toyama-Sorimachi, N.; Saido, T. C.; Kawasaki, H.; Sugita, H.; Miyasaka, M.; Arahata, K. I.; Ishiura, S.; Suzuki, K. Muscle-Specific Calpain, P94, Is Degraded by Autolysis Immediately after Translation, Resulting in Disappearance from Muscle. *J. Biol. Chem.* **1993**, *268*, 10593–10605.

149. Ono, Y.; Ojima, K.; Torii, F.; Takaya, E.; Doi, N.; Nakagawa, K.; Hata, S.; Abe, K.; Sorimachi, H. Skeletal Muscle-Specific Calpain Is an Intracellular Na^{+}- Dependent Protease. *J. Biol. Chem.* **2010**, *285*, 22986–22998. https://doi.org/10.1074/jbc.M110.126946.

150. Ono, Y.; Torii, F.; Ojima, K.; Doi, N.; Yoshioka, K.; Kawabata, Y.; Labeit, D.; Labeit, S.; Suzuki, K.; Abe, K.; et al. Suppressed Disassembly of Autolyzing P94/CAPN3 by N2A Connectin/Titin in a Genetic Reporter System. *J. Biol. Chem.* **2006**, *281*, 18519–18531. https://doi.org/10.1074/jbc.M601029200.

151. Kramerova, I.; Kudryashova, E.; Venkatraman, G.; Spencer, M. J. Calpain 3 Participates in Sarcomere Remodeling by Acting Upstream of the Ubiquitin - Proteasome Pathway. *Hum. Mol. Genet.* **2005**, *14*, 2125–2134. https://doi.org/10.1093/hmg/ddi217.

152. Ojima, K.; Ono, Y.; Ottenheijm, C.; Hata, S.; Suzuki, H.; Granzier, H.; Sorimachi, H. Non-Proteolytic Functions of Calpain-3 in Sarcoplasmic Reticulum in Skeletal Muscles. *J. Mol. Biol.* **2011**, *407*, 439–449. https://doi.org/10.1016/j.jmb.2011.01.057.

153. Kramerova, I.; Kudryashova, E.; Wu, B.; Ottenheijm, C.; Granzier, H.; Spencer, M. J. Novel Role of Calpain-3 in the Triad-Associated Protein Complex Regulating Calcium Release in Skeletal Muscle. *Hum. Mol. Genet.* **2008**, *17*, 3271–3280. https://doi.org/10.1093/hmg/ddn223.

154. Dayanithi, G.; Richard, I.; Viero, C.; Mazuc, E.; Mallie, S.; Valmier, J.; Bourg, N.; Herasse, M.; Marty, I.; Lefranc, G.; et al. Alteration of Sarcoplasmic Reticulum Ca^{2+} Release in Skeletal Muscle from Calpain 3-Deficient Mice. *Int. J. Cell Biol.* **2009**, *2009*, 340346. https://doi.org/10.1155/2009/340346.

155. Baghdiguian, S.; Martin, M.; Richard, I.; Pons, F.; Astier, C.; Bourg, N.; Hay, R. T.; Chemaly, R.; Halaby, G.; Loiselet, J.; et al. Calpain 3 Deficiency Is Associated with Myonuclear Apoptosis and Profound Perturbation of the Iκβα/NF-Kβ Pathway in Limb-Girdle Muscular Dystrophy Type 2A. *Nat. Med.* **1999**, *5*, 503–511. https://doi.org/10.1038/8385.

156. Sorimachi, H.; Kinbara, K.; Kimura, S.; Takahashi, M.; Ishiura, S.; Sasagawa, N.; Sorimachi, N.; Shimada, H.; Tagawa, K.; Maruyama, K.; et al. Muscle-Specific Calpain, P94, Responsible for Limb Girdle Muscular Dystrophy Type 2A, Associates with Connectin through IS2, a P94-Specific Sequence. *J. Biol. Chem.* **1995**, *270*, 31158–31162. https://doi.org/10.1074/jbc.270.52.31158.

157. Santoso, J. W.; McCain, M. L. Neuromuscular Disease Modeling on a Chip. *Dis. Model. Mech.* **2020**, *13*, dmm044867. https://doi.org/10.1242/dmm.044867.

158. Menconi, M.; Gonnella, P.; Petkova, V.; Lecker, S.; Hasselgren, P.-O. Dexamethasone and Corticosterone Induce Similar, but Not Identical, Muscle Wasting Responses in Cultured L6 and C2C12 Myotubes. *J. Cell. Biochem.* **2008**, *105*, 353–364. https://doi.org/10.1002/jcb.21833.

159. Zhao, Q.; Yang, S. T.; Wang, J. J.; Zhou, J.; Xing, S. S.; Shen, C. C.; Wang, X. X.; Yue, Y. X.; Song, J.; Chen, M.; et al. TNF Alpha Inhibits Myogenic Differentiation of C2C12 Cells through NF-Kβ Activation and Impairment of IGF-1 Signaling Pathway. *Biochem. Biophys. Res. Commun.* **2015**, *458*, 790–795. https://doi.org/10.1016/j.bbrc.2015.02.026.

160. Hashimoto, N.; Kiyono, T.; Wada, M. R.; Umeda, R.; Goto, Y.; Nonaka, I.; Shimizu, S.; Yasumoto, S.; Inagawa-Ogashiwa, M. Osteogenic Properties of Human Myogenic Progenitor Cells. *Mech. Dev.* **2008**, *125*, 257–269. https://doi.org/https://doi.org/10.1016/j.mod.2007.11.004.

161. Decary, S.; Mouly, V.; Hamida, C. B.; Sautet, A.; Barbet, J. P.; Butler-Browne, G. S. Replicative Potential and Telomere Length in Human Skeletal Muscle: Implications for Satellite Cell-Mediated Gene Therapy. *Hum. Gene Ther.* **1997**, *8*, 1429–1438. https://doi.org/10.1089/hum.1997.8.12-1429.

162. Zhu, C.-H. H.; Mouly, V.; Cooper, R. N.; Mamchaoui, K.; Bigot, A.; Shay, J. W.; Di Santo, J. P.; Butler-Browne, G. S.; Wright, W. E. Cellular Senescence in Human Myoblasts Is Overcome by Human Telomerase Reverse Transcriptase and Cyclin-Dependent Kinase 4: Consequences in Aging Muscle and Therapeutic Strategies for Muscular Dystrophies. *Aging Cell* **2007**, *6*, 515–523. https://doi.org/10.1111/j.1474-9726.2007.00306.x.

163. Saini, J.; Faroni, A.; Abd Al Samid, M.; Reid, A. J.; Lightfoot, A. P.; Mamchaoui, K.; Mouly, V.; Butler-Browne, G.; McPhee, J. S.; Degens, H.; et al. Simplified *in Vitro* Engineering of Neuromuscular Junctions between Rat Embryonic Motoneurons and Immortalized Human Skeletal Muscle Cells. *Stem Cells Cloning* **2019**, *12*, 1–9. https://doi.org/10.2147/SCCAA.S187655.

164. Morris, T. A.; Naik, J.; Fibben, K. S.; Kong, X.; Kiyono, T.; Yokomori, K.; Grosberg, A. Striated

Myocyte Structural Integrity: Automated Analysis of Sarcomeric z-Discs. *PLoS Comput. Biol.* **2020**, *16*, e1007676. https://doi.org/10.1371/journal.pcbi.1007676.

165. Salani, S.; Donadoni, C.; Rizzo, F.; Bresolin, N.; Comi, G. P.; Corti, S. Generation of Skeletal Muscle Cells from Embryonic and Induced Pluripotent Stem Cells as an *in Vitro* Model and for Therapy of Muscular Dystrophies. *J. Cell. Mol. Med.* **2012**, *16*, 1353–1364. https://doi.org/10.1111/j.1582-4934.2011.01498.x.

166. Soblechero-Martín, P.; Albiasu-Arteta, E.; Anton-Martinez, A.; Garcia-Jimenez, I.; González-Iglesias, G.; Larrañaga-Aiestaran, I.; López-Martinez, A.; Poyatos-García, J.; Ruiz-Del-Yerro, E.; Gonzalez, F.; et al. A CRISPR/Cas9-Based Approach For Editing Immortalised Human Myoblasts To Model Duchenne Muscular Dystrophy *In Vitro*. *bioRxiv* **2020**, 2020.02.24.962316. https://doi.org/10.1101/2020.02.24.962316.

167. Selvaraj, S.; Filareto, A.; Kiley, J.; Voytas, D.; Kyba, M.; Perlingeiro, R. Gene Correction of LGMD2A Patient-Specific IPS Cells for Targeted Autologous Cell Therapy. *Mol. Ther.* **2016**, *24*, S125–S126. https://doi.org/10.1016/s1525-0016(16)33121-5.

168. Lin, C.-Y.; Yoshida, M.; Li, L.-T.; Ikenaka, A.; Oshima, S.; Nakagawa, K.; Sakurai, H.; Matsui, E.; Nakahata, T.; Saito, M. K. IPSC-Derived Functional Human Neuromuscular Junctions Model the Pathophysiology of Neuromuscular Diseases. *JCI insight* **2019**, *4*. https://doi.org/10.1172/jci.insight.124299.

169. Rao, L.; Tang, W.; Wei, Y.; Bao, L.; Chen, J.; Chen, H.; He, L.; Lu, P.; Ren, J.; Wu, L.; et al. Highly Efficient Derivation of Skeletal Myotubes from Human Embryonic Stem Cells. *Stem cell Rev. reports* **2012**, *8*, 1109–1119. https://doi.org/10.1007/s12015-012-9413-4.

170. Hellbach, N.; Peterson, S.; Haehnke, D.; Shankar, A.; LaBarge, S.; Pivaroff, C.; Saenger, S.; Thomas, C.; McCarthy, K.; Ebeling, M.; et al. Impaired Myogenic Development, Differentiation and Function in HESC-Derived SMA Myoblasts and Myotubes. *PLoS One* **2018**, *13*, e0205589. https://doi.org/10.1371/journal.pone.0205589.

171. Takahashi, K.; Yamanaka, S. Induction of Pluripotent Stem Cells from Mouse Embryonic and Adult Fibroblast Cultures by Defined Factors. *Cell* **2006**, *126*, 663–676. https://doi.org/10.1016/j.cell.2006.07.024.

172. Darabi, R.; Arpke, R. W.; Irion, S.; Dimos, J. T.; Grskovic, M.; Kyba, M.; Perlingeiro, R. C. R. Human ES- and IPS-Derived Myogenic Progenitors Restore DYSTROPHIN and Improve Contractility upon Transplantation in Dystrophic Mice. *Cell Stem Cell* **2012**, *10*, 610–619. https://doi.org/10.1016/j.stem.2012.02.015.

173. Lainé, J.; Skoglund, G.; Fournier, E.; Tabti, N. Development of the Excitation-Contraction Coupling Machinery and Its Relation to Myofibrillogenesis in Human IPSC-Derived Skeletal Myocytes. *Skelet. Muscle* **2018**, *8*, 1. https://doi.org/10.1186/s13395-017-0147-5.

174. Juretić, N.; Jorquera, G.; Caviedes, P.; Jaimovich, E.; Riveros, N. Electrical Stimulation Induces Calcium-Dependent up-Regulation of Neuregulin-1β in Dystrophic Skeletal Muscle Cell Lines. *Cell. Physiol. Biochem.* **2012**, *29*, 919–930. https://doi.org/10.1159/000188068.

175. Nikolić, N.; Skaret Bakke, S.; Tranheim Kase, E.; Rudberg, I.; Flo Halle, I.; Rustan, A. C.; Thoresen, G. H.; Aas, V. Electrical Pulse Stimulation of Cultured Human Skeletal Muscle Cells as an *in Vitro* Model of Exercise. *PLoS One* **2012**, *7*, 1–10. https://doi.org/10.1371/journal.pone.0033203.

176. Scheler, M.; Irmler, M.; Lehr, S.; Hartwig, S.; Staiger, H.; Al-Hasani, H.; Beckers, J.; de Angelis,

M. H.; Häring, H.-U.; Weigert, C. Cytokine Response of Primary Human Myotubes in an *in Vitro* Exercise Model. *Am. J. Physiol. Cell Physiol.* **2013**, *305*, C877-86. https://doi.org/10.1152/ajpcell.00043.2013.

177. Bandi, E.; Jevsek, M.; Mars, T.; Jurdana, M.; Formaggio, E.; Sciancalepore, M.; Fumagalli, G.; Grubic, Z.; Ruzzier, F.; Lorenzon, P. Neural Agrin Controls Maturation of the Excitation-Contraction Coupling Mechanism in Human Myotubes Developing *in Vitro*. *Am. J. Physiol. Cell Physiol.* **2008**, *294*, C66–C73. https://doi.org/10.1152/ajpcell.00248.2007.

178. Rezonja, K.; Sostaric, M.; Vidmar, G.; Mars, T. Dexamethasone Produces Dose-Dependent Inhibition of Sugammadex Reversal in in Vitro Innervated Primary Human Muscle Cells. *Anesth. Analg.* **2014**, *118*, 755–763. https://doi.org/10.1213/ANE.0000000000000108.

179. Tanaka, H.; Furuya, T.; Kameda, N.; Kobayashi, T.; Mizusawa, H. Triad Proteins and Intracellular Ca^{2+} Transients during Development of Human Skeletal Muscle Cells in Aneural and Innervated Cultures. *J. Muscle Res. Cell Motil.* **2000**, *21*, 507–526. https://doi.org/10.1023/A:1026561120566.

180. Guo, X.; Gonzalez, M.; Stancescu, M.; Vandenburgh, H. H.; Hickman, J. J. Neuromuscular Junction Formation between Human Stem Cell-Derived Motoneurons and Human Skeletal Muscle in a Defined System. *Biomaterials* **2011**, *32*, 9602–9611. https://doi.org/10.1016/j.biomaterials.2011.09.014.

181. Tagawa, K.; Taya, C.; Hayashi, Y.; Nakagawa, M.; Ono, Y.; Fukuda, R.; Karasuyama, H.; Toyama-Sorimachi, N.; Katsui, Y.; Hata, S.; et al. Myopathy Phenotype of Transgenic Mice Expressing Active Site-Mutated Inactive P94 Skeletal Muscle-Specific Calpain, the Gene Product Responsible for Limb Girdle Muscular Dystrophy Type 2A. *Hum. Mol. Genet.* **2000**, *9*, 1393–1402. https://doi.org/10.1093/hmg/9.9.1393.

182. Ojima, K.; Kawabata, Y.; Nakao, H.; Nakao, K.; Doi, N.; Kitamura, F.; Ono, Y.; Hata, S.; Suzuki, H.; Kawahara, H.; et al. Dynamic Distribution of Muscle-Specific Calpain in Mice Has a Key Role in Physical-Stress Adaptation and Is Impaired in Muscular Dystrophy. *J. Clin. Invest.* **2010**, *120*, 2672–2683. https://doi.org/10.1172/JCI40658.

183. Spencer, M. J.; Guyon, J. R.; Sorimachi, H.; Potts, A.; Richard, I.; Herasse, M.; Chamberlain, J.; Dalkilic, I.; Kunkel, L. M.; Beckmann, J. S. Stable Expression of Calpain 3 from a Muscle Transgene *in Vivo*: Immature Muscle in Transgenic Mice Suggests a Role for Calpain 3 in Muscle Maturation. *Proc. Natl. Acad. Sci. U. S. A.* **2002**, *99*, 8874–8879. https://doi.org/10.1073/pnas.132269299.

184. Ermolova, N.; Kudryashova, E.; Difranco, M.; Vergara, J.; Kramerova, I.; Spencer, M. Pathogenity of Some Limb Girdle Muscular Dystrophy Mutations Can Result from Reduced Anchorage to Myofibrils and Altered Stability of Calpain 3. *Hum. Mol. Genet.* **2011**, *20*, 3331–3345. https://doi.org/10.1093/hmg/ddr239.

185. Richard, I.; Roudaut, C.; Marchand, S.; Baghdiguian, S.; Herasse, M.; Stockholm, D.; Ono, Y.; Suel, L.; Bourg, N.; Sorimachi, H.; et al. Loss of Calpain 3 Proteolytic Activity Leads to Muscular Dystrophy and to Apoptosis-Associated IκBα/Nuclear Factor KB Pathway Perturbation in Mice. *J. Cell Biol.* **2000**, *151*, 1583–1590. https://doi.org/10.1083/jcb.151.7.1583.

186. Ojima, K.; Ono, Y.; Doi, N.; Yoshioka, K.; Kawabata, Y.; Labeit, S.; Sorimachi, H. Myogenic Stage, Sarcomere Length, and Protease Activity Modulate Localization of Muscle-Specific Calpain. *J. Biol. Chem.* **2007**, *282*, 14493–14504. https://doi.org/10.1074/jbc.M610806200.

187. Gunning, P. W.; Hardeman, E. C.; Lappalainen, P.; Mulvihill, D. P. Tropomyosin - Master Regulator of Actin Filament Function in the Cytoskeleton. *J. Cell Sci.* **2015**, *128*, 2965–2974. https://doi.org/10.1242/jcs.172502.

188. Escolar, D. M.; O'Carroll, P.; Leshner, R. *Treatment and Management of Muscular Dystrophies*; Philadelphia, The United Staes of America,; Bertorini, T. E., Ed.; 2011; https://doi.org/10.1016/B978-1-4377-0372-6.00019-0.

189. Taveau, M.; Bourg, N.; Sillon, G.; Roudaut, C.; Bartoli, M.; Richard, I. Calpain 3 Is Activated through Autolysis within the Active Site and Lyses Sarcomeric and Sarcolemmal Components. *Mol. Cell. Biol.* **2003**, *23*, 9127–9135. https://doi.org/10.1128/MCB.23.24.9127-9135.2003.

190. Zak, R.; Martin, A. F.; Prior, G.; Rabinowitz, M. Comparison of Turnover of Several Myofibrillar Proteins and Critical Evaluation of Double Isotope Method. *J. Biol. Chem.* **1977**, *252*, 3430–3435.

191. Isaacs, W. B.; Kim, I. S.; Struve, A.; Fulton, A. B. Biosynthesis of Titin in Cultured Skeletal Muscle Cells. *J. Cell Biol.* **1989**, *109*, 2189–2195. https://doi.org/10.1083/jcb.109.5.2189.

192. Beckmann, J. S.; Spencer, M. Calpain 3, the "Gatekeeper" of Proper Sarcomere Assembly, Turnover and Maintenance. *Neuromuscul. Disord.* **2008**, *18*, 913–921. https://doi.org/10.1016/j.nmd.2008.08.005.

193. Ono, Y.; Iemura, S. I.; Novak, S. M.; Doi, N.; Kitamura, F.; Natsume, T.; Gregorio, C. C.; Sorimachi, H. PLEIAD/SIMC1/C5orf25, a Novel Autolysis Regulator for a Skeletal-Muscle-Specific Calpain, CAPN3, Scaffolds a CAPN3 Substrate, CTBP1. *J. Mol. Biol.* **2013**, *425*, 2955–2972. https://doi.org/10.1016/j.jmb.2013.05.009.

194. Vallejo-Illarramendi, A.; Toral-Ojeda, I.; Aldanondo, G.; López de Munain, A. Dysregulation of Calcium Homeostasis in Muscular Dystrophies. *Expert Rev. Mol. Med.* **2014**, *16*, e16. https://doi.org/10.1017/erm.2014.17.

195. Sacco, A.; Mourkioti, F.; Tran, R.; Choi, J.; Llewellyn, M.; Kraft, P.; Shkreli, M.; Delp, S.; Pomerantz, J. H.; Artandi, S. E.; et al. Short Telomeres and Stem Cell Exhaustion Model Duchenne Muscular Dystrophy in Mdx/MTR Mice. *Cell* **2010**, *143*, 1059–1071. https://doi.org/10.1016/j.cell.2010.11.039.

196. Jaka, O.; Casas-Fraile, L.; Azpitarte, M.; Aiastui, A.; López de Munain, A.; Sáenz, A. FRZB and Melusin, Overexpressed in LGMD2A, Regulate Integrin B1D Isoform Replacement Altering Myoblast Fusion and the Integrin- Signalling Pathway. *Expert Rev. Mol. Med.* **2017**, *19*, 1–16. https://doi.org/10.1017/erm.2017.3.

197. Amici, D. R.; Pinal-Fernandez, I.; Mázala, D. A. G.; Lloyd, T. E.; Corse, A. M.; Christopher-Stine, L.; Mammen, A. L.; Chin, E. R. Calcium Dysregulation, Functional Calpainopathy, and Endoplasmic Reticulum Stress in Sporadic Inclusion Body Myositis. *Acta Neuropathol. Commun.* **2017**, *5*, 24. https://doi.org/10.1186/s40478-017-0427-7.

198. Michel, L. Y. M.; Hoenderop, J. G. J.; Bindels, R. J. M. Calpain-3-Mediated Regulation of the Na^+-Ca^{2+} Exchanger Isoform 3. *Pflugers Arch. Eur. J. Physiol.* **2016**, *468*, 243–255. https://doi.org/10.1007/s00424-015-1747-8.

199. Matsakas, A.; Patel, K. Intracellular Signalling Pathways Regulating the Adaptation of Skeletal Muscle to Exercise and Nutritional Changes. *Histol. Histopathol.* **2009**, *24*, 209–222. https://doi.org/10.14670/HH-24.209.

200. Cohen, N.; Kudryashova, E.; Kramerova, I.; Anderson, L. V. B.; Beckmann, J. S.; Bushby, K.;

Spencer, M. J. Identification of Putative *in Vivo* Substrates of Calpain 3 by Comparative Proteomics of Overexpressing Transgenic and Nontransgenic Mice. *Proteomics* **2006**, *6*, 6075–6084. https://doi.org/10.1002/pmic.200600199.

201. Kramerova, I.; Beckmann, J. S.; Spencer, M. J. Molecular and Cellular Basis of Calpainopathy (Limb Girdle Muscular Dystrophy Type 2A). *Biochim. Biophys. Acta* **2007**, *1772*, 128–144. https://doi.org/10.1016/j.bbadis.2006.07.002.

202. Sáenz, A.; Azpitarte, M.; Armañanzas, R.; Leturcq, F.; Alzualde, A.; Inza, I.; García-Bragado, F.; De la Herran, G.; Corcuera, J.; Cabello, A.; et al. Gene Expression Profiling in Limb-Girdle Muscular Dystrophy 2A. *PLoS One* **2008**, *3*, e3750. https://doi.org/10.1371/journal.pone.0003750.

203. Kroemer, G.; Galluzzi, L.; Brenner, C. Mitochondrial Membrane Permeabilization in Cell Death. *Physiol. Rev.* **2007**, *87*, 99–163. https://doi.org/10.1152/physrev.00013.2006.

204. Handschin, C.; Rhee, J.; Lin, J.; Tarr, P. T.; Spiegelman, B. M. An Autoregulatory Loop Controls Peroxisome Proliferator-Activated Receptor Gamma Coactivator 1alpha Expression in Muscle. *Proc. Natl. Acad. Sci. U. S. A.* **2003**, *100*, 7111–7116. https://doi.org/10.1073/pnas.1232352100.

205. Guo, C.; Sun, L.; Chen, X.; Zhang, D. Oxidative Stress, Mitochondrial Damage and Neurodegenerative Diseases. *Neural Regen. Res.* **2013**, *8*, 2003–2014. https://doi.org/10.3969/j.issn.1673-5374.2013.21.009.

206. Bellinger, A. M.; Reiken, S.; Carlson, C.; Mongillo, M.; Liu, X.; Rothman, L.; Matecki, S.; Lacampagne, A.; Marks, A. R. Hypernitrosylated Ryanodine Receptor/Calcium Release Channels Are Leaky in Dystrophic Muscle Andrew. *Nat. Med.* **2009**, *15*, 325–330. https://doi.org/10.1038/nm.1916.Hypernitrosylated.

207. Raney, M. A.; Turcotte, L. P. Evidence for the Involvement of CaMKII and AMPK in Ca^{2+}-Dependent Signaling Pathways Regulating FA Uptake and Oxidation in Contracting Rodent Muscle. *J. Appl. Physiol.* **2008**, *104*, 1366–1373. https://doi.org/10.1152/japplphysiol.01282.2007.

208. Shan, T.; Zhang, P.; Liang, X.; Bi, P.; Yue, F.; Kuang, S. Lkb1 Is Indispensable for Skeletal Muscle Development, Regeneration, and Satellite Cell Homeostasis. *Stem Cells* **2014**, *32*, 2893–2907. https://doi.org/10.1002/stem.1788.

209. Morita, M.; Gravel, S. P.; Hulea, L.; Larsson, O.; Pollak, M.; St-Pierre, J.; Topisirovic, I. MTOR Coordinates Protein Synthesis, Mitochondrial Activity. *Cell Cycle* **2015**, *14*, 473–480. https://doi.org/10.4161/15384101.2014.991572.

210. Morita, M.; Gravel, S. P.; Chénard, V.; Sikström, K.; Zheng, L.; Alain, T.; Gandin, V.; Avizonis, D.; Arguello, M.; Zakaria, C.; et al. MTORC1 Controls Mitochondrial Activity and Biogenesis through 4E-BP-Dependent Translational Regulation. *Cell Metab.* **2013**, *18*, 698–711. https://doi.org/10.1016/j.cmet.2013.10.001.

211. Rosales, X. Q.; Malik, V.; Sneh, A.; Chen, L.; Lewis, S.; Kota, J.; Gastier-Foster, J. M.; Astbury, C.; Pyatt, R.; Reshmi, S.; et al. Impaired Regeneration in LGMD2A Supported by Increased PAX7-Positive Satellite Cell Content and Muscle-Specific Microrna Dysregulation. *Muscle and Nerve* **2013**, *47*, 731–739. https://doi.org/10.1002/mus.23669.

212. Roberts, T. C.; Blomberg, K. E. M.; McClorey, G.; Andaloussi, S. El; Godfrey, C.; Betts, C.; Coursindel, T.; Gait, M. J.; Smith, C. E.; Wood, M. J. Expression Analysis in Multiple Muscle Groups and Serum Reveals Complexity in the MicroRNA Transcriptome of the Mdx Mouse with Implications for Therapy. *Mol. Ther. - Nucleic Acids* **2012**, *1*, e39. https://doi.org/10.1038/mtna.2012.26.

213. Chen, J. F.; Tao, Y.; Li, J.; Deng, Z.; Yan, Z.; Xiao, X.; Wang, D. Z. MicroRNA-1 and MicroRNA-206 Regulate Skeletal Muscle Satellite Cell Proliferation and Differentiation by Repressing Pax7. *J. Cell Biol.* **2010**, *190*, 867–879. https://doi.org/10.1083/jcb.200911036.

214. Dey, B. K.; Gagan, J.; Dutta, A. MiR-206 and -486 Induce Myoblast Differentiation by Downregulating Pax7. *Mol. Cell. Biol.* **2011**, *31*, 1329–1329. https://doi.org/10.1128/mcb.05013-11.

215. Liu, N.; Bezprozvannaya, S.; Shelton, J. M.; Frisard, M. I.; Hulver, M. W.; McMillan, R. P.; Wu, Y.; Voelker, K. A.; Grange, R. W.; Richardson, J. A.; et al. Mice Lacking MicroRNA 133a Develop Dynamin 2-Dependent Centronuclear Myopathy. *J. Clin. Invest.* **2011**, *121*, 3258–3268. https://doi.org/10.1172/JCI46267.

216. Stuelsatz, P.; Pouzoulet, F. F.; Lamarre, Y.; Dargelos, E.; Poussard, S.; Leibovitch, S.; Cottin, P.; Veschambre, P. Down-Regulation of MyoD by Calpain 3 Promotes Generation of Reserve Cells in C2C12 Myoblasts. *J. Biol. Chem.* **2010**, *285*, 12670–12683. https://doi.org/10.1074/jbc.M109.063966.

217. Kramerova, I.; Kudryashova, E.; Wu, B.; Spencer, M. J. Regulation of the M-Cadherin-b-Catenin Complex by Calpain 3 during Terminal Stages of Myogenic Differentiation. *Mol. Cell. Biol.* **2006**, *26*, 8437–8447. https://doi.org/10.1128/MCB.01296-06.

218. Li, H.; Malhotra, S.; Kumar, A. Nuclear Factor-Kappa β Signaling in Skeletal Muscle Atrophy. *J. Mol. Med.* **2008**, *86*, 1113–1126. https://doi.org/10.1007/s00109-008-0373-8.

219. Benayoun, B.; Baghdiguian, S.; Lajmanovich, A.; Bartoli, M.; Daniele, N.; Gicquel, E.; Bourg, N.; Raynaud, F.; Pasquier, M.; Suel, L.; et al. NF-Kβ-Dependent Expression of the Antiapoptotic Factor c-FLIP Is Regulated by Calpain 3, the Protein Involved in Limb-Girdle Muscular Dystrophy Type 2A. *FASEB J.* **2008**, *22*, 1521–1529. https://doi.org/10.1096/fj.07-8701com.

220. Elbaz, M.; Yanay, N.; Laban, S.; Rabie, M.; Mitrani-Rosenbaum, S.; Nevo, Y. Life or Death by NF-Kβ, Losartan Promotes Survival in Dy2J/Dy2J Mouse of MDC1A. *Cell Death Dis.* **2015**, *6*, e1690. https://doi.org/10.1038/cddis.2015.60.

221. Groenendyk, J.; Lynch, J.; Michalak, M. Calreticulin, Ca^{2+}, and Calcineurin-Signaling from the Endoplasmic Reticulum. *Mol. Cells* **2004**, *17*, 383–389.

222. Evans, W. J. Skeletal Muscle Loss: Cachexia, Sarcopenia, and Inactivity. *Am. J. Clin. Nutr.* **2010**, *91*, 1123S-1127S. https://doi.org/10.3945/ajcn.2010.28608A.

223. Bonaldo, P.; Sandri, M. Cellular and Molecular Mechanisms of Muscle Atrophy. *Dis. Model. Mech.* **2013**, *6*, 25–39. https://doi.org/10.1242/dmm.010389.

224. Bachiller, S.; Alonso-Bellido, I. M.; Real, L. M.; Pérez-Villegas, E. M.; Venero, J. L.; Deierborg, T.; Armengol, J. Á.; Ruiz, R. The Ubiquitin Proteasome System in Neuromuscular Disorders: Moving Beyond Movement. *Int. J. Mol. Sci.* **2020**, *21*. https://doi.org/10.3390/ijms21176429.

225. Bilodeau, P. A.; Coyne, E. S.; Wing, S. S. The Ubiquitin Proteasome System in Atrophying Skeletal Muscle: Roles and Regulation. *Am. J. Physiol. Cell Physiol.* **2016**, *311*, C392-403. https://doi.org/10.1152/ajpcell.00125.2016.

226. Fanin, M.; Nascimbeni, A. C.; Angelini, C. Muscle Atrophy in Limb Girdle Muscular Dystrophy 2A: A Morphometric and Molecular Study. *Neuropathol. Appl. Neurobiol.* **2013**, *39*, 762–771. https://doi.org/10.1111/nan.12034.

227. Ono, Y.; Hayashi, C.; Doi, N.; Kitamura, F.; Shindo, M.; Kudo, K.; Tsubata, T.; Yanagida, M.; Sorimachi, H. Comprehensive Survey of P94/Calpain 3 Substrates by Comparative Proteomics--

Possible Regulation of Protein Synthesis by P94. *Biotechnol. J.* **2007**, *2*, 565–576. https://doi.org/10.1002/biot.200700018.

228. Briguet, A.; Erb, M.; Courdier-Fruh, I.; Barzaghi, P.; Santos, G.; Herzner, H.; Lescop, C.; Siendt, H.; Henneboehle, M.; Weyermann, P.; et al. Effect of Calpain and Proteasome Inhibition on Ca^{2+}-Dependent Proteolysis and Muscle Histopathology in the Mdx Mouse. *FASEB J.* **2008**, *22*, 4190–4200. https://doi.org/10.1096/fj.07-099036.
229. Fanin, M.; Nascimbeni, A. C.; Angelini, C. Muscle Atrophy, Ubiquitin-Proteasome, and Autophagic Pathways in Dysferlinopathy. *Muscle Nerve* **2014**, *50*, 340–347. https://doi.org/10.1002/mus.24167.
230. Körner, Z.; Fontes-Oliveira, C. C.; Holmberg, J.; Carmignac, V.; Durbeej, M. Bortezomib Partially Improves Laminin A2 Chain–Deficient Muscular Dystrophy. *Am. J. Pathol.* **2014**, *184*, 1518–1528. https://doi.org/https://doi.org/10.1016/j.ajpath.2014.01.019.
231. Gastaldello, S.; D'Angelo, S.; Franzoso, S.; Fanin, M.; Angelini, C.; Betto, R.; Sandona, D. Inhibition of Proteasome Activity Promotes the Correct Localization of Disease-Causing Alpha-Sarcoglycan Mutants in HEK-293 Cells Constitutively Expressing Beta-, Gamma-, and Delta-Sarcoglycan. *Am. J. Pathol.* **2008**, *173*, 170–181. https://doi.org/10.2353/ajpath.2008.071146.
232. Rajakumar, D.; Senguttuvan, S.; Alexander, M.; Oommen, A. Involvement of Oxidative Stress, Nuclear Factor Kappa B and the Ubiquitin Proteasomal Pathway in Dysferlinopathy. *Life Sci.* **2014**, *108*, 54–61. https://doi.org/10.1016/j.lfs.2014.05.005.
233. Carmignac, V.; Quere, R.; Durbeej, M. Proteasome Inhibition Improves the Muscle of Laminin Alpha2 Chain-Deficient Mice. *Hum. Mol. Genet.* **2011**, *20*, 541–552. https://doi.org/10.1093/hmg/ddq499.
234. Nastasi, T.; Bongiovanni, A.; Campos, Y.; Mann, L.; Toy, J. N.; Bostrom, J.; Rottier, R.; Hahn, C.; Conaway, J. W.; Harris, A. J.; et al. Ozz-E3, a Muscle-Specific Ubiquitin Ligase, Regulates Beta-Catenin Degradation during Myogenesis. *Dev. Cell* **2004**, *6*, 269–282.
235. Vandesompele, J.; De Preter, K.; Pattyn, F.; Poppe, B.; Van Roy, N.; De Paepe, A.; Speleman, F. Accurate Normalization of Real-Time Quantitative RT-PCR Data by Geometric Averaging of Multiple Internal Control Genes. *Genome Biol.* **2002**, *3*, RESEARCH0034. https://doi.org/10.1186/gb-2002-3-7-research0034.
236. Azakir, B. A.; Di Fulvio, S.; Kinter, J.; Sinnreich, M. Proteasomal Inhibition Restores Biological Function of Mis-Sense Mutated Dysferlin in Patient-Derived Muscle Cells. *J. Biol. Chem.* **2012**, *287*, 10344–10354. https://doi.org/10.1074/jbc.M111.329078.
237. Hellemans, J.; Mortier, G.; De Paepe, A.; Speleman, F.; Vandesompele, J. QBase Relative Quantification Framework and Software for Management and Automated Analysis of Real-Time Quantitative PCR Data. *Genome Biol.* **2007**, *8*, R19. https://doi.org/10.1186/gb-2007-8-2-r19.
238. Azakir, B. A.; Erne, B.; Di Fulvio, S.; Stirnimann, G.; Sinnreich, M. Proteasome Inhibitors Increase Missense Mutated Dysferlin in Patients with Muscular Dystrophy. *Sci. Transl. Med.* **2014**, *6*, 250ra112. https://doi.org/10.1126/scitranslmed.3009612.
239. Vissing, J. Limb Girdle Muscular Dystrophies: Classification, Clinical Spectrum and Emerging Therapies. *Curr. Opin. Neurol.* **2016**, *29*, 635–641. https://doi.org/10.1097/WCO.0000000000000375.
240. Sveen, M. L.; Andersen, S. P.; Ingelsrud, L. H.; Blichter, S.; Olsen, N. E.; Jønck, S.; Krag, T. O.;

Vissing, J. Resistance Training in Patients with Limb-Girdle and Becker Muscular Dystrophies. *Muscle and Nerve* **2013**, *47*, 163–169. https://doi.org/10.1002/mus.23491.

241. Sczesny-Kaiser, M.; Kowalewski, R.; Schildhauer, T. A.; Aach, M.; Jansen, O.; Grasmücke, D.; Güttsches, A. K.; Vorgerd, M.; Tegenthoff, M. Treadmill Training with HAL Exoskeleton-A Novel Approach for Symptomatic Therapy in Patients with Limb-Girdle Muscular Dystrophy-Preliminary Study. *Front. Neurosci.* **2017**, *11*, 1–9. https://doi.org/10.3389/fnins.2017.00449.

242. Bartoli, M.; Poupiot, J.; Vulin, A.; Fougerousse, F.; Arandel, L.; Daniele, N.; Roudaut, C.; Noulet, F.; Garcia, L.; Danos, O.; et al. AAV-Mediated Delivery of a Mutated Myostatin Propeptide Ameliorates Calpain 3 but Not α-Sarcoglycan Deficiency. *Gene Ther.* **2007**, *14*, 733–740. https://doi.org/10.1038/sj.gt.3302928.

243. Wagner, K. R.; Fleckenstein, J. L.; Amato, A. A.; Barohn, R. J.; Bushby, K.; Escolar, D. M.; Flanigan, K. M.; Pestronk, A.; Tawil, R.; Wolfe, G. I.; et al. A Phase I/II Trial of MYO-029 in Adult Subjects with Muscular Dystrophy. *Ann. Neurol.* **2008**, *63*, 561–571. https://doi.org/10.1002/ana.21338.

244. Liu, J.; Campagna, J.; John, V.; Damoiseaux, R.; Mokhonova, E.; Becerra, D.; Meng, H.; McNally, E. M.; Pyle, A. D.; Kramerova, I.; et al. A Small-Molecule Approach to Restore a Slow-Oxidative Phenotype and Defective CaMKIIβ Signaling in Limb Girdle Muscular Dystrophy. *Cell Reports Med.* **2020**, *1*, 100122. https://doi.org/https://doi.org/10.1016/j.xcrm.2020.100122.

245. Straub, V.; Bertoli, M. Where Do We Stand in Trial Readiness for Autosomal Recessive Limb Girdle Muscular Dystrophies? *Neuromuscul. Disord.* **2015**, *26*, 111–125. https://doi.org/10.1016/j.nmd.2015.11.012.

246. Roudaut, C.; Le Roy, F.; Suel, L.; Poupiot, J.; Charton, K.; Bartoli, M.; Richard, I. Restriction of Calpain3 Expression to the Skeletal Muscle Prevents Cardiac Toxicity and Corrects Pathology in a Murine Model of Limb-Girdle Muscular Dystrophy. *Circulation* **2013**, *128*, 1094–1104. https://doi.org/10.1161/CIRCULATIONAHA.113.001340.

247. Coalition to Cure Calpain 3. Avaiable online: http://www.curecalpain3.org (accessed on15 May, 2019).

248. Rodino-Klapac, L. R.; Janssen, P. M. L.; Shontz, K. M.; Canan, B.; Montgomery, C. L.; Griffin, D.; Heller, K.; Schmelzer, L.; Handy, C.; Clark, K. R.; et al. Micro-Dystrophin and Follistatin Co-Delivery Restores Muscle Function in Aged DMD Model. *Hum. Mol. Genet.* **2013**, *22*, 4929–4937. https://doi.org/10.1093/hmg/ddt342.

249. Sondergaard, P. C.; Griffin, D. A.; Pozsgai, E. R.; Johnson, R. W.; Grose, W. E.; Heller, K. N.; Shontz, K. M.; Montgomery, C. L.; Liu, J.; Clark, K. R.; et al. AAV. Dysferlin Overlap Vectors Restore Function in Dysferlinopathy Animal Models. *Ann. Clin. Transl. Neurol.* **2015**, *2*, 256–270. https://doi.org/10.1002/acn3.172.

250. Gruntman, A. M.; Flotte, T. R. Delivery of Adeno-Associated Virus Gene Therapy by Intravascular Limb Infusion Methods. *Hum. Gene Ther. Clin. Dev.* **2015**, *26*, 159–164. https://doi.org/10.1089/humc.2015.116.

251. Sarepta Therapeutics. Avaiable online: https://www.sarepta.com/ (accessed on16 May, 2019).

252. Echigoya, Y.; Mouly, V.; Garcia, L.; Yokota, T.; Duddy, W. In Silico Screening Based on Predictive Algorithms as a Design Tool for Exon Skipping Oligonucleotides in Duchenne Muscular Dystrophy. *PLoS One* **2015**, *10*, e0120058. https://doi.org/10.1371/journal.pone.0120058.

253. Echigoya, Y.; Lim, K. R. Q.; Trieu, N.; Bao, B.; Miskew Nichols, B.; Vila, M. C.; Novak, J. S.; Hara, Y.; Lee, J.; Touznik, A.; et al. Quantitative Antisense Screening and Optimization for Exon 51 Skipping in Duchenne Muscular Dystrophy. *Mol. Ther.* **2017**, *25*, 2561–2572. https://doi.org/10.1016/j.ymthe.2017.07.014.

254. UCSC Genome Browser. Avaiable online: https://genome.ucsc.edu/cgi-bin/hgPcr (accessed on6 November, 2019).

255. Thermo Fisher Scientific. Avaiable online: https://www.thermofisher.com/fr/fr/home/brands/thermo-scientific/molecular-biology/molecular-biology-learning-center/molecular-biology-resource-library/thermo-scientific-web (accessed on6 November, 2019).

256. Ren, H.; Li, F.; Tian, C.; Nie, H.; Wang, L.; Li, H.-H.; Zheng, Y. Inhibition of Proteasome Activity by Low-Dose Bortezomib Attenuates Angiotensin II-Induced Abdominal Aortic Aneurysm in Apo E−/− Mice. *Sci. Rep.* **2015**, *5*, 15730. https://doi.org/10.1038/srep15730.

257. Cunningham, J. T.; Rodgers, J. T.; Arlow, D. H.; Vazquez, F.; Mootha, V. K.; Puigserver, P. MTOR Controls Mitochondrial Oxidative Function through a YY1–PGC-1α Transcriptional Complex. *Nature* **2007**, *450*, 736–740. https://doi.org/10.1038/nature06322.

258. Salguero Palacios, R.; Roderfeld, M.; Hemmann, S.; Rath, T.; Atanasova, S.; Tschuschner, A.; Gressner, O. A.; Weiskirchen, R.; Graf, J.; Roeb, E. Activation of Hepatic Stellate Cells Is Associated with Cytokine Expression in Thioacetamide-Induced Hepatic Fibrosis in Mice. *Lab. Investig.* **2008**, *88*, 1192–1203. https://doi.org/10.1038/labinvest.2008.91.

259. Luca, A. De. Use of Grip Strength Meter to Assess the Limb Strength of Mdx Mice. *TREAT-NMD Neuromusclar Netw.* **2008**, *DMD_M.2.2.*, 1–11.

260. Capogrosso, R. F.; Mantuano, P.; Uaesoontrachoon, K.; Cozzoli, A.; Giustino, A.; Dow, T.; Srinivassane, S.; Filipovic, M.; Bell, C.; Vandermeulen, J.; et al. Ryanodine Channel Complex Stabilizer Compound S48168/ARM210 as a Disease Modifier in Dystrophin-Deficient Mdx Mice: Proof-of-Concept Study and Independent Validation of Efficacy. *FASEB J.* **2017**, *32*, 1025–1043. https://doi.org/10.1096/fj.201700182RRR.

261. Kobayashi, Y. M.; Rader, E. P.; Crawford, R. W.; Campbell, K. P. Endpoint Measures in the Mdx Mouse Relevant for Muscular Dystrophy Pre-Clinical Studies. *Neuromuscul. Disord.* **2012**, *22*, 34–42. https://doi.org/10.1016/j.nmd.2011.08.001.

262. Gazzerro, E.; Assereto, S.; Bonetto, A.; Sotgia, F.; Scarfì, S.; Pistorio, A.; Bonuccelli, G.; Cilli, M.; Bruno, C.; Zara, F.; et al. Therapeutic Potential of Proteasome Inhibition in Duchenne and Becker Muscular Dystrophies. *Am. J. Pathol.* **2010**, *176*, 1863–1877. https://doi.org/10.2353/ajpath.2010.090468.

263. Kane, R. C.; Bross, P. F.; Farrell, A. T.; Pazdur, R. Velcade: U.S. FDA Approval for the Treatment of Multiple Myeloma Progressing on Prior Therapy. *Oncologist* **2003**, *8*, 508–513. https://doi.org/10.1634/theoncologist.8-6-508.

264. Araújo, K. P. C.; Moreira, D. F.; Gaiad, T. P.; Miglino, M. A.; Gorniak, S. L.; Feder, D.; Belizário, J. E.; Ambrósio, C. E. T.P.4.03 Treatment with Bortezomib (PS-341) of Golden Retriever Muscular Dystrophy (GRMD): Analysis of Proteasome Inhibition and Morphology of Dystrophic Skeletal Muscle. *Neuromuscul. Disord.* **2009**, *19*, 613. https://doi.org/10.1016/j.nmd.2009.06.218.

265. Guglielmi, V.; Nowis, D.; Tinelli, M.; Malatesta, M.; Paoli, L.; Marini, M.; Manganotti, P.; Sadowski, R.; Wilczynski, G.; Meneghini, V.; et al. Bortezomib-Induced Muscle Toxicity in

Multiple Myeloma. *J. Neuropathol. Exp. Neurol.* **2017**, *76*, 620–630. https://doi.org/10.1093/jnen/nlx043.

266. Warnez Soulie, J. Dystrophie Musculaire Des Ceintures de Type 2A : Étude de Phénomènes Inflammatoires et Développement d'outils de Thérapie Génique, Aix-Marseille Université, 2018.

267. DiFranco, M.; Kramerova, I.; Vergara, J. L.; Spencer, M. J. Attenuated Ca^{2+} Release in a Mouse Model of Limb Girdle Muscular Dystrophy 2A. *Skelet. Muscle* **2016**, *6*, 11. https://doi.org/10.1186/s13395-016-0081-y.

268. Carter, G. T.; Wineinger, M. A.; Walsh, S. A.; Horasek, S. J.; Abresch, R. T.; Fowler, W. M. Effect of Voluntary Wheel-Running Exercise on Muscles of the Mdx Mouse. *Neuromuscul. Disord.* **1995**, *5*, 323–332. https://doi.org/https://doi.org/10.1016/0960-8966(94)00063-F.

269. Folker, E.; Baylies, M. Nuclear Positioning in Muscle Development and Disease. *Front. Physiol.* **2013**, *4*, 363. https://doi.org/10.3389/fphys.2013.00363.

270. Duddy, W.; Duguez, S.; Johnston, H.; Cohen, T. V; Phadke, A.; Gordish-Dressman, H.; Nagaraju, K.; Gnocchi, V.; Low, S.; Partridge, T. Muscular Dystrophy in the Mdx Mouse Is a Severe Myopathy Compounded by Hypotrophy, Hypertrophy and Hyperplasia. *Skelet. Muscle* **2015**, *5*, 16. https://doi.org/10.1186/s13395-015-0041-y.

271. Huebsch, K. A.; Kudryashova, E.; Wooley, C. M.; Sher, R. B.; Seburn, K. L.; Spencer, M. J.; Cox, G. A. Mdm Muscular Dystrophy: Interactions with Calpain 3 and a Novel Functional Role for Titin's N2A Domain. *Hum. Mol. Genet.* **2005**, *14*, 2801–2811. https://doi.org/10.1093/hmg/ddi313.

272. Burks, T. N.; Cohn, R. D. Role of TGF-β Signaling in Inherited and Acquired Myopathies. *Skelet. Muscle* **2011**, *1*, 19. https://doi.org/10.1186/2044-5040-1-19.

273. Spurney, C. F.; Sali, A.; Guerron, A. D.; Iantorno, M.; Yu, Q.; Gordish-Dressman, H.; Rayavarapu, S.; van der Meulen, J.; Hoffman, E. P.; Nagaraju, K. Losartan Decreases Cardiac Muscle Fibrosis and Improves Cardiac Function in Dystrophin-Deficient Mdx Mice. *J. Cardiovasc. Pharmacol. Ther.* **2011**, *16*, 87–95. https://doi.org/10.1177/1074248410381757.

274. Taniguti, A. P. T.; Pertille, A.; Matsumura, C. Y.; Santo Neto, H.; Marques, M. J. Prevention of Muscle Fibrosis and Myonecrosis in Mdx Mice by Suramin, a TGF-B1 Blocker. *Muscle Nerve* **2011**, *43*, 82–87. https://doi.org/10.1002/mus.21869.

275. Nozaki, M.; Li, Y.; Zhu, J.; Ambrosio, F.; Uehara, K.; Fu, F. H.; Huard, J. Improved Muscle Healing after Contusion Injury by the Inhibitory Effect of Suramin on Myostatin, a Negative Regulator of Muscle Growth. *Am. J. Sports Med.* **2008**, *36*, 2354–2362. https://doi.org/10.1177/0363546508322886.

276. Chan, Y.-S.; Li, Y.; Foster, W.; Horaguchi, T.; Somogyi, G.; Fu, F. H.; Huard, J. Antifibrotic Effects of Suramin in Injured Skeletal Muscle after Laceration. *J. Appl. Physiol.* **2003**, *95*, 771–780. https://doi.org/10.1152/japplphysiol.00915.2002.

277. Gosselin, L. E.; Williams, J. E.; Deering, M.; Brazeau, D.; Koury, S.; Martinez, D. A. Localization and Early Time Course of TGF-?1 MRNA Expression in Dystrophic Muscle. *Muscle Nerve* **2004**, *30*, 645–653. https://doi.org/10.1002/mus.20150.

278. Nevo, Y.; Halevy, O.; Genin, O.; Moshe, I.; Turgeman, T.; Harel, M.; Biton, E.; Reif, S.; Pines, M. Fibrosis Inhibition and Muscle Histopathology Improvement in Laminin-Alpha2-Deficient Mice. *Muscle Nerve* **2010**, *42*, 218–229. https://doi.org/10.1002/mus.21706.

279. Hemeryck, A.; Geerts, R.; Monbaliu, J.; Hassler, S.; Verhaeghe, T.; Diels, L.; Verluyten, W.; van

Beijsterveldt, L.; Mamidi, R. N. V. S.; Janssen, C.; et al. Tissue Distribution and Depletion Kinetics of Bortezomib and Bortezomib-Related Radioactivity in Male Rats after Single and Repeated Intravenous Injection of 14 C-Bortezomib. *Cancer Chemother. Pharmacol.* **2007**, *60*, 777–787. https://doi.org/10.1007/s00280-007-0424-9.

280. European Medicines Agency. Scientific discussion for the approval of Velcade. Avaiable online: https://www.ema.europa.eu/en/documents/scientific-discussion/velcade-epar-scientific-discussion_en.pdf.

281. Yu, Q.; Stamenkovic, I. Cell Surface-Localized Matrix Metalloproteinase-9 Proteolytically Activates TGF-Beta and Promotes Tumor Invasion and Angiogenesis. *Genes Dev.* **2000**, *14*, 163–176.

282. Xu, C.; Bailly-Maitre, B.; Reed, J. C. Endoplasmic Reticulum Stress: Cell Life and Death Decisions. *J. Clin. Invest.* **2005**, *115*, 2656–2664. https://doi.org/10.1172/JCI26373.

283. Jiang, Z.; Clemens, P. R. Cellular Caspase-8-like Inhibitory Protein (CFLIP) Prevents Inhibition of Muscle Cell Differentiation Induced by Cancer Cells. *FASEB J. Off. Publ. Fed. Am. Soc. Exp. Biol.* **2006**, *20*, 2570–2572. https://doi.org/10.1096/fj.06-6347fje.

284. Ikezoe, K.; Nakamori, M.; Furuya, H.; Arahata, H.; Kanemoto, S.; Kimura, T.; Imaizumi, K.; Takahashi, M. P.; Sakoda, S.; Fujii, N.; et al. Endoplasmic Reticulum Stress in Myotonic Dystrophy Type 1 Muscle. *Acta Neuropathol.* **2007**, *114*, 527–535. https://doi.org/10.1007/s00401-007-0267-9.

285. Ikezoe, K.; Furuya, H.; Ohyagi, Y.; Osoegawa, M.; Nishino, I.; Nonaka, I.; Kira, J.-I. Dysferlin Expression in Tubular Aggregates: Their Possible Relationship to Endoplasmic Reticulum Stress. *Acta Neuropathol.* **2003**, *105*, 603–609. https://doi.org/10.1007/s00401-003-0686-1.

286. Nagaraju, K.; Casciola-Rosen, L.; Lundberg, I.; Rawat, R.; Cutting, S.; Thapliyal, R.; Chang, J.; Dwivedi, S.; Mitsak, M.; Chen, Y.-W.; et al. Activation of the Endoplasmic Reticulum Stress Response in Autoimmune Myositis: Potential Role in Muscle Fiber Damage and Dysfunction. *Arthritis Rheum.* **2005**, *52*, 1824–1835. https://doi.org/10.1002/art.21103.

287. Zito, E. Targeting ER Stress/ER Stress Response in Myopathies. *Redox Biol.* **2019**, *26*, 101232. https://doi.org/https://doi.org/10.1016/j.redox.2019.101232.

288. Langen, R. C. J.; Schols, A. M. W. J.; Kelders, M. C. J. M.; Wouters, E. F. M.; Janssen-Heininger, Y. M. W. Enhanced Myogenic Differentiation by Extracellular Matrix Is Regulated at the Early Stages of Myogenesis. *Vitr. Cell. Dev. Biol. - Anim.* **2003**, *39*, 163–169. https://doi.org/10.1007/s11626-003-0011-2.

289. Mamchaoui, K.; Trollet, C.; Bigot, A.; Negroni, E.; Chaouch, S.; Wolff, A.; Kandalla, P.; Marie, S.; Di Santo, J.; St Guily, J.; et al. Immortalized Pathological Human Myoblasts: Towards a Universal Tool for the Study of Neuromuscular Disorders. *Skelet. Muscle* **2011**, *1*, 34. https://doi.org/10.1186/2044-5040-1-34.

290. Milic, A.; Daniele, N.; Lochmüller, H.; Mora, M.; Comi, G. P.; Moggio, M.; Noulet, F.; Walter, M. C.; Morandi, L.; Poupiot, J.; et al. A Third of LGMD2A Biopsies Have Normal Calpain 3 Proteolytic Activity as Determined by an *in Vitro* Assay. *Neuromuscul. Disord.* **2007**, *17*, 148–156. https://doi.org/10.1016/j.nmd.2006.11.001.

291. Sáenz, A.; Leturcq, F.; Cobo, A. M.; Poza, J. J.; Ferrer, X.; Otaegui, D.; Camaño, P.; Urtasun, M.; Vílchez, J.; Gutiérrez-Rivas, E.; et al. LGMD2A: Genotype-Phenotype Correlations Based on a Large Mutational Survey on the Calpain 3 Gene. *Brain* **2005**, *128*, 732–742.

https://doi.org/10.1093/brain/awh408.

292. Fanin, M.; Nardetto, L.; Nascimbeni, A. C.; Tasca, E.; Spinazzi, M.; Padoan, R.; Angelini, C. Correlations between Clinical Severity, Genotype and Muscle Pathology in Limb Girdle Muscular Dystrophy Type 2A. *J. Med. Genet.* **2007**, *44*, 609–614. https://doi.org/10.1136/jmg.2007.050328.

293. Bianchini, E.; Testoni, S.; Gentile, A.; Calì, T.; Ottolini, D.; Villa, A.; Brini, M.; Betto, R.; Mascarello, F.; Nissen, P.; et al. Inhibition of Ubiquitin Proteasome System Rescues the Defective Sarco(Endo)Plasmic Reticulum Ca^{2+}-ATPase (SERCA1) Protein Causing Chianina Cattle Pseudomyotonia. *J. Biol. Chem.* **2014**, *289*, 33073–33082. https://doi.org/10.1074/jbc.M114.576157.

294. Teicher, B. A.; Ara, G.; Herbst, R.; Palombella, V. J.; Adams, J. The Proteasome Inhibitor PS-341 in Cancer Therapy. *Clin. Cancer Res.* **1999**, *5*, 2638 LP – 2645.

295. Adams, J. Development of the Proteasome Inhibitor PS-341. *Oncologist* **2002**, *7*, 9–16. https://doi.org/10.1634/theoncologist.7-1-9.

296. Sharma, A.; Preuss, C. V. Bortezomib.; Treasure Island (FL),; 2020; Treasure Island (FL), 2020.

297. Levêque, D.; Carvalho, M. C. M.; Maloisel, F. Review. Clinical Pharmacokinetics of Bortezomib. *In Vivo* **2007**, *21*, 273–278.

298. Reece, D. E.; Sullivan, D.; Lonial, S.; Mohrbacher, A. F.; Chatta, G.; Shustik, C.; Burris, H. 3rd; Venkatakrishnan, K.; Neuwirth, R.; Riordan, W. J.; et al. Pharmacokinetic and Pharmacodynamic Study of Two Doses of Bortezomib in Patients with Relapsed Multiple Myeloma. *Cancer Chemother. Pharmacol.* **2011**, *67*, 57–67. https://doi.org/10.1007/s00280-010-1283-3.

299. Chauhan, D.; Catley, L.; Li, G.; Podar, K.; Hideshima, T.; Velankar, M.; Mitsiades, C.; Mitsiades, N.; Yasui, H.; Letai, A.; et al. A Novel Orally Active Proteasome Inhibitor Induces Apoptosis in Multiple Myeloma Cells with Mechanisms Distinct from Bortezomib. *Cancer Cell* **2005**, *8*, 407–419. https://doi.org/https://doi.org/10.1016/j.ccr.2005.10.013.

300. Colson, K. Treatment-Related Symptom Management in Patients with Multiple Myeloma: A Review. *Support. care cancer Off. J. Multinatl. Assoc. Support. Care Cancer* **2015**, *23*, 1431–1445. https://doi.org/10.1007/s00520-014-2552-1.

301. Richardson, P.; Schlossman, R.; Munshi, N.; Avigan, D.; Jagannath, S.; Alsina, M.; Doss, D.; McKenney, M.; Hande, K.; Farrell, M.; et al. A Phase 1 Trial of Lenalidomide (REVLIMID®) with Bortezomib (VELCADE®) in Relapsed and Refractory Multiple Myeloma. *Blood* **2005**, *106*, 365. https://doi.org/10.1182/blood.V106.11.365.365.

302. Miguel, J. F. S.; Richardson, P.; Sonneveld, P.; Schuster, M.; Irwin, D.; Stadtmauer, E.; Facon, T.; Harousseau, J.; Ben-Yehuda, D.; Lonial, S.; et al. Frequency, Characteristics, and Reversibility of Peripheral Neuropathy (PN) in the APEX Trial. *Blood* **2005**, *106*, 366. https://doi.org/10.1182/blood.V106.11.366.366.

303. Field-Smith, A.; Morgan, G. J.; Davies, F. E. Bortezomib (Velcadetrade Mark) in the Treatment of Multiple Myeloma. *Ther. Clin. Risk Manag.* **2006**, *2*, 271–279. https://doi.org/10.2147/tcrm.2006.2.3.271.

304. Rosenthal, N.; Brown, S. The Mouse Ascending: Perspectives for Human-Disease Models. *Nat. Cell Biol.* **2007**, *9*, 993–999. https://doi.org/10.1038/ncb437.

305. Urtasun, M.; Sáenz, a; Roudaut, C.; Poza, J. J.; Urtizberea, J. a; Cobo, a M.; Richard, I.; García

Bragado, F.; Leturcq, F.; Kaplan, J. C.; et al. Limb-Girdle Muscular Dystrophy in Guipúzcoa (Basque Country, Spain). *Brain* **1998**, *121 (Pt 9*, 1735–1747.

306. Bohlmeyer, T. J.; Wu, A. H.; Perryman, M. B. Evaluation of Laboratory Tests as a Guide to Diagnosis and Therapy of Myositis. *Rheum. Dis. Clin. North Am.* **1994**, *20*, 845–856.
307. Heizmann, C. W.; Berchtold, M. W.; Rowlerson, A. M. Correlation of Parvalbumin Concentration with Relaxation Speed in Mammalian Muscles. *Proc. Natl. Acad. Sci. U. S. A.* **1982**, *79*, 7243–7247. https://doi.org/10.1073/pnas.79.23.7243.
308. Kho, A. T.; Kang, P. B.; Kohane, I. S.; Kunkel, L. M. Transcriptome-Scale Similarities between Mouse and Human Skeletal Muscles with Normal and Myopathic Phenotypes. *BMC Musculoskelet. Disord.* **2006**, *7*, 23. https://doi.org/10.1186/1471-2474-7-23.
309. Barclay, C. J.; Weber, C. L. Slow Skeletal Muscles of the Mouse Have Greater Initial Efficiency than Fast Muscles but the Same Net Efficiency. *J. Physiol.* **2004**, *559*, 519–533. https://doi.org/https://doi.org/10.1113/jphysiol.2004.069096.
310. Feng, H.-Z.; Chen, M.; Weinstein, L. S.; Jin, J.-P. Improved Fatigue Resistance in Gsα-Deficient and Aging Mouse Skeletal Muscles Due to Adaptive Increases in Slow Fibers. *J. Appl. Physiol.* **2011**, *111*, 834–843. https://doi.org/10.1152/japplphysiol.00031.2011.
311. Bassel-Duby, R.; Olson, E. N. Signaling Pathways in Skeletal Muscle Remodeling. *Annu. Rev. Biochem.* **2006**, *75*, 19–37. https://doi.org/10.1146/annurev.biochem.75.103004.142622.
312. U. S. National Library of Medicine. Proteasomal Inhibition for Patients With Mis-sense Mutated Dysferlin (Dysferlin). Avaiable online: https://clinicaltrials.gov/ct2/history/NCT01863004?V_8=View (accessed on1 December, 2020).
313. Manivannan, S. N.; Darouich, S.; Masmoudi, A.; Gordon, D.; Zender, G.; Han, Z.; Fitzgerald-Butt, S.; White, P.; McBride, K. L.; Kharrat, M.; et al. Novel Frameshift Variant in MYL2 Reveals Molecular Differences between Dominant and Recessive Forms of Hypertrophic Cardiomyopathy. *PLOS Genet.* **2020**, *16*, e1008639.
314. Jacob, H. J.; Kwitek, A. E. Rat Genetics: Attaching Physiology and Pharmacology to the Genome. *Nat. Rev. Genet.* **2002**, *3*, 33–42. https://doi.org/10.1038/nrg702.
315. Larcher, T.; Lafoux, A.; Tesson, L.; Remy, S.; Thepenier, V.; François, V.; Le Guiner, C.; Goubin, H.; Dutilleul, M.; Guigand, L.; et al. Characterization of Dystrophin Deficient Rats: A New Model for Duchenne Muscular Dystrophy. *PLoS One* **2014**, *9*, e110371. https://doi.org/10.1371/journal.pone.0110371.
316. Andreetta, F.; Bernasconi, P.; Baggi, F.; Ferro, P.; Oliva, L.; Arnoldi, E.; Cornelio, F.; Mantegazza, R.; Confalonieri, P. Immunomodulation of TGF-Beta 1 in Mdx Mouse Inhibits Connective Tissue Proliferation in Diaphragm but Increases Inflammatory Response: Implications for Antifibrotic Therapy. *J. Neuroimmunol.* **2006**, *175*, 77–86. https://doi.org/10.1016/j.jneuroim.2006.03.005.
317. Gosselin, L. E.; Williams, J. E.; Personius, K.; Farkas, G. A. A Comparison of Factors Associated with Collagen Metabolism in Different Skeletal Muscles from Dystrophic (Mdx) Mice: Impact of Pirfenidone. *Muscle Nerve* **2007**, *35*, 208–216. https://doi.org/10.1002/mus.20681.
318. Li, H.; Mittal, A.; Makonchuk, D. Y.; Bhatnagar, S.; Kumar, A. Matrix Metalloproteinase-9 Inhibition Ameliorates Pathogenesis and Improves Skeletal Muscle Regeneration in Muscular Dystrophy. *Hum. Mol. Genet.* **2009**, *18*, 2584–2598. https://doi.org/10.1093/hmg/ddp191.
319. Zsebo, K.; Yaroshinsky, A.; Rudy, J. J.; Wagner, K.; Greenberg, B.; Jessup, M.; Hajjar, R. J.

Long-Term Effects of AAV1/SERCA2a Gene Transfer in Patients with Severe Heart Failure: Analysis of Recurrent Cardiovascular Events and Mortality. *Circ. Res.* **2014**, *114*, 101–108. https://doi.org/10.1161/CIRCRESAHA.113.302421.

320. Mázala, D. A. G.; Pratt, S. J. P.; Chen, D.; Molkentin, J. D.; Lovering, R. M.; Chin, E. R. SERCA1 Overexpression Minimizes Skeletal Muscle Damage in Dystrophic Mouse Models. *Am. J. Physiol. Physiol.* **2015**, *308*, C699–C709. https://doi.org/10.1152/ajpcell.00341.2014.

321. Kang, S.; Dahl, R.; Hsieh, W.; Shin, A.; Zsebo, K. M.; Buettner, C.; Hajjar, R. J.; Lebeche, D. Small Molecular Allosteric Activator of the Sarco/Endoplasmic Reticulum Ca^{2+}-ATPase (SERCA) Attenuates Diabetes and Metabolic Disorders. *J. Biol. Chem.* **2016**, *291*, 5185–5198. https://doi.org/10.1074/jbc.M115.705012.

322. Taguchi, K.; Kobayashi, T.; Hayashi, Y.; Matsumoto, T.; Kamata, K. Enalapril Improves Impairment of SERCA-Derived Relaxation and Enhancement of Tyrosine Nitration in Diabetic Rat Aorta. *Eur. J. Pharmacol.* **2007**, *556*, 121–128. https://doi.org/https://doi.org/10.1016/j.ejphar.2006.11.026.